SYNTHESIS, MODIFICATION AND CATALYTIC EVALUATION OF HIGH-SILICA ZEOLITES

BY

SHAKEEL AHMED

A Dissertation Presented to the

FACULTY OF THE COLLEGE OF GRADUATE STUDIES

KING FAHD UNIVERSITY OF PETROLEUM & MINERALS

DHAHRAN, SAUDI ARABIA

In Partial Fulfillment of the
Requirements for the Degree of

DOCTOR OF PHILOSOPHY

In

CHEMISTRY

May 1995

بسم الله الرحمن الرحيم

. . . وما أوتيتم من العلم الا قليلا

(الآسراء ٨٥)

KING FAHD UNIVERSITY OF PETROLEUM AND MINERALS
DHAHRAN 31261, SAUDI ARABIA

COLLEGE OF GRADUATE STUDIES

This dissertation, written by Mr. Shakeel Ahmed under the direction of his Dissertation Advisor and approved by his Dissertation Committee, has presented to and accepted by the Dean of the College of Graduate Studies, in partial fulfillment of the requirements for the degree of DOCTOR OF PHILOSOPHY in Chemistry.

Dissertation Committee:

Professor M.Z. El-Faer
Dissertation Advisor

Dr. M.M. Abdillahi
Member

Professor M.F. Ali
Member

Professor U.K.A. Klein
Member

Dr. A.M. Abdennabi
Member

Dr. Abdul-Rehman Al-Arfaj
Department Chairman

Dr. M. Atiqullah
Member

Professor Ala H. Al-Rabeh
Dean, College of Graduate Studies

Date: June 4, 1996

Dedicated to
my parents, wife and son Saa'd

ACKNOWLEDGMENT

Praise be to Allah, the Almighty, for giving me the help and guidance that enabled me to accomplish this work successfully.

I wish to express my appreciation to Professor Mohammad Z. El-Faer who served as my Dissertation Advisor. I am also indebted to my Co-Advisor, Dr. M.M. Abdillahi. The completion of this work would not have been possible without his sincere help and cooperation. I wish to thank the other members of my Dissertation Committee, Dr. M. Atiqullah, Professor M.F. Ali, Professor U.K.A. Klein and Dr. A.M. Abdennabi for their constructive suggestions.

I wish to thank Dr. S.A. Barri, of the KFUPM Research Institute, for reviewing the Dissertation carefully and providing valuable comments.

I am thankful to all my colleagues and friends who helped me during the work. I wish to mention Azfar, Zaka, Zaki, Naseem, Imran, Dr. Farooq and Dr. Saleem-ur-Rehman.

I would like to thank all of members of the Zeolite Research Group of the KFUPM Research Institute. Specifically, I need to mention K. Alam, M.A.B. Siddique, M.S. Al-Gharami, S.M.J. Zaidi, S.A. Ali and A.M. Aitani.

I am thankful to Dr. Abdul-Rehman Al-Arfaj, Chairman Chemistry Department, for his generous help and cooperation.

Finally, I wish to thank Petroleum and Gas Technology Division, KFUPM Research Institute, for providing me the opportunity to conduct this work.

TABLE OF CONTENTS

CHAPTER 3. EXPERIMENTAL

CHAPTER 5. CONCLUSIONS AND RECOMMENDATIONS

LIST OF TABLES

LIST OF FIGURES

DISSERTATION ABSTRACT

NAME	SHAKEEL AHMED
TITLE OF STUDY	SYNTHESIS, MODIFICATION AND CATALYTIC EVALUATION OF HIGH-SILICA ZEOLITES
MAJOR FIELD	CHEMISTRY
DATE OF DEGREE	MAY 1995

High-silica zeolites of MFI type were synthesized by rapid crystallization method. The major factors affecting the hydrothermal synthesis were screened using Plackett-Burman experimental design. The pH of the crystallizing mixture was found to be the most important factor. A pH of 10.0 ±0.5 was found to be the optimum for the crystallization of high-silica zeolites by this method. The results of the rapid crystallization method were compared with that of conventional method. A narrow particle size distribution was found in the case of rapid crystallization method. This finding was rationalized on the basis of nucleation rate relative to the crystallization rate. The synthesized zeolites were modified by varying Si/Al ratio, metal incorporation and steaming. A quantitative relationship was found between the Si/Al ratio of the gel and that of the zeolite product. The least square fit to the data gave: $(Si/Al)_{zeolite} = 3.53 + 0.777(Si/Al)_{gel}$ with a correlation coefficient of 0.999. This was consistent with the silica having higher solubility than aluminosilicate species and that the pH of the hydrogel, within the range of Si/Al ratios investigated, was constant. The synthesized and modified zeolites were characterized by FTIR, XRD, SEM, ESR, thermal analysis and particle size distribution analysis. Acidity measurements of some of the synthesized and modified zeolites were performed by TPD of ammonia and FTIR of adsorbed pyridine. A bench scale high-pressure flow reactor system was designed and fabricated for the catalytic evaluation of the high-silica zeolites. Some of the selected zeolite catalysts were evaluated for MTBE synthesis and methanol to olefins (MTO) conversion. In the case of MTBE, the effect of temperature, Si/Al ratio, space velocity and methanol to isobutene molar ratio was investigated for the conversion of isobutene. Higher yields of MTBE were obtained at 80 °C for lower Si/Al ratio. The space velocity and molar ratio had minor effect. The acidity of the zeolite was correlating with the conversion of isobutene. Steam-modified zeolite performed better in term of selectivity for MTBE than commercial Amberlyst-15 resin catalyst. The yield of MTBE was comparable for both catalysts. The higher activity of the steamed catalyst was explained on the basis of enhanced acidity. Steaming at higher severity caused reduction in activity resulting from excessive loss of acid sites. The results of catalytic evaluation for MTO showed that Fe-containing synthesized zeolite gave highest selectivity for the C_2 - C_4 olefins. This was attributed to the dilute acidity of the catalyst.

DOCTOR OF PHILOSOPHY DEGREE
KING FAHD UNIVERSITY OF PETROLEUM AND MINERALS
Dhahran, Saudi Arabia

الخلاصة

اســـم الطالب : شكيل احمد
عنوان الدراسة : التحضير والتعديل والتقويم الحفزي للزيولايت مرتفعة السيليكا
التخصص : الكيمياء
تاريخ الشهادة : ذو الحجة ١٤١٥هـ (مايو ١٩٩٥م)

تم إعـداد الزيولايت ذات السيليكا العـالي نوع (MFI) بواسطة طريقة التبلر السريع . واستـخدم التصميم التجريبي (Plackett-Burman) لتحديد العـوامل الرئيسية المؤثرة في عمليـة الإعداد الحراري-المائي للزيولايت . وأظهرت النتائج أن الرقم الهيدروجيني لمزيج التبلر هو العامل الأكثر أهمية حيث وجد أن الرقم الهيـدروجيني ١٠ر٠ ± ٥ر٠ هو المـعدل الأمثـل لتبلر الزيولايت ذات السـيليكا العاليـة باتباع هذه الطريقة . وتمت مقارنة نتائج طريقة التبلر السريـع بالطريقة التقليدية لإعداد الزيولايت فوجد أن التوزيع الضيق لحجم الحـبيبات هو المـتوفر في طريقة التبلر السـريع . وتم تبرير هذه النتيجـة بناء على معدل تشكل النوى نسـبة إلى مـعدل التـبلر . وتم كـذلك تعـديل الزيولايت المعـدة بتغـيير مـعدل السـيليكا/الألومينا (Si/Al) ودمج المعـادن إضافة إلى المعـالجة بالبخار . وأظهـرت النتائج وجود علاقـة ترابطية كميـة بين معدل (Si/Al) لكل من الجل والزيولايت . وأعطت الطريقـة التوافقـية للمربع الأقل بالنسـبة للبيانات المعادلة التالية : (Si/Al) زيولايـت = ٣ر٥٣ + ٠ر٧٧٧ (Si/Al) جل ووجد ان المعـامل الترابطي هو (٠ر٩٩٩) . ويتوافق هذا مع السـيليكا التي لديها ذوبانيـة أكثر من أصناف الألـومينا سيليكات إضـافة إلى ثبات الرقم الهيدروجيني للجل ضمن معـدلات (Si/Al) قيد الدراسة . وتم تعيين خواص الحفازات المعدة والمعدلة بواسطة مطيافيـة فوريير تحـت الحمراء (FTIR) وحيـود الأشعة السينية (XRD) والمجهر الإلكتروني الماسح (SEM) والرنين الدوري الإلكتـروني (ESR) والتحليل الـحراري إضافـة إلى توزيع حجم الحبيبات . وتم كـذلك قـياس حمضية بعض الزيولايت المعدة والمعدلة باسـتخدام طريقة المج الحراري المبرمج للنشادر ومطيافية (FTIR) لامتصاص البيريدين . وتم تصـميم وتصنيع وحدة مفاعل ذات ضغط مرتفع للتقـويم الحفزي للزيولايت ذات السيليكا العاليـة . وأجريت التجارب لتقـويم بعض الحفازات في تفاعل ثالثي بيوتيل ميثيل الأثير (MTBE) وتحويل الميثانول إلى الأليفينات (MTO) . وبالنسبة لتفاعل (MTBE) فـقـد تم دراســة تأثير درجـة الحـرارة ومـعـدل (Si/Al) وسـرعة الدفـق والمعـدل الجـزيئي للمـيـثـانول/الأيسـوبيـوتيلين بالنسبـة لتحـويل الأيسـوبيوتيلين . وأظهـرت النتائج إرتفـاعاً فـي إنتاجـية (MTBE) عند (٨٠) درجة مـئوية ومعـدلات منخـفضة من (Si/Al) . أما سـرعة الدفق والمعـدل الجزيئي فوجد أن لهما تأثير ثانوي على التفاعل . وتناسبت حمضية الزيولايت مع تحويل الأيسوبيوتيلين . وأظهرت النتائج كـذلك أن الزيولايت المعدل بالبخره أداء حفزياً أفضل بالنسبة لإنتقائية (MTBE) مقارنة بالحفاز التجاري راتينج (Amberlyst-15) . في حين تساوت الإنتاجية لكلا الحـفازين . إن النشاط الحفزي المرتفع للحفـاز المعـالج بالبخـار يعود إلى الحـمضيـة المتـزايدة . غير أن المـعالجـة الشديدة بالبـخار أدت إلى إنخفاض النشاط الناتج عن الفقد الكبير في المواقع الحمضية . وأشارت نتائج التقويم الحفزي لتحويل الميثانول (MTO) إلى أن الزيولايت المـعد والمـحتـوي على الحديد يـعطي أفضل إنتـقائيـة للأليفـينات الخفيفة (C2 - C4) . وتعود هذه النتيجة إلى تأثير الحمضية المخففة للحفاز .

درجة الدكتوراة في الفلسفة
جامعة الملك فهد للبترول والمعادن
الظهران . المملكة العربية السعودية

CHAPTER 1

INTRODUCTION

1.1 Background

Zeolites are porous aluminosilicates that exhibit three dimensional structures by interconnecting frameworks of $[AlO_4]^{-5}$ and $[SiO_4]^{-4}$ tetrahedra. However, isomorphous substitutions of both aluminum and silicon are possible to extend this definition to various aluminophosphates, gallosilicates, borosilicates etc. Zeolites are distinguished from each other by structural differences in their unit cell. The shape-selectivity of zeolites, allowing the passage of organic molecules with critical dimensions while inhibiting others, makes them very attractive catalysts. Therefore, zeolites are of great significance as catalysts in petroleum chemistry and in the synthesis of organic intermediates, and fine chemicals [1-5]. The catalytic properties of zeolites can be widely varied by isomorphous substitutions or by subsequent post-synthesis modifications.

The natural zeolites have formed under aqueous, alkaline condition in matrices of basalt rock and as sedimentary deposits. These conditions are typical of hydrothermal systems and have guided the laboratory technique of synthesis. The role of water as a mineralizing agent, aided by alkaline conditions, drew the attention of mineralogists and chemists to hydrothermal synthesis. Systematic studies began in Barrer's laboratory in early 1940's. The first made being analcime, mordenite zeolites with the

edingtonite framework[6] also with the framework of that subsequently termed ZK-5[7,8]. ZK-5 was thus the first zeolite without a natural counterpart to be synthesized.

In the recent years there have been considerable academic and industrial research efforts carried out in the field of zeolite synthesis[9-13]. There are 34 known natural zeolites and about 150 zeolites from aluminosilicate systems have been reported in the published literature[10]. Compared to the large number of known zeolite and related materials, the number of observed zeolite structure types remain relatively small, currently approximately 87, with many different materials adopting the same framework topology [14,15].

High-silica zeolites (Si/Al >10) are usually formed from neutral or basic hydrogels containing sources of silica and alumina, alkali or ammonium ions and organic molecules such as (alkyl)amines or quaternary ammonium compounds [16,17]. For pH values usually higher than 10, the high OH^- concentration enhances the dissociation rate of the amorphous gel and consequently the crystal growth rate [18].

The presence or absence of particular cations in the gel may significantly influence the course of zeolite formation [19]. Organic species present in the gel are responsible for the formation of high silica zeolites by templating and/or space-filling effect [16, 20]. Organic bases favor strongly the formation of particular double ring silicate anions which constitute secondary building units for different zeolites [21, 22].

Recently, elements such as Fe, B, As, Cr, V, and Ge have been used to replace aluminum and silicon in the framework of the pentasil family of zeolites. Pentasil-zeolite has been proposed recently to encompass all members of high silica zeolites [23].

1.2 Historical Development

The history of zeolite dates back to 1756, when the Swedish mineralogist Cronstedt discovered the first zeolite mineral, Stilbite. He recognized zeolites as a new class of minerals consisting of hydrated aluminosilicates of the alkali and alkaline earths.

The early literature described the ion exchange, adsorption, molecular sieve and structural properties of zeolite minerals as well as a number of reported syntheses of zeolites. Barrer's pioneering work in zeolite adsorption and synthesis in the mid-1930's to 1940's inspired Milton of the Linde Division of Union Carbide Corporation to initiate studies in zeolite synthesis in search of new approaches for separation and purification of air. Between 1949 and 1954, Milton and his co-worker Breck discovered a number of commercially significant zeolites, types A, X, and Y. In 1959 a zeolite Y-based catalyst was marketed by Union Carbide as an isomerization catalyst [24].

In 1962 Mobil Oil introduced the use synthetic zeolite X as a cracking catalyst. In 1969 Grace described the first modification chemistry based on steaming zeolite Y to form an "ultrastable" Y. In

1967 to 1969, Mobil Oil reported the synthesis of the high silica zeolite beta and ZSM-5. In 1974 Henkel introduced zeolite A in detergents as a replacement for the environmentally suspect phosphates. By 1977 industry-wide 22,000 tons of zeolite Y were in use in catalytic cracking. In 1977 Union Carbide introduced zeolites for ion-exchange separations.

In the 1980's extensive work was carried out on the synthesis and applications of ZSM-5 and a proliferating number of other members of the high silica zeolite family. In 1982 microporous crystalline aluminophosphate molecular sieves were described by Wilson et al. [25] at Union Carbide, and additional members of the aluminophosphate-based molecular sieve family, for example, SAPO, MeAPO, MeAPSO, ElAPO and ElAPSO, subsequently discovered by 1986 [26]. Considerable effort in synthesizing metallosilicate molecular sieves was reported where the metals iron, gallium, titanium, germanium, and others were incorporated during synthesis into the silica or aluminosilicate frameworks, typically with the ZSM-5 (MFI) topology [27]. The major events in the historical development of zeolites are summarized in Table 1.1.

The development of commercial zeolites selected from newly discovered compositions and structures, chemical modifications of present products to generate new useful properties, and a re-evaluation of the known zeolites which never achieved commercial success should be attempted. With the world-wide expansion of scientific zeolite centers with the capability of synthesizing zeolites and finding their potential

Table 1.1 Chronological development of zeolite.

Year	Event	Ref.
1938	Early synthesis of zeolites by R. M. Barrer.	6,28
1946	Barrer reported new zeolites	7
1948	Synthesis of mordenite.	29
1956	Synthesis of A zeolite by Breck, (UC).	30
1959	Synthesis of X zeolite by Milton et al.	31
1962	FCC catalyst by Mobil Company.	32
1964	Synthesis of Y zeolite by Breck.	33
1967	US-Y zeolite by Mc Daniel.	34
1972	ZSM-5 by Argauer et al., (Mobil).	35
1988	VPI-5 by Davies.	36

applications, it is likely that this will offer new opportunities in the field of catalysis and reactor design.

The industrial application of zeolite used as catalysts will open up entirely new vistas in chemical, petroleum, and petrochemical industries.

In parts of the world where there is no oil, coal becomes a developing source of hydrocarbon fuels and chemicals, where by zeolites should dominate the down-stream secondary catalytic processes used to upgrade products of the Fischer-Tropsche converter. In the oil producing countries, like Saudi Arabia, zeolite catalysts will offer the interhydrocarbon conversions for the production of the more value-added feedstocks and products. The future of zeolite catalysis looks bright.

1.3 Objectives

The overall objective of this research is to synthesize, modify and characterize high-silica zeolites for the methyl-tertiary butyl ether (MTBE) synthesis and methanol to olefins (MTO) conversion reactions.

However, the specific objectives are as follows:

1. Prepare various high-silica zeolites in the laboratory with different properties.

2. Modify the synthesized zeolite catalysts to obtain the requirements for the ether and light olefin synthesis.
3. Characterize the synthesized /modified zeolites using the relevant analytical techniques.
4. Perform the catalytic evaluation of the zeolite catalysts for MTO and MTBE reactions.

CHAPTER 2

LITERATURE REVIEW

2.1 Hydrothermal Synthesis of Zeolites

The laboratory synthesis has been mostly successful by duplicating the conditions which produced natural zeolites. However, one of the conditions that can be hardly duplicated is crystallization time of thousand years and beyond. Thus laboratory systems operate at high pH (usually >12) and higher temperature, and produce smaller, less-perfect crystal. So the majority of the synthetic zeolites are formed under non-equilibrium condition and consits of metastable phases.

Zeolites are generally synthesized by a hydrothermal process [13], from a source of alumina (e.g., sodium aluminate or aluminum sulfate) and of silica (e.g., a silica sol, fumed silica or sodium silicate) and an alkali such as NaOH, and/or organic additive (e.g., a quaternary ammonium salt). The main factors influencing the hydrothermal synthesis and crystallization will be reviewed in what follows.

2.1.1 Factors Affecting the Hydrothermal Synthesis

Thermodynamic variables in the synthesis of zeolites are temperature, alkalinity(pH) and chemical composition of the reacting mixtures. The kinetical variables include the treatment of the reactants before crystallization, their chemical and physical nature [37,38]. Even

though each variable contributes to a specific aspect of crystallization, substantial interaction occur between these elements during the course of crystallization.

2.1.1.1 *Temperature*

Zeolite forms over a considerable range of temperatures. Based on geological evidence, an upper limit of 350°C has been suggested in a hydrothermal synthesis [39], although high-temperature synthesis of analcime (360°C), clinoptilolite (370°C), ferrierite (375°C), and mordenite (430°C) have been cited [13].

The temperature range for crystallization increases with increasing Si/Al ratio in the zeolite, from 25°C to 125°C for the aluminum-rich zeolites, A and X zeolites, from 100°C to 150°C for intermediate Si/Al zeolites, L, omega and mordenite and from near 125°C to 200°C for the high-silica zeolites as exemplified by ZSM-5 [40,41]. This is consistent with the suggested relationship of pore volume and synthesis temperature [42]. The higher the synthesis temperature, the smaller tends to be the water content and intracrystalline porosity of any zeolite. The most porous zeolites such as A, X, Y, chabazite, RHO and ZK-5, with pore volumes in the range of 0.25 to 0.36 cm^3/g of crystal do not form at temperatures much above 100°C. Silica-rich phases such as mordenite, L, omega, ZSM-5, -11, and -39 and KZ-1 and -2, all with rather low intracrystalline porosities (0.15 - 0.20 cm^3/g), are usually best made at temperatures in the range 100°C - 200°C [42].

The temperature obviously affects the rate of nucleation and crystal growth. Zhdanov et al., demonstrated a linear rate of crystal growth with

rising temperature for NaX zeolite [43]. It is also observed that the temperature strongly affects the induction time. This behavior is typical of that found with other zeolites, such as NaY, by Xu Qinhua [9] or ZSM-5 by Chao [45].

2.1.1.2 *Chemical Composition*

The zeolite framework which crystallizes from a given batch is determined mainly by its composition. Table 2.1 broadly lists individual components of the mixture and the primary influence of each component on that reaction mixture [17].

Table 2.1. Primary influence of the composition of reaction mixture.

Molar Ratio	Primary Influence
SiO_2/Al_2O_3	Framework composition
H_2O/SiO_2	Rate, and crystallization mechanism
OH^-/SiO_2	Rate, Silicate molecular weight, and OH^- concentration
Inorganic cation(s)/SiO_2	Structure, and cation distribution
Organic additives/SiO_2	Structure, and framework aluminum content

The crystallization of a particular zeolite structure from the gel system containing these components strongly depends on the SiO_2/Al_2O_3 ratio of the starting gel mixture[46]. The inorganic or organic cations not only influence the structure crystallized they may also influence other

features of the final crystalline products, such as morphology and crystal size. Therefore, although K^+ appears to favor the formation of the NU-10 structure [46], in the $NH_2(CH_2)_6NH_2/K^+$ system, addition of this alkali cation to a reaction mixture containing tetrapropyl ammonium (TPA^+) cation as the organic component has been shown to change only the size of the ZSM-5 crystals produced from this mixture [47].

2.1.1.3 *Water*

In hydrothermal chemistry, water is present as a major component of crystallizing magmas. It has been recognized for a long time that, water is an excellent mineralizer [13,48], assisted in this role by OH^- ions in particular. This mineralizing property is the basis of hydrothermal chemistry. In zeolite synthesis, water is essential as a guest species which stabilizes the host lattice. The zeolite water may then be removed leaving the unchanged anhydrous zeolite. In hydrothermal systems, the good solvent powers of water promote mixing and transport of materials and facilitates nucleation and crystal growth. Water stabilizes zeolite crystals by filling the cavities and forming a type of solid solution. The stabilizing effect is such that porous aluminosilicate will not form in absence of a "guest" molecule, which may be a salt molecule as well as water [49].

The highly siliceous zeolites become progressively more hydrophobic as the silica content increases. This means that zeolite water stabilizes them less and intracrystalline organic species more. For example, the water concentration or the degree of dilution is of minor

importance for the synthesis of ZSM-5 which can crystallize out of gels with H_2O/SiO_2 ratio ranging from 7 to 22 [50].

Suzuki et al. [51] found that average diameter of the zeolite crystallites (ZSM-5) increased as the water content of the reaction mixture increases. The bulk Si/Al ratio remained constant even though the water-silica ratio of the mixture was varied from 7.8 to 80. In contrast, the Si/Al ratio at the outer shell of the crystallites decreased as the water content of the reaction mixture increased.

Though the presence of organic species in solution exerts a strong influence on the structure crystallized, water can also "tip the balance" of which structure crystallizes. In an experiment of the synthesis system containing pyrrolidine, Suzuki et al.[52] found that in the crystallization of ZSM-39, ZSM-48, and KZ-1(ZSM-23), only changing the H_2O/SiO_2 ratio from 20 to 80 shifted the structure of the zeolite obtained from the synthesis mixture. At low water content and high SiO_2/Al_2O_3 ratios, ZSM-39 is crystallized, whereas KZ-1(ZSM-23) is formed in more aluminum-rich gels. In more dilute systems, ZSM-48 is observed to crystallize at high SiO_2/Al_2O_3 ratios.

2.1.1.4 *Alkalinity(pH)*

In the inorganic system, the alkalinity is the key parameter in determining the crystallization rate [53]. The mineralizing role of free OH^- has been discussed in detail by Barrer [54], and Derouane et al. [55].

An increasing OH^- concentration will generally accelerate the growth and shorten induction period before viable nuclei are formed.

The OH^- is also a powerful minralizer. It is a good complexing agent which can bring amphoteric oxides and hydroxides into solution. The decrease in nucleation time and enhanced rate of crystal growth with rising pH can be attributed at least partially to the much greater concentration of dissolved species. In alkaline media the solubility of silica increases nearly exponentially with concentration of alkali. According to the ratio of M_2O/SiO_2 in the resultant mixture, a range of silicate anions may appear of various degree of oligomerization. In the case of alumina at high pH minimal oligomerization occurs, the dominant anion always being $Al(OH)_4$ [13]. The high alkalinity causes a high supersaturation of silicate and aluminate, and the formation of a large number of nuclei. The growth of the nuclei proceeds until the aluminum in the gel is exhausted. Alkaline media thus enable ready mixing of reactants and facilitate nucleation and crystal growth.

The hydroxide concentration can alter crystallization time for a particular structure as well as change the crystalline phase and composition produced. In the synthesis of Nu-10, increasing the OH^- concentration by a factor of 10 dramatically decreases the crystallization time. The amount of aluminum present in the crystalline product also increases with OH^- concentration, with SiO_2/Al_2O_3 changing from 97 to 82 to 55 in this example upon 10-fold and 20-fold increases in hydroxide, respectively. With increasing alumina content, a shift in the structure

formed also occurs. Instead of crystalline Nu-10, the Nu-4 structure is obtained [56].

Kulkarni et al.[57], discussed the role of pH on the aluminum distribution in the framework of ZSM-5 and experimentally showed that pH 6.7 was the lowest limit for the crystallization of ZSM-5. Obviously a longer period of time for crystallization (30 days) at this pH was required. However, the minimum autoclaving time (60 hrs) was found for the pH range 8.6 to 11, it was also observed that the final pH of the reaction mixture was always higher than the initial pH. Similar results were obtained by Casci and Lowe [58], during the crystallization of zeolite EU-1. The increase in the [free base] to [SiO_2] ratio, that is, ([M_2O] - [Al_2O_3])/[SiO_2], by removal of SiO_2 accompanied by the formation of zeolite increases the pH of the solution.

2.1.1.5 *Silica/Alumina ratio*

The SiO_2/Al_2O_3 ratio in the gel places a constraint on the framework composition of the zeolite produced. Ideally, the desired SiO_2/Al_2O_3 ratio of a zeolite chosen for a specific application should be obtainable through adjusting that ratio in the synthesis mixture. Unfortunately, changing the ratio of silica to alumina in the reaction mixture to produce the desired aluminum content not only changes the aluminum concentration in the zeolite structure, but it also changes the final structure obtained. For example, analcime can be obtained with SiO_2/Al_2O_3 ratio of between 4 and 5, with mordenite appearing around 8.

The nonzeolite, crystalline quartz phase follows at SiO_2/Al_2O_3 approaching 12 [13].

This type of dependency is also observed in the crystallization of higher-silica-containing materials. Zeolite EU-1 crystallizes at a SiO_2/Al_2O_3 between 30 and 120 in the presence of hexamethonium cation. Little crystalline material is observed to crystallize from a reaction mixture containing SiO_2/Al_2O_3 below 30. At $SiO_2/Al_2O_3 > 120$, the zeolite EU-2 structure is formed [59].

Not all zeolites are so sensitive to the composition of the starting reaction mixture. In the zeolite ZSM-5 system, crystallization occurs over a wide range of SiO_2/Al_2O_3, from 15 to infinity [35,60]. Zeolite ZSM-11 also has been synthesized under a broad range of SiO_2/Al_2O_3 from 15 to the pure silica polymorph, Silicalite-2 [60-62]. Attempts to prepare zeolite ZSM-5 at SiO_2/Al_2O_3 ratios less than 15 results in the crystallization of a mordenite or other less silica-rich phases.

Several workers have investigated the influence of the aluminum content on the rate of ZSM-5 crystallization [63-66]. All data show that the rate of crystallization of ZSM-5 becomes faster when the aluminum content of the gel is lower and all other factors remaining equal. This is opposite to the normal hydrothermal behavior of zeolites with lower SiO_2/Al_2O_3 ratio, such as A, X, Y etc., in which high SiO_2/Al_2O_3 ratio give a system with higher viscosity of the solution and a lower reaction rate.

2.1.1.6 *Time*

The synthesis time is important in two ways:

(i) an induction period during which the reaction mixture is held near ambient temperature prior to raising to the crystallization temperature often optimize zeolite yield (as in X, Y synthesis);
(ii) often different zeolite crystallize from one reaction mixture at different times [67].

Here, Ostwald's law of successive transformations is obeyed, in which an initial metastable phase is transformed successively into one or more phases of higher stability [68]. At constant temperature and initial mixture composition, the transformation proceeds from amorphous to metastable to more stable phase. Time, as a parameter, can be optimized in the synthesis of many zeolites. Increasing the temperature or hydroxide component of the reaction mixture and addition of inorganic or organic cations can all be applied to minimize the crystallization time which is important from a practical stand point. Difficulties arise in the preparation of desired materials in which additional metastable zeolite (or non-zeolite) phases are observed. Crystallization parameters must be adjusted to minimize the production of other phases while simultaneously minimizing the time needed to obtain the desired crystalline phase.

A considerable reduction in time of crystallization of zeolite was achieved by Inui et al [69]. In this procedure, called as 'rapid zeolite crystallization method', the gel precursor was treated by temperature-

programmed heating and the crystals formed within 2 h. The zeolites prepared by rapid crystallization method performed better than that of catalysts prepared by conventional methods. The possibility of incorporation of hetero elements (other than Si or Al) inside crystals was also studied [70].

2.1.2 Templating Action

Cations present in a reaction mixture are often the dominant factor determining the zeolite type [37]. Flanigen [16] pointed out that the two basic roles of a cation are: (i) a limited structure directing role and (ii) a general role of providing a source of hydroxyl ion and stabilizing the formation of sol-like aluminosilicate species. The cation is said to have a structure-directing function which influence the structure of the forming zeolite. Such a structure-directing effect has been termed "templating". More recently, the concept of cation templating in zeolite synthesis has been developed and summarized by Rollmann [17].

Although the exact mechanism of the templating effect still is not fully understood, it is visualized that the zeolite structure grows around the template, thus stabilizing certain pore structures or subunits. The relative sizes of the polyhedral cages and the related specific cations are shown in Table 2.2 [16]. A good fit for the anhydrous diameter is observed for the TMA(tetramehtyl ammonium) ion in the gmelinite and sodalite cages. The K, Ba, and Rb ions in the cancrinite cage and for the diameter of the hydrated Na ion in the gmelinite and sodalite cages. Table

2.2 also shows that the Ba and Rb ions can substitute for K ion, and TMA can substitute for the hydrated Na ion in their structure-forming roles. This analysis tends to support the cation-templating concept for most of the polyhedral cages considered.

Jarman and Melchior [170] studied the occupancy sites of TMA^+ ion in zeolite A and ZK-4, using ^{13}C NMR spectroscopy. Isotropic ^{13}C NMR chemical shifts distinguished between TPA^+ ions trapped in the α and β cages of these zeolites and were insensitive to Si/Al ratio. The observed intensities indicated near complete occupancy of the β cage over the complete composition range.

Table 2.2. Cation-specific building units in zeolite structures [16].

BUILDING UNIT		SPECIFIC CATION		
	FREE DIMENSIONS, A^O		DIAMETER (A^O)	
			ANHYDROUS	HYDRATED
D-4	2.3	Na	2.0	7.2
Alpha	11.4	Na	2.0	7.2
Sodalite	6.6	Na or TMA	2.0 (NA), 6.9 (TMA)	7.2 (Na), 7.3 (TMA)
Gmelinite	6.0 * 7.4	Na or TMA	2.0 (NA), 6.9 (TMA)	7.2 (Na), 7.3 (TMA)
Cancrinite	3.5-5.0	K, Ba, or Rb	2.8 (K), 2.7 (Ba), 3.0 (Rb)	6.6 (K), 8.1 (Ba), 6.6 (Rb)
D-6	3.6	Na, K, Sr, or Ba	2.0-2.8	7.2-8.2

The synthesis of ZSM-5 using TPA^+ (tetrapropyl ammonium) was reported by Argauer and Landolt [35]. Further it has been shown that the TPA^+ ion is needed preferably in the nucleation step of the crystallization process [21]. During the nucleation process whereby the organic cation organizes oxide tetrahedra into a particular geometric topology around itself and thus provides the initial building block for a particular structure type. In the case of ZSM-5 formation, the TPA^+ ion is obviously used as a template around which the channel intersections are formed. Crystallographic examination of the TPA cation in the ZSM-5 structure indicates a channel-directing role for this cation as the trapped amine is oriented in the channel intersections with the (C_3H_7) "arms" extended into the straight and sinusoidal channels of this zeolite structure [71]. It has also been proved by Boxhoorn et al [72], by ^{13}C MAS NMR measurements that

the TPA^+ ion is localized in the intersections of the channels of the ZSM-5 structure. In direct contrast, however, is the orientation of the same organic cation amine in the $AlPO_4$-5 structure [73]. $AlPO_4$-5 contains straight tunnel-like 12 ring channels and is also readily synthesized in the presence of the TPA cation.

Using ^{29}Si and ^{27}Al MAS NMR, IR, thermal and textural analysis, Scholle and coworkers [74] have confirmed the presence of increasing amounts of TPA-ZSM-5 entities with dimensions less than or comparable to an unit cell at early stages of crystallization. It is demonstrated that just for any other zeolite crystallization, ZSM-5 also crystallizes according to the successive nucleation and growth processes.

On the other hand, the zeolite ZSM-5 and ZSM-11 have similar framework topology, with the structure that crystallizes dependent on the organic quaternary amine used in the initial gel composition. Both structures containing intersecting channel systems; ZSM-5 contains the straight and a sinusoidal intersecting system, whereas ZSM-11 structure contains two straight intersecting systems with four intersections per unit cell [14]. TPA is used to promote ZSM-5 structural development, whereas TBA (tetrabutyl ammonium) cation or TBP, (the phosphorus-containing analog), promotes ZSM-11 formation. Although TPA has been found to aid in crystallizing two different channel systems (ZSM-5 and $AlPO_4$-5), here different templates induce crystallization of similar channel structures (ZSM-5 and ZSM-11). All three systems occlude the organic cation in their pore system upon crystallization. The generality of a

specific "lock and key" role for cations in the crystallization of zeolite structures is still unclear.

Although many studies indicate a great contribution by the cation to crystallizing individual structures, finding a direct correlation between specific cations and any one structural building unit has been less than satisfactory in any case. Flanigen [16], attempted to relate the structural units composing the zeolites with the necessity of having specific inorganic cation or groups of cations to direct that structure. Examination of a large number of the reported cation systems known at that time revealed that those structures containing only single rings of four, five, six, and eight tetrahedra show little structural cation specificity. The zeolite mordenite, for example, has been synthesized from Na, Li, Na-Li, Sr and Ca cation base systems and appears to show little cation preference. Analcime, containing 4 and 6 rings, and harmotome/phlipsite frameworks, containing 4 and 8 rings, have been synthesized in a large number of alkali and alkaline earth cation-base systems as well. Nevertheless, some definite trends can be observed between cation and structure. Strong cation specificity could be found for the double 4 ring, the cancrinite, gmelinite, sodalite, and a cages, and the zeolite frameworks composed of these units. The double 6 ring, on the one hand, did not show any favoritism for a specific cation; but, on the other hand, this unit does appear limited in the cation system chosen, as double 6 ring-containing structures have not been found in systems containing either Li or Ca ions.

Thus, "templating effect" attributed to the growth of zeolite structures around a given cation template cannot be used as a blanket description of the role of that cation in structure direction. The close relationship between its influence on structure as well as its interaction with other components of the gel make it difficult to completely interpret the role of the cation in zeolite crystallization at this time.

Now it is possible to synthesize ZSM-5 in the absence of any organic compounds [75,76]. Nastro et al. [77] started a systematic study of ZSM-5 synthesis in the $(Na, K)_2O$. $(Al_2O_3)x$. $(SiO_2)y$. $(H_2O)z$ system. They suggested that the hydrated Na^+ ions are able to function as a template for the formation of following secondary building units (SBU), which are common to ZSM-5 and also the mordenite structure. It was proposed that in a suitable environment Na^+ ions allow the very slow assembly of these units to give the precursor structures of ZSM-5 nuclei (Figure 2.1).

Dai et al. [78] studied the effects of starting composition and silica source for the formation of Na-ZSM-5 in the absence of organic template. It was reported that the liquid phase SiO_2/Al_2O_3 ratio is important in controlling the formation of Na-ZSM-5 and mordenite, and the silica source influences the liquid phase composition. High yield of Na-ZSM-5 was obtained only when small-sized sol was employed.

Schwieger and coworkers [79], have studied samples of pentasil zeolites synthesized with and without organic templates using ^1H and ^{27}Al NMR. By varying the SiO_2/Al_2O_3 ratio and the length of crystallization at

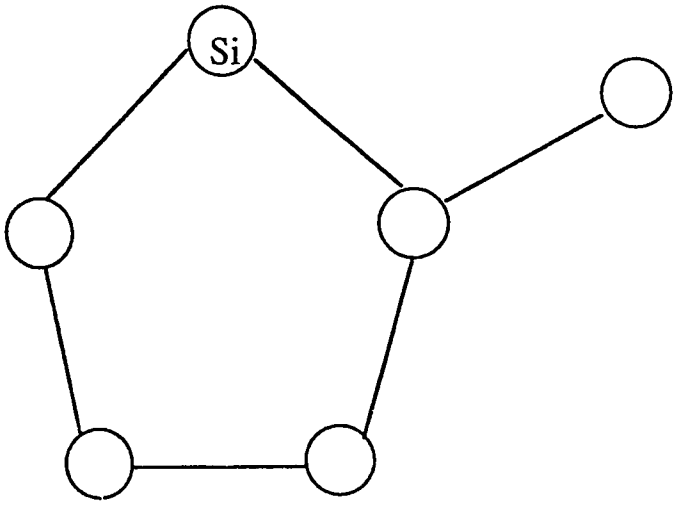

Figure 2.1 The secondary building unit of ZSM-5 zeolite.

175°C, H_2O/SiO_2 = 30, Na_2O/SiO_2 =0.1 they have arrived optimal reaction conditions for a template-free synthesis of zeolites of ZSM-5 type at SiO_2/Al_2O_3 ratio =30-50 and 36-48 h.

2.1.3. The Nature of Reactants

The variety of species used as sources of the alumina, silica and base has been listed in Table 2.3 [13]. It has been shown in many systems that the product obtained is often dependent on the sources selected as well as their treatment prior to formulation. When hydrated sodium silicate [80], especially sodium metasilicate pentahydrate, was the source of silica, zeolite NaX was formed at 100°C, much more readily than when "inactive" solid and colloidal silica were used. The "inactive" sources under the conditions of synthesis resulted primarily in gismondine type NaP. The "activity" of the soluble sodium silicates appeared to depend on the presence of very small amount of Al in them.

In alkaline sodium aluminate solutions the important anion is $Al(OH)_4^-$. At pH values below 7, ^{27}Al NMR indicates that $(Al(H_2O)_6)^{3+}$, $(Al(OH)_2(H_2O)_n)^+$ and $Al(OH)_3$. nH_2O are important species while above pH 10.5, $Al(OH)_4^-$ is exclusively present [55]. In alkaline silicate solutions, on the other hand, polymeric anions are common. The viscosity of waterglass indicates a high degree of polymerization, the extent of which can be expected to vary with concentrations of the sodium silicate and free alkali [81].

Table 2.3. Some sources of cations, aluminum and silicon in zeolite crystallization [13].

Charge compensating cation	Aluminum	Silicon
Alkali metal hydroxides	Metal aluminates	Silicates and silicate hydrates
Alkaline earth hydroxides and oxides	$Al(OH)_3$, A_2O_3,AlOOH	Water glass
Other oxides and hydroxides	Al alkoxide	Silica sols
Salts (fluorides, halides, carbonates, phosphates, sulphates, etc.)	Al salts	Silica gels
Organic bases and ammonium hydroxide especially quaternary bases	Glasses	Silica and other synthetic glasses
Silicates and aluminates	Sediments	Silicon esters
Mixtures of two or more of the above.	Minerals, especially clay minerals, feldspars, felspathoids, and other zeolites	Tuffs and volcanic glasses
		Minerals including clay minerals, feldspars, felspathoids and other zeolites
		Basalt and mineral mixtures
		Sediments
		Combination of two or more of the above

The synthesis of zeolite ZSM-5 is also very sensitive to the starting silicate reagents used. Mostowicz and Sand [82] examined the crystallization of ZSM-5 using four different sources of silica. Crystallization of ZSM-5 using either Ludox or silicate produced a very sharp crystallization due to rapid nucleation of the desired structure after 5 hours. Using precipitated silica (QUSO-F-20) resulted in a lengthening of the induction period before crystals were observed. Both Cab-O-Sil and QUSO produced slower growth of the ZSM-5 structure. Crystallization was complete after 15 hours using Cab-O-Sil and beyond 25 hours for QUSO. The silicate and Ludox produced crystalline material within 6 to 8 hours.

Kühl [83], in his study of the synthesis of faujasite materials, examined the effect of the starting reagent on the crystallization of the faujasite structure. He found that the crystallization of certain structures from starting gels used was dependent on the degree of polymerization of the silicate starting material. Very polymeric silicates were found to give ZK-15 or chabazite-like phases (low-silica ZSM-14) in the same free [OH] (pH) range where the less polymeric, metasilicate causes zeolite Y to crystallize. Kuhl proposed that possibly the depolymerization of the more polymeric silicate (waterglass) is slow, or any soluble silicate precursors formed are stabilized sufficiently to prevent further rapid depolymerization [83]. A trend from Y to ZK-14 to ZK-15 to zeolite B follows the degree of polymerization of the silicate starting material used.

2.2 Mechanism of Zeolite Crystallization

During the past two decades a number of papers have been appeared on the mechanism of zeolite crystallization. In most cases the synthesis of zeolite A and faujasite was studied[16,21,38,66,80,84-94]. Recently also highly siliceous zeolites, such as the ZSM-5 [21,66] and mordenite systems [91] have received much attention. Breck and Flanigen [95] and McNicol [92,93] have been presented evidences for crystallization by solid phase transformation in studying A and faujasite type zeolites. Zhadanov et al. [38,43], Sand et al. [84], Kacirek and Lechert [89] have, by contrast, demonstrated the role of liquid phase ion transformation in the growth of different zeolite nuclei and presented evidences in support of a solution transport mechanism.

Initially, Barrer et al. [85] and later many other investigators [66, 80, 84, 86-91] have proposed the nucleation to be the result of the polymerization of aluminate, silicate and possibly more complex ions in the liquid phase, the ions being continuously supplied by the dissolution of the solid gel material. Derouane et al. [21] have suggested that both the liquid phase ion transformation mechanism and solid hydrogel phase transformation mechanism are important in studying the synthesis of ZSM-5 zeolite depending on the silica source and the gel formulation used. In general, based on the evidence presented to date, it appears that the mechanism for crystallization of these systems is strongly directed by the components making up the reaction system and the conditions of synthesis.

2.2.1 Crystallization by Solid Phase Transformation Mechanism

Crystallization of the zeolite structure directly from the solid-gel phase has been suggested based on several pieces of evidence. On the basis of electron microscopic studies and chemical analysis of aluminosilicate gels, Flanigen and Breck [95,96], showed that the crystallization occurs from the solid-gel phase. The induction period was postulated to be a time during which the nuclei formed in the solid phase growing into a definite size. The elemental composition of the crystalline zeolite was almost identical to that of the initial solid phase extracted from the gel [38]. During crystallization neither the hydrogel phase is dissolved nor the formation and growth of the crystal nuclei is occurred in the liquid phase.

Flanigen [97] proposed the use of IR and Raman spectroscopy for examining the micro-structure of the pre-crystalline solid phase. These

spectroscopic techniques were not dependent on a threshold particle size, as found for X-ray diffraction techniques. Examination of the mid-infrared range (1200 to 300 cm^{-1}) of the solid-gel phase during crystallization of NaX zeolite does show several changes occurring in the spectrum. The range between 650 and 500 cm^{-1} is attributed to vibrations arising from movements of the substructural ring units. The band observed at 575 cm^{-1} was tentatively assigned to the presence of such substructural units as the double 6 ring. However, it is still not possible definitely to: (1) determine the contribution of the solution in the transport of the species, either as substructural units such as the secondary building units or as monomeric silicate and aluminate; or (2) differentiate nucleation directly on the solid phase or in the solution phase.

Recently, Kyu-Heon and Son-Ki Ihm [98] studied the crystallization mechanism for atmospheric synthesis of high-silica ZSM-5. They observed that the nucleation starts in the solid phase originated from thin, plate-like lamellae during the induction period, which was evidenced from ^{29}Si NMR and SEM. After nucleation, both amorphous and crystalline phases appear simultaneously. It was believed that the Al-rich amorphous phase was dissolved and recrystallized on the Si-rich crystal surface later.

2.2.2 Crystallization by a Solution Transport Mechanism

Kerr [86,87] reported on crystallization of zeolites A and X in specific systems in which he postulated growth from solution. A direct solid-solid transformation of amorphous substrate to crystalline product

does not occur. Amorphous solid dissolves in the alkaline solution to form a soluble active species. The concentration this species remains constant most of the growth period.

Angell et al. [90] have determined the mechanistic pathway in 4A zeolite synthesis, by using several different characterization techniques as a function of time. The evidence also support a solution transport mechanism. The results of the Raman spectroscopy, particularly during the crystallization stage can be contrasted with a report of McNicol [93], who observed no changes with time other than the appearance of zeolite A. In the early stages, i.e., during induction, the alumina concentration decreased after 3 hours when crystallization of zeolite A has set in . From the results of Raman spectroscopy and chemical analysis by Roozeboom et al. [99], aluminate disappeared from solution and is incorporated in the solid phase. As to the silicate concentration of the liquid phase, this concentration decreased less drastically to comparable low levels. Whereas, in case of both zeolite X and zeolite Y, before any crystallites were detected, aluminate was disappearing from solution and incorporated in the amorphous aluminosilicate phase. In the same period an increase in silicate concentration in the liquid and a decrease in silicon concentration of the solid phase have been found. From the results it is clear that in the first 2-3 hours of the crystallization or nucleation some silicon containing ions (monomeric or polymeric) were dissolved from the amorphous (alumino) silicate gel. These hydroxylated ions apparently condensed with $Al(OH)_4^-$ ions present to form a large variety of aggregates, which may

be the nuclei for crystal growth. Thus the whole mechanism of zeolite A, X and Y formation is a solution transport mechanism.

2.2.3 Crystallization by Two Mechanisms in the Same System

The zeolite crystallization may occur following two different mechanisms, in which nucleation occurs in the hydrogel phase or in the liquid phase. Derouane et al. [21], were able to synthesize ZSM-5 by either the solution method (method A) or the gel nucleation method (method B), depending mainly on the relative concentrations of the reactants and the nature of the silica source, to study the mechanism of zeolite crystallization. Summarizing the results obtained by measurements of XRD, TGA, SEM and chemical analysis, synthesis of type A and B for ZSM-5 zeolite were two disinct ways from a solution or gel nucleation mechanism, respectively. It seems that a high basicity and/or the presence of foreign ions in the nutrient and also the polymeric nature of the silica source and the Si/Al ratio of the gel direct the reaction to solution nucleation, and that TPA content and the degree of dilution are less important as determining parameters for the nucleation mechanism.

Therefore, two different mechanisms occur in the synthesis of ZSM-5 zeolites, depending on the source of silica and the Si/Al, Al/Na and (Si+Al)/TPA ratios in the reaction mixture. The first is a liquid phase ion transportatin process (solution transport mechanism) in which few nuclei are formed and large crystallites are obtained. The second is a solid hydrgel phase transformation process (solid phase transformation

mechanism) in which numerous nuclie are formrd, leading to polycrystalline aggreates.

Bodart et al. [100] have showed, in a comparative study of the crystallization mechanisms of zeolites Y, mordenite and ZSM-5, that mordenite and ZSM-5 (synthesis of type A) are crystallized through liquid phase ion transport mechanism. Where as, the mechanism of crystallization for ZSM-5 (synthesis of type B) was explained by direct hydrogel transformation (or surface nucleation). In the case of zeolite Y a combination of these two mechanisms was reported.

2.3 Kinetics of Zeolite Crystallization

The yield of zeolite crystals in a hydrothermal synthesis is typically an S-shaped function of time. The crystals may be considered to grow from nuclei, although the precise nature of a nucleus is unknown. Typical nucleation and growth curves are illustrated schematically in Figure 2.2. There may be a period after preparation of a hydrothermal system in which no nucleation appears to take place. This is followed by a nucleation period in which the rate of nucleation first increases with time, then, as significant growth of crystalline material occurs, passes through a maximum and decreases. Crystal growth continues until, ultimately, the amount of crystalline material reaches a maximum as the source is depleted.

There have been a number of attempts to model or predict zeolite growth curves, as reviewed by Thompson and Dyer [101]. Many

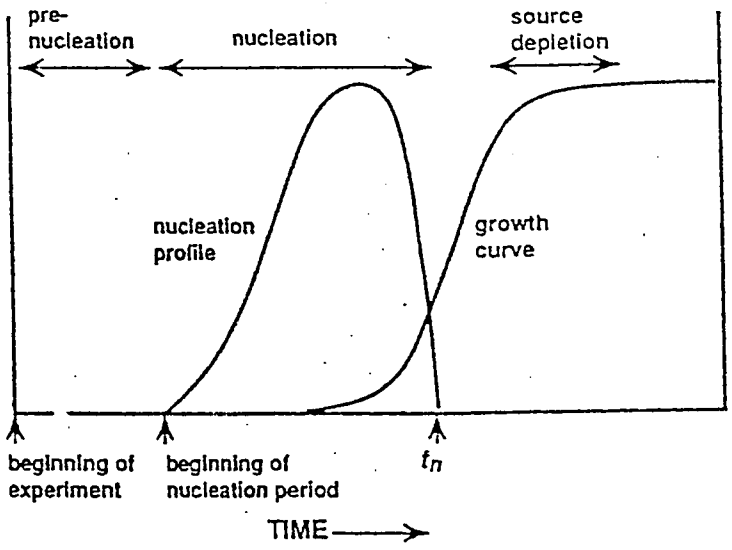

Figure 2.2 Schematic illustration of nucleation and growth curves for a hydrothermal zeolite synthesis [110].

mathematical expressions have been suggested to describe nucleation rates such as, constant rate, power law, exponential decay, exponential increase, etc [13]. However, a comprehensive treatment that fully explains the experimental observations on zeolite nucleation and growth has yet to emerge.

Kinetic studies of zeolite growth have been carried out mostly for A and X type zeolites. The growing of A and X-type zeolites has to be regarded as an autocatalytic process and the formation of zeolites was accelerated by nuclei already present [86,87,95,102,103]. From the experiments using nuclei the growth can be regarded as a reaction of first order, whereas the nucleation is a reaction of high order. A typical kinetic experiment for the formation of zeolite A gave the rate of formation of crystalline product to the first-order kinetics with respect to the quantity of crystalline zeolite present [86]:

$$dz/dt = kz \qquad (2.1)$$

where z = zeolite % in solid phase at time t and k is proportionality constant. The rate of any crystallization process is determined by the rate of nuclei formation and crystal growth. Equation 2.1 indicates the increase in either the linear rate of crystal growth or the rate of nuclei formation during the period of crystallization. The formation of nuclei takes place during the entire process of crystallization, but the rate of nucleation increases only in the initial stage. The process can be described by the common equation in the form $z = kt^n$. The values of the constants k and n are easily calculated from the plot of log z versus log t. The results of crystallization of A, X and mordenite are given in Figure 2.3. The calculated points agree quite well with the experimental curve [38].

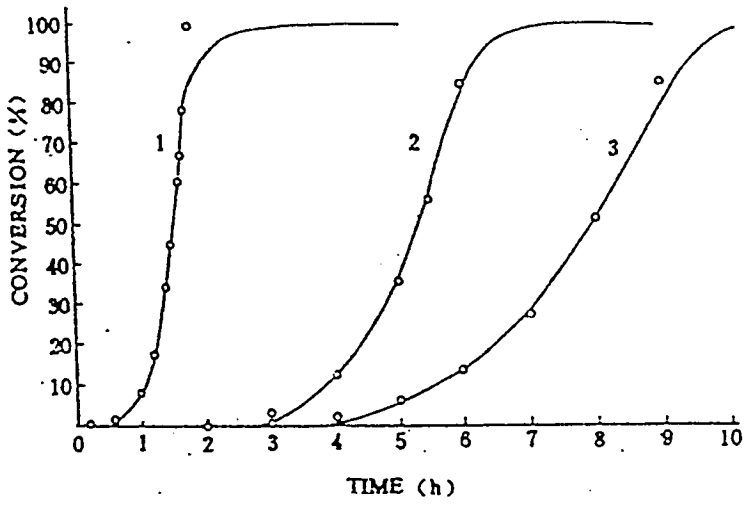

Figure 2.3 Crystallization of zeolites as a function of time [38].
1. Zeolite A, 373 K
2. Zeolite X, 373 K
3. Mordenite, 573 K
—— Experimental curves o Points calculated from $Z = kt^n$

Several kinetic models of crystallization in non-spontaneous and spontaneous nucleation systems are presented in the literature. Spontaneous nucleation system is the system without adding any seed crystals during synthesis of zeolites or gel. The curves showing yield of crystals against time are characteristically sigmoid in shape. This behavior has been observed for zeolite A [102], X and Y [89,104,105], sodalite hydrate [49], mordenite [106] and ZSM-5 [66] . As a law of crystal growth for such system Meise and Schwochow [107] have formulated the expression:

$$r = \beta t \qquad (2.2)$$

and assumed that the crystals are spherical configuration whose radius r increases in proportion to reaction time t and β is a proportionality constant. An estimate of the percent increase in the number of particles N in the reaction time t suggests an exponential function of the form

$$\frac{dN}{dt} = A(e^{Et} - 1) \qquad (2.3)$$

as a law of nucleation, where A and E are coefficients. The curves of crystal growth against time have also been represented by the model-based reaction [108]:

$$\frac{Z_t}{Zf} = 1 - \exp(-kt^n) \qquad (2.4)$$

The ratio Z_t/Z_f is of mass Z_t of crystal at time t to the mass Z_f in the final product and k is a constant. At the reaction time t the normalized contribution to the final yield Z_f arising only from nuclei formed at time (less than t) in the interval $d\tau$ is

$$d(Z_t/Z_f) = 4/3\ \pi\beta^3(t-\tau)\ A(e^{Et} - 1)d\tau \qquad (2.5)$$

Reaction was assumed to be complete after a time t_e when $Z_t/Z_f = 1$. Integration of equation (2.5) over all values of t between 0 and t gave:

$$Z_t/Z_f = \frac{4}{3}\pi\frac{AB^3}{E}\left[\frac{6}{E^3}\{\exp(Et)-1\}-\frac{6}{E^2}t-\frac{3}{E}t^2-t^3-\frac{1}{4}t^4\right] \qquad (2.6)$$

Where A, B, and E are constants. The experimental and calculated curves for the course of the reaction and particle size distribution are illustrated in Figure 2.4 [107]. It was concluded that as time increased, both nucleation and crystal growth were accelerated.

The crystal size growth of NaX zeolite during crystallization of reaction mixture and the histogram of crystal size distribution in the final product are given in Figure 2.5 [43]. Curve 1 of Figure 2.5 and 2.6 gives the linear growth rates of largest crystals. Each point on the curve was obtained by microscope measurements of diameters of 10-20 largest crystals observed in identical samples. The period of constant linear growth rate for crystals of different size extended for about 115 h and thereafter declined asymptotically towards zero. Curve 2 in Figure 2.5 describes the average size distribution of crystals. From the time for nucleation of crystals of each mode, the size distribution curve of Figure 2.5 gives the nucleation rate curve 2 of Figure 2.6. This rate passes through a maximum. When comparing the crystallization curve 3 in Figure 2.6, which was derived from curve 1 and 2 of Figure 2.5 with curve 1, the rate of linear crystal growth remains constant all over the

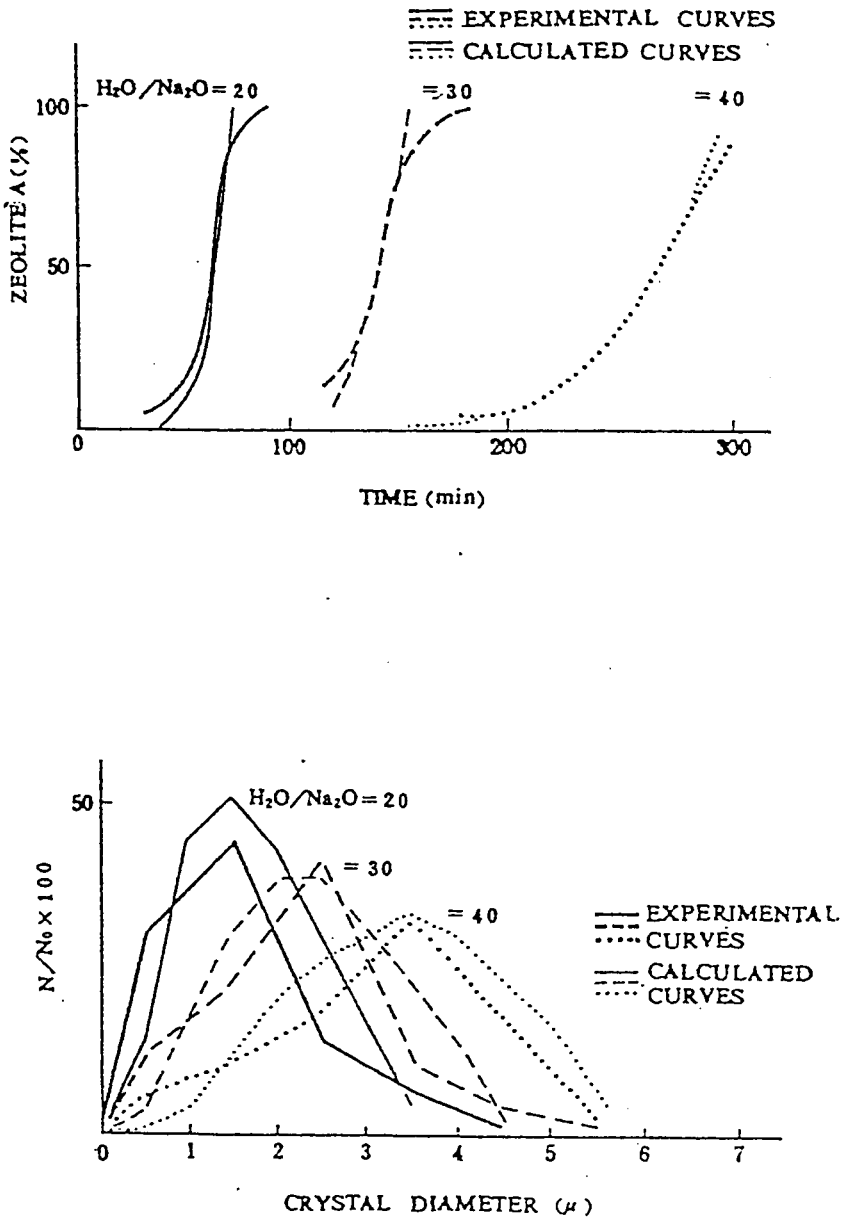

Figure 2.4 Influence of alkalinity on zeolite A crystallization (top) and on crystal size distribution (bottom), showing agreement between experimental and calculated values [107].

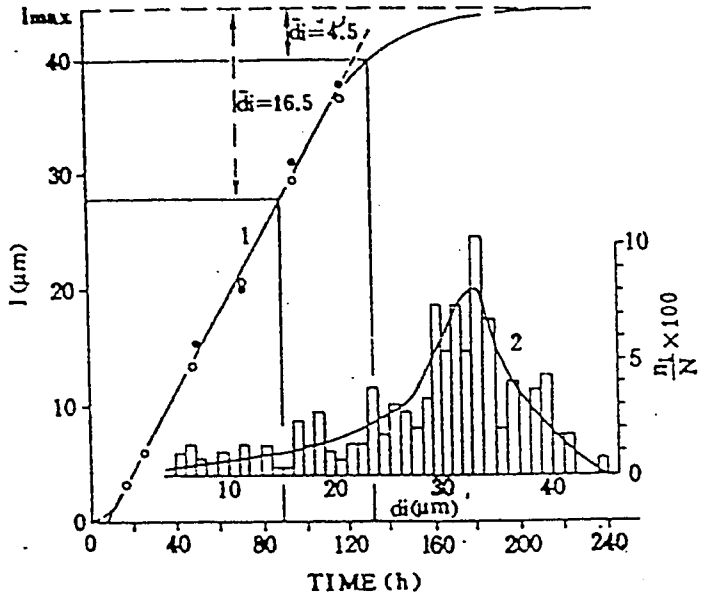

Figure 2.5 Crystal size growth of Na-X zeolite during crystallization of the gel (1) and the histogram of crystal size distribution in the final product (2) [43].

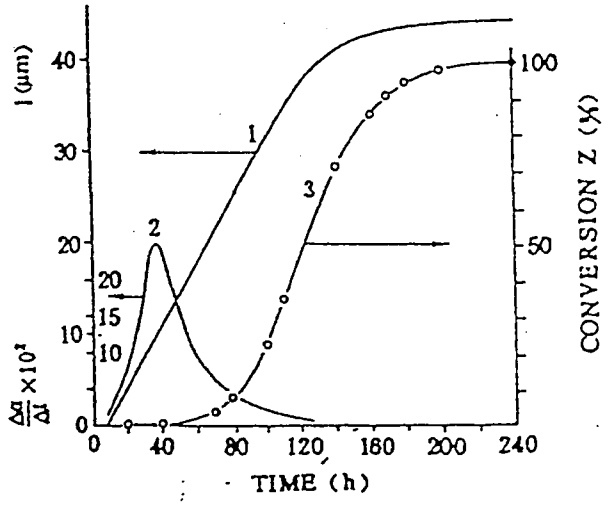

Figure 2.6 Nucleation kinetic curve (2) and the crystal mass growth curve (3) for Na-X zeolite calculated form data of Fig. 2.4 [43].

autocatlytic stage of the crystallization process. The stage of delayed crystal mass growth begins when the linear rate has begun to decrease. It implies that linear growth rates are independent of crystal size.

The crystallization kinetics of Silicalite-1 was studied by Culfaz et al. [109], using TPA-Br and TPA-Cl as template in the range of 100 to 175 °C in the batch system. The activation energies and of nucleation and crystallization were determined as 37.2 and 66.5 kj/mol, respectively. A longer induction period for crystallization and larger crystals were obtained in the case of TPA-Cl. The crystallization was complete within 5 h at 175 °C whereas it took over 5 days at 100 °C for completion of crystal growth.

Recently an emprical model for the nucleation and growth of zeolites was developed by Budd et al. [110]. The rate of nucleation of zeolite crystals, which typically passes trough a maximum, was described by the following function:

$$n(x) = S\left[x^m - \left(x^m / t_n^{(m'-m)}\right)\right] \qquad (2.7)$$

where n(x) is the rate of nucleation at a time x and t_n denotes the end of the primary nucleation period m and m´ are constants and S, a scaling factor. Crystalline growth curves calculated gave linear growth rate for individual crystals. The model was applied to the results for the hydrothermal synthesis of NaA zeolite. The calculated results agreed with the experimental valves.

2.4 Modification by Metals Incorporation

The replacement of T-atoms (tetrahedral) in a crystalline lattice of zeolite is referred as isomorphous substitution. Commonly encountered T-atoms are silicon and aluminum. In the early literature, reviewed by Breck [111], as potential candidates are described for substitution in tetrahedral sites: Ga^{3+}, P^{5+}, Ge^{4+} and Fe^{3+}. The existance of Zr-, Ti- and Cr-silicates "zeolites" has been claimed as well. All this work refers to substitution in so-called first generation zeolites with low silicon content.

The isomorphous substitution in high-silica medium pore zeolites (so called second generation materials) is also extensively reported in the literature. In the patent literature a whole variety of metallosilicates with medium pore size and high-silica content has been claimed. A non exhaustive enumeration of such materials is given in Table 2.4 [112].

Another approach to substitution of metal atoms into zeolite structures has been to replace the typical silica alumina gel with gels containing other metal atoms. This concept has resulted in numerous unique molecular sieve compositions containing: aluminum and phosphorus [25,129]; silicon, aluminum and phosphorus [130,131]; and with other metal atoms present in the framework with the alumiun and phosphorus as well [132,133].

The incorporation of element in a given structure may well modify the catalytic properties of the zeolite. The T-element introduced either by

Table 2.4 Survey of different metallosilicates claimed in patent literature.

Nature of Silicate	Si/M	Si/Al	Remarks	Ref.
AMS-1B borosilicate	52.3	1410	Specific XRD	113
ZBH borosilicate zeolite	48.8	-	Pentasil-type	114
Boroaluminosilicate	4.5	1667	Offretite-type	115
Borolite	120.0	-	Various structures	116
Gallosilicate	68.3	-	Theta-1	117
Chromosilicate zeolite	86.8	275.1	MFI	118
TRS-27 beryliumsilicate	12.0	-	-	119
TRS-66 : zincsilicate	15	-	-	119
TRS-64 titaniumsilicate	3	-	-	119
TRS-48 vanadiumsilicate	17	-	-	119
Titanoaluminosilicate	21.3	87.0	MFI	120
Zirconoaluminosilicate	28.6	76.9	MFI	121
AMS-1 Cr chromosilicate	32.6	1515.2	AMS	122
Zincosilicate	0.8	-	Zeolite A	123
Zincaluminnumsilicate	13.4	94.5	-	124
Arsenesilicate	207.3	375.2	Zeolite structure	125
Organosilicate containing tin	7.6	1787.0	Zeolite	126
Iron-silicate	200	0.0	Zeolitic	127
Iron-alumino-silicates	23.0	163.1	MFI	128

direct synthesis or by post-synthetic (chemical) modification, may occupy one of the following positions:

- actual incorporation into framework sites (tetrahedral)
- formation or deposition of cluster oxide in the porous network or at the external surface of the zeolite microcrystals
- siting at exchange position
- occupation of defect sites derived from tetrahedral coordination (internal-grafting)
- grafting at the external surface.

In addition, the presence of the modifier may alter the crystallinity of the zeolite or possibly reduce the free-volume and even considerably reduce the access to the porous network. This will result in the exclusion of molecules which would normally enter the porous network [134].

Poncelet et al. [135,136], reported the earliest synthesis of zeolite comprising framework elements other than silicon and alumiun. Although, the first synthesis was germanium substituted faujasite, iron was also recognized to be hosted partly in exchange and partly in framework position in many zeolites. The incorporation of iron in framework sites was achieved mostly in the case of MFI structure [137-140].

Inui et al. [141,142], studied the acidic properties of ZSM-5 by substitution of Al with various transition elements. The elements were incorporated at the preparation stage of gel formation by the rapid crystallization method. The prepared crystalline catalysts were offered to

the conversion of methanol, light olefins, light parafins, paraffinic heavy oil and methane. For Ga [141] and Fe [143], it was claimed that these metals were incorporated into the structure of zeolite. Performance for methanol conversion of various metallosilcates having a Si/metal ratio of 3200 was measured. H-Ga-silicate exhibited a better performance for gasoline synthesis from methanol than H-Al-silicate, that is, H-ZSM-5. On the other hand, the iron-group metal substituted silicates such as H-Ni-, H-Fe-, and H-Co-silicates yielded light olefins with higher selectivity than H-ZSM-5.

The hydrothermal synthesis of the titanium-containing derivative of high-silica ZSM-5 (TS-1) was first reported by Tarmasso et al. [144]. Subsequent studies on TS-1 have shown that it is an active catalyst in oxidative processes with hydrogen peroxide [144-148]. Due to the outstanding catalytic activity of this material, TS-1 is being used commercially in Italy for the production of catechol and hydroquinone [147]. Additionally, the TS-1 catalyzed conversion of cyclohexanone into cyclohexanone oxime is operating at pilot-plant scale [149].

Very recently, Khouw and Davis [150] synthesized titanium containing aluminium-free ZSM-5 (TS-1) in the presence and absence of alkali metal and alkaline earth ions. The catalysts were investigated for the selective oxidation of alkanes and alkenes using aqueous H_2O_2 as oxidant at temperatures below 100 °C. Sodium-exchanged TS-1 was not active for alkane oxidation. Similarly, no catalytic activity was observed for TS-1 synthesized in the presence high concentrations of alkali metal ions (Si/Na

<20). For both cases, the catalytic activity was restored by washing the solid with 1M H_2SO_4 prior to catalytic evaluation.

Double substitutions in silicalite by direct synthesis were also reported in the literature. Several patents claimed the synthesis of zeolites containing both Ti and a trivalent element [120,152-155]. However, only in few of them proofs about the presence of both elements in lattice position are given [153-155]. Bellussi et al. [156], synthesized silicalites containing both Ti and a trivalent element (Al, Ga, Fe) in lattice position. Titanium content decreased with increasing content of the trivalent metal. Isomophous substitution of both elements were confirmed by physico-chemical analyses, oxidizing and acidic catalytic activities.

2.5 Hydrothermal Modification of Zeolites

Steam or hydrothermal treatment is used to modify activity as well as product selectivity in various reactions [157,158].The Bronsted acidity of zeolites is a function of the equilibrium established between the SiOH silanol group and its associated aluminum site. The proton is renderd acidic through the interaction between the unshared pair of electrons on the oxygen atom and the unoccupied orbital of the aluminum atom [159], which weakens the bond between the oxygen atom and the proton coordinated to it so that the proton has donor (Bröensted) acidity.

A role for aluminum, dislodged from the framework, in the generation of stronger acid sites was first proposed for faujasitic zeolites [160]. An additional peak, at 570 K, in the TPDA spectrum was assigned to Lewis-Bronsted interactions shown in Sheme 1, and the modified zeolites showed increased catalytic activity.

Sheme 1 Proposed Superacid Sites [160] (Arrows show electron withdrawl).

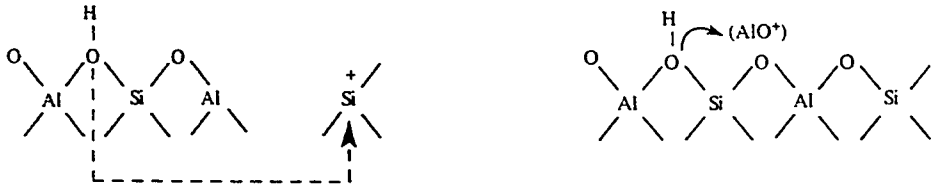

(i) (ii)

Enhanced catalytic activity following mild steaming of H-ZSM-5 was reported without explanation [160] and a subsequent study [161] related results, for n-hexane cracking, to the presence of non-framework aluminum pointing out that it might involve either synergism between framework Broensted sites and dislodged aluminum or the generation of a new type of active site. This work also pointed to an optimum ratio of non-framework to framework aluminum and demonstrated that the optima; steamed zeolites contained sites which retained ammonia to higher temperatures than did the parent zeolite. The sites of enhanced activity were shown to be more rapidly deactivated, during coke formation, than the sites of normal activity.

An explanation for enhanced activity, following steaming, assumes that Al in ZSM-5 is randomly distributed only within the four rings which

leads to increased pairing (AlOSiOAl) with increase in Al content up to eight Al per unit cell when pairing is complete. Mild steaming could dislodge or partly dislodge one of the paired aluminiums which remains in proximity to its Al neighbor in the four ring giving rise, by synergistic interaction, to a site of enhanced activity. This explanation was first shown to be incorrect [163] on the basis of existing ^{29}Si NMR results and this view has recently been confirmed by a more detailed NMR investigation [164].

The recent NMR study conducted by Brunner et al. [164] suggests that there is no enhancement of Broensted acidity, in steamed H-ZSM-5, since there is no significant shift in the ^{1}H NMR band nor in the infrared hydroxyl stretch. Instead the enhanced activity is attributed to the presence of dislodged aluminum generated under conditions of mild steaming, which is not readily extracted by 0.5 M HCl nor by reaction with formic acid. The catalytically effective non-framework aluminum is said to exist as uncharged unstable complexes which are mostly non-hydroxylated and are immobilized. Optimal enhancement in cracking of n-hexane is reported for a ratio of total non-framework aluminum to framework aluminum of around 1.3 which is not grossly different from the earlier value reported by Ashton et al. [162] (the earlier value is probably low since current procedures for detection of all the non-framework aluminum represent an improvement over the earlier methods). Only insignificant amounts of cationic aluminum are reported and no evidence is found for aluminum partially dislodged from the framework.

On the other hand infrared studies on steamed Y zeolites show clear evidence for ionic aluminum species [165] and new hydroxyl bands are detected which are poisoned by traces of sodium ions and are assigned to a small number of very strong Broensted sites produced by interaction of framework hydroxyls and non-framework ionic aluminum [166]. In other work strongly 'superacidic' non-framework hydroxyl groups are tentatively assigned to an amorphous silica-alumina phase generated by steam treatment. Moreover, the interaction between CO and Broensted sites in H-ZSM-5 is increased when the parent zeolite is impregnated with $Al(NO_3)_3$ and calcined to give H-ZSM-5/Al_2O_3.

Whatever the mode of operation there is considerable evidence that mild hydrothermal treatment, can result in enhanced catalytic activity in several types of zeolite. Infrared studies of the hydroxyl region have been interpreted in terms of stronger Broensted sites [166] and uv-vis results for the protonation of aromatics by dealuminated mordenite are also consistent with this view [167]. However, some NMR investigations [164] and associated catalytic cracking of hexane are interpreted in terms of a new site, produced in H-ZSM-5 by mild steaming, which enhances activity by providing a dehydrogenation function. Olefins produced by the initial dehydrogenation are then captured and rapidly converted on Broensted sites. The new site is considered to be a non-framework aluminum species and no evidence is found for enhanced Broensted acidity (see previous). This view, expressed previously for solid acid catalysis, is supported by the effect of added olefins which results in an increase in the cracking rate constant for the parent H-ZSM-5 at lower concentration of olefin

(0.1-10%) but in a decrease in rate for the steamed zeolite. This reduction in rate is presumed to arise from poisoning of the strong Lewis sites by olefins which may be dehydrogenated to diolefins [168]. Of course, dehydrogenation is possible on strong Broensted sites (C-H protonation) or on radical centers so that it is difficult to be certain about initial activation, as discussed earlier.

Support for a synergistic interaction between framework Broensted sites and non-framework species comes from the enhanced catalytic activity which is observed when lanthanum ions are exchanged into zeolite H-Y [166]. Lanthanum is reported to form multivalent complex ions such as $[La(OH)_2La]^{4+}$, $[LaO_2La]^{2+}$ or $La(OH)^{2+}$ in the b-cages of zeolite Y. These species can function as electron withdrawal sites for bridged oxygens which support protic hydrogens in the larger cages. The result is sites of enhanced Broensted acidity. By analogy a similar function can be performed by non-framework aluminum species such as $[Al(OH)_2Al]^{4+}$ which are previously reported to be present in β-cages.

A recent study of steamed H-ZSM-5 by Luk'Yanov [169] finds that the sites associated with enhanced activity mainly affect the rate of bimolecular hydrogen transfer and suggests that the initial rate of alkane activation (per site) is unchanged which would seem to disagree with the proposed role for strong Lewis sites discussed above [164]. These recent results [166] demonstrate that the sites having enhanced activity are more rapidly deactivated by coking than sites having normal activity which is in agreement with previous catalytic studies [162] but disagrees with NMR

results [164]. Further work is needed to clarify the mechanistic role of sites with enhanced activity. If enhanced bimolecular hydrogen transfer is their main contribution to enhanced rates then the role of sorption sites associated with dislodged aluminums which are close to Broensted sites should be considered since the hydrogen transfer depends upon sorption and site proximity as well as upon the acid strength of the site.

Summarizing, there is no doubt that enhanced catalytic activity in hydrocarbon transformation over acid zeolites can be generated by hydrothermal processes which dislodge framework aluminum. There is some evidence that sites of enhanced acidity are also produced in these catalysts. Consequently, it is reasonable to connect these results and postulate that the enhanced acidity arises from synergistic interaction between dislodged aluminum species, either neutral or ionic and framework Broensted sites. This is the view currently accepted by most workers. However, the role of sorption at the reactive site and the possibility that strong Lewis sites may function independently requires further study. A difficulty concerns the wide variety of pre-treatments used to generate the hydrothermally treated catalysts which may mean that comparisons do not, in all cases, refer to similar materials.

2.6 Synthesis of Methyl tert-Butyl Ether

Methyl *tert*-butyl ether (MTBE) has gained wide acceptance in recent years as a clean, non-polluting gasoline additive and a good octane

enhancer. This is due to its favorable physical properties for mixing with gasoline, excellent anti knocking behavior, and reduction in the emission of toxic compounds from vehicle exhausts [171]. The worldwide production of MTBE is currently increasing faster than that of most other commodity chemicals [172]. Some estimates are that by 1995 demand for MTBE could increase at a rate of 25% / year [173]. Emission standards imposed by the 1990 US Clean Air Act Amendments (CAAA) are expected to require oxygenates in nearly 70% of the US gasoline pool by year 2000 [174]. As a result of the CAAA, much interest has been focused on the use of oxygenates and especially tertiary alkyl ethers as gasoline components [171, 175].

MTBE is produced by reacting methanol with isobutene in the presence of an acidic catalyst such as acidic ion-exchange resins via:

$$CH_3OH + (CH_3)_2C{=}CH_2 \rightleftharpoons (CH_3)_3COCH_3$$
$$\Delta_R H^{\circ}_{298} = -37.7 \text{ kJ/mol}$$

The reaction is rapid, selective, moderately exothermic and is equilibrium-limited. Reaction temperature is 90 °C or below to increase equilibrium conversion and prolong catalyst life. Pressure is substantially above atmospheric, to keep the reaction system liquid [176].

The main side reactions are the dimerization and oligomerization of isobutene [177,178]. Other possible side reactions, with less significance, are the formation of tert-butyl alcohol, the formation of traces of

dimethyl ether [179] and the double-bond isomerization of 1-butene. The latter is only 1% of the dimmer formation [177,180].

The primary function of the catalyst seems to be to donate a hydrogen ion to isobutene to form a tertiary carbonium ion [181]. Methanol acts as a nucleophile and attacks the carbonium ion to form the ether. Isobutene is also an acceptable nucleophile, although not as good as methanol, and can react with carbonium ion to form the dimer. Therefore, methanol is used in excess to avoid the isobutene dimer formation. Water, if present, is better nucleophile than methanol and will form tert-butyl alcohol (TBA). These reaction are given in Figure 2.7.

Batch rate studies indicate that the reaction is first order with respect to isobutene and independent of catalyst and methanol concentrations [177]. This coincides with the proposed mechanism and implies the rate determining step is the protonation of isobutene to form carbonium ion. The attack of the nucleophile, methanol, is much faster. If isobutene is in stoichiometric excess, the rate is independent on methanol, but the MTBE reaction is not normally run under these conditions.

It has been shown that the reaction is not mass transfer limited in the liquid phase [182]. This is convenient because it allows the use of the rate law as determined from a batch reactor to be easily used to design a continuous process. The fact that the liquid to solid catalyst ratio is much larger in a batch reactor is not important because the reaction is not limited by the liquid phase.

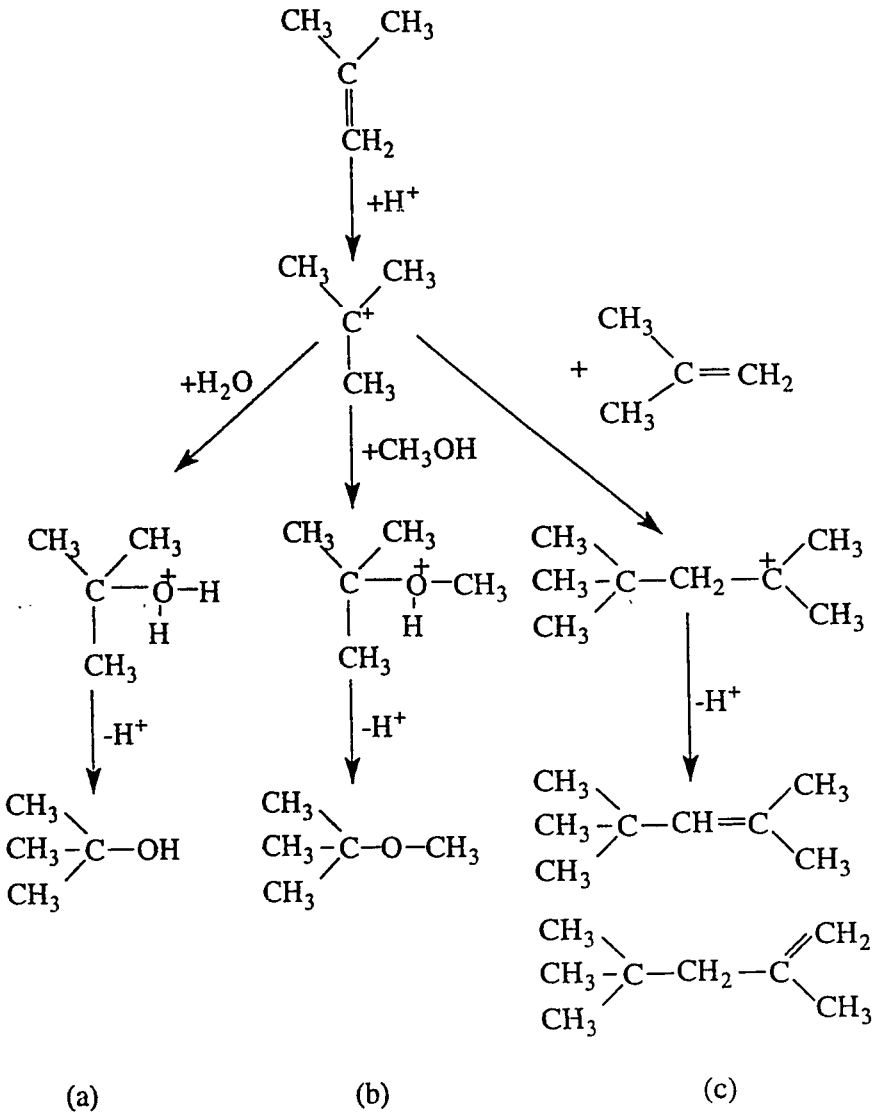

Figure 2.7 Mechanism for the production of (a) *tert*-butanol, (b) MTBE, (c) diolefins [226].

A widely used and thoroughly studied catalyst for MTBE production is Amberlyst 15 (Rohm and Hass Co., USA). It is a strongly acidic cation-exchange macroreticular resin composed of sulphonated copolymer of styrene and 20% divinylbenzene. The resin has surface area of 43 ±1 m^2/g and a mean pore diameter of 240 °A. The ion-exchange capacity determined by titration is 4.8 mequi. of HSO_3/g of dry resin [183].

In 1977, researchers at Snamprogetti published the first research report on the use of Amberlyst 15 (A-15) for the production of ethers [184]. The experiments were conducted at 60 °C in an autoclave, the ion-exchange resin was found to display a higher activity than the soluble anhydrous p-toluene sulphonic acid for MTBE synthesis. Liquid phase mass-transfer resistance was negligible and no induction period was observed. The reactivity of primary alcohols with isobutene was observed to follow the order as:

n-butanol > n-propanol > ethanol > methanol.

The results also showed a zero order dependence of rate on methanol concentrations and a first order dependence on isobutene concentration.

Gicquel and Torck [186] examined the influence of methanol concentration on the activity of the Amberlyst 15 resin for the formation of MTBE, together with the effect of the polarity of the medium on the reaction thermodynamics. The synthesis and decomposition of MTBE were carried out in the temperature range of 50 - 95 °C using a stainless steel double-jacked batch reactor. It was concluded that the resin catalysts

are sensitive to the concentration of methanol, with the reaction rates increasing sharply when the concentration is lowered. Furthermore, at a given temperature, the variation in the apparent equilibrium constant is mainly due to the variation of the methanol activity coefficient as a function of its molar fraction.

The catalytic evaluation of Amberlyst 15 for MTBE synthesis under non-isothermal conditions believed to be compatible with those in industry has been reported [185] . The study was carried out in a bench-scale, plug-flow reactor system. Variables considered were temperature, flow rate and feed composition. An integrated rate expression was used to estimate kinetic constants at 26, 51 and 67 °C using data obtained from the plug-flow reactor. Conditions which maximize selectivity and productivity, together with other catalyst characteristics, were also determined.

Ancillotti et al. [187] have described the modified Snamprogetti process for the synthesis of MTBE from butadiene-rich stream cracking C4 cuts. The presence of butadiene in the feed streams are undesirable. The peroxidation, polymerization, and the reaction with methanol to produce butenyl ethers are the problems associated with butadiene. The reaction rates for the addition of methanol to the three olefinic substrates in units of l/(acid equiv.)(sec) at 80 C were as follows:

isobutene	1×10^{-2}
butadiene	2×10^{-6}
cis-2-butene	2×10^{-7}.

The data shows that the reaction rate for butadiene is greater than the n-butene but less than isobutene. This order of rates is reflected in the relative carbocation stability, as follows:

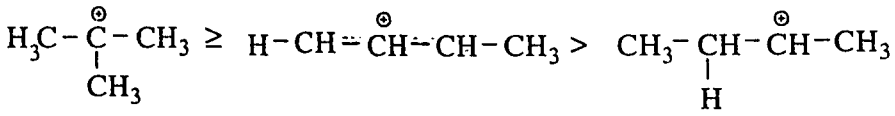

This is in accordance with the two-step reaction mechanism where the olefin protonation is regarded as the first and rate controlling step.

The butenyl ethers identified in the reaction product were essentially 3-methoxy, 1-butene and 1-methoxy, 2-butene obtained from 1-2 and 1-4 methanol addition respectively. The reactivity difference between isobutene and butadiene is large enough to allow isobutene to react selectively, but only in a narrow area of operating conditions. The use of contact times exceeding the minimum value required to reach the equilibrium in MTBE synthesis led to an increased butenyl ether formation and to MTBE decomposition due to the competitive reaction of methanol with butadiene. A detailed analysis of the product shows the presence of very low amounts of impurities, such as the above-mentioned butenyl ethers, along with minor amounts of TBA, methanol, 2-methoxy butane and dimer [188].

Rehfinger and Hoffmann [189] determined the microkinetics for the liquid-phase synthesis of MTBE using Amberlyst 15. The results were compared with a specially prepared resin, CVT, which had a lower degree of cross-linking, that is, 7.5 % divinyl benzene. The experiments were

conducted in a continuously stirred-tank reactor in the temperature range of 50 to 90 °C. The developed microkinetic model was found to be independent of the degree of cross-linking of the resin in the investigated range of 7.5 to 20 % DVB by weight. The nature of the C4 solvent, n-olefin or n-alkane, does not influence the intrinsic rate of MTBE synthesis. Also, no pressure dependence was observed up to 21 atmosphere. The influence of the macropore diffusion of methanol on the activity and selectivity of the resin catalyst was also examined. The results were in agreement with a shell-core model, according to which almost none of the methanol-containing core produces the by-product diisobutene. However, only the outer shell forms the main product MTBE.

The vapor phase addition of methanol to isobutene over Amberlyst 15 catalyst was studied by Tejero et al. [190]. The equilibrium constant for the reaction was determined experimentally in a continuous-flow reactor at atmospheric pressure and in the temperature range of 40 to 110 °C. When a mixture in equilibrium was fed into the reactor, the temperature of the catalyst bed did not change. Given that the MTBE synthesis reaction is fairly exothermic, this was considered a rough indication that the composition of the mixture did correspond to the equilibrium composition at the particular temperature. This method was found to be suitable and the equilibrium constants obtained were found to agree satisfactorily with the predicted values calculated from literature data. The results are given Table 2.5.

Table 2.5 Standard free-energy, enthalpy, and entropy changes of the reaction for obtaining MTBE at 298 K in vapour phase [190].

	ΔG° (cal/mol)	ΔH° (cal/mol)	ΔS° (cal/mol-K)
Determined by assuming that ΔH° is constant	-3160 ± 150	-15570 ± 175	-41.61 ± 0.50
Determined by assuming that ΔH° varies with temp.	-3170 ± 150	-15670 ± 175	-41.55 ± 0.50
Estimated from literature data	-3080	-15630	-42.09

Rate data were also obtained in the range of 41 to 61.5 °C [183]. The rate determining step was the reaction between the methanol adsorbed molecularly on one center and the isobutene adsorbed on two centers. The authors also concluded that the proposed mechanism is thermodynamically consistent.

Sundmacher and Hoffman [191] developed a mathematical model to analyze the interaction of the internal mass and heat transport with the macrokinetics of MTBE synthesis. A macroporous acidic ion-exchange resin was applied as catalyst for the liquid phase synthesis of fuel ethers. The multicomponent mass transfer in the macropore was formulated in terms of chemical potential gradients, due to the extreme nonideality of the mixture. The simulated effectiveness factor and the selectivity were in good agreement with experimental results for MTBE formation in a continuos stirred tank reactor.

A catalytic distillation process for the production of MTBE was developed by Dixon et al. [192] . This process refers to an operation

which performs a catalyzed reaction coincident with primary fractionation of the reaction components. It is carried out in a fractionation tower containing catalyst system that allows both catalytic reaction and distillation to occur simultaneously. In this process, the current commercial catalyst, Amberlyst 15, is contained in a fiberglass cloth with stainless steel wire mesh. The resulting layered high surface structure acts as a mass transfer medium. The stacked bales constitute the catalyst bed and form the basis for catalytic distillation. The process simplifies the MTBE production by requiring only one reactor and no reactor intercoolers, as needed in the conventional process. The isobutene is mixed with methanol inside the column. The reactor temperature is maintained at the reaction mixture boiling point causing the feed to boil up through the catalyst to react with methanoi to form MTBE. The distillation trays above and below the catalyst packing separate the isobutene-methanol and methanol-MTBE azeotropes. MTBE is continuously removed as it is formed by the distillation. A high conversion of isobutene (99.9%) can be achieved by this process.

A reactive distillation column for the synthesis of MTBE was simulated using a steady-state equilibrium stage model. For identical column and feed specifications, two distinctly different composition profiles were obtained, which correspond to high and low conversion of isobutene. The residue curve maps for simultaneous physical and chemical equilibrium showed that the two conversion profiles correspond to the residue curves which have their starting points in distinctly different composition regions [193].

Nijhuis et al. [194] performed the computer simulations for the synthesis of methyl tert-butyl ether in a fixed-bed reactor using a reactive distillation column. The calculations clearly showed the advantages of MTBE synthesis in a catalytic distillation tower. Furthermore, the computer simulations showed that multiple steady states may occur in the reactive distillation column during MTBE synthesis in a broad range of operating conditions. An analysis of some sensitivity studies was presented.

The use of zeolite catalysts for MTBE production has the potential of overcoming the temperature limitations of the existing commercial resin catalyst. The zeolite catalyst will have improved activity, selectivity and stability. Early work identified that MTBE could be synthesized from methanol and tert-butyl alcohol or isobutene in the presence of mineral acids, such as sulphuric acid [195,196]. However, such a method was not particularly selective due to by-product formation from dehydration reactions. More recently, Bitar et al. [197] have reviewed the following features that should be considered in the design of an optimized process:

1. *Temperature:* this is required to be as low as possible to maximize the equilibrium isobutene conversion and to minimize by-product formation.

2. *Methanol/isobutene ratio:* this should be as near stoichiometric as possible to reduce the cost of recovery and recycle of the unreacted methanol.

3. *Isobutene conversion:* for single stage operation with acidic ion-exchange resins, 90 - 96 % conversion of isobutene is readily achievable; conversions above this level require the operation of an additional conversion stage. Clearly, novel catalysts need to match or better these criteria.

4. *Catalyst lifetime:* for single stage operation with acidic exchange resin catalysts permits lifetimes up to two years to be achieved and this must therefore serve as a benchmark for the design of improved catalysts. With respect to catalyst lifetime for heterogeneous catalysts, it is well-known that for acid-catalyzed reactions, zeolites, particularly the pentasil zeolite ZSM-5, can demonstrate long operational life, for example, as demonstrated by HZSM-5 for the methanol-to-gasoline process. It is therefore not surprising that zeolites have been studied as catalysts for MTBE production.

A number of studies have been reported in the literature for the synthesis and/or modification of commercial zeolites for their catalytic application in the reaction of methanol with isobutene to produce MTBE.

Chu and Kuhl [198] studied zeolite beta, ZSM-5, ZSM-11, rare earth exchanged Y zeolite and mordenite as catalysts for vapor phase conversion of methanol and isobutene to MTBE. Two reaction systems were used for the screening of the catalysts, vapor phase and liquid or mixed phase. The vapor phase reaction tests were conducted in packed bed

glass reactor at atmospheric pressure for preliminary screening. The results of vapor phase synthesis of MTBE are given in Table 2.6.

Table 2.6 Formation of MTBE over zeolite catalysts in the vapor phase.

Zeolite[a]	Mordenite (26)		Beta (22)		REHY (5.3)[b]		REAlY (5.1)[c]		ZSM-5 (70)		ZSM-11 (25)	
Reaction conditions[d]												
molar ratio[e]	1.07	1.14	1.46	1.53	1.20	1.18	1.06	1.04	1.04	1.105	0.98	0.98
temp.,°C	82	93	82	93	82	93	82	93	82	93	82	93
Conversion of isobutene												
to MTBE, %	8.4	7.1	13.9	9.1	11.3	10.6	25.3	23.4	30.5	25.3	25.1	21.0
to C_8 olefin, %	6.0	14.1	23.0	27.3	0.47	1.9	0.3	1.3	0	0.1	0.1	0.2
Selectivity to MTBE, %	58.3	33.5	37.7	25.0	96.0	85.0	98.8	94.9	100	99.6	99.6	99.9

[a]Figure in parethesis gives SiO2/Al2O3 ratio.
[b]REHY prepared by ion-exchange of calcined RENaY with (NH4)2SO4, RE = rare earth.
[c]REAlY prepared by ion-exchange of calcined RENaY with $Al_2(SO_4)_3$.
[d]WHSV = 3.4 h-1, total weight of methanol and isobutene per g of catalyst.
[e]Molar ratio methanol/isobutene.

Although the conversion was low, but based on the performance in this test, catalysts were selected for the liquid phase study. The liquid phase reactions were carried out in packed bed stainless steel tube reactor. It was concluded from this work that the medium pore zeolites such as ZSM-5 and ZSM-11 gave the highest isobutene conversion and MTBE selectivity. The zeolite beta and mordenite showed poorest selectivity. On the other hand, the small pore zeolites e.g. ferrierite were found inactive for this reaction, since isobutene cannot enter the zeolite cage structure. They rationalized the relative reactivity of the zeolites in terms of the differences in diffusion rate of the reactants within the zeolite channels. For the medium pore zeolites, ZSM-5 and ZSM-ll, methanol diffuses more

rapidly than isobutene. Therefore, an isobutene molecule migrating within the zeolite pore system encounters a high excess of adsorbed methanol and reacts to form MTBE at a higher selectivity. The lower selectivity observed for mordenite and zeolite beta were due to the lack of shape selectivity in the diffusion of methanol and isobutene as compared to large pore zeolites such as Y zeolites. The high selectivity observed for rare earth exchanged zeolites Y was considered to be due to the preferential adsorption of methanol by the more polar zeolite of lower SiO_2/Al_2O_3 ratio. The similarity between the large pore zeolites tested and the commercial Amberlyst 15 resin catalyst was that the selectivity of MTBE increased with temperature. However, this was not observed for ZSM-5 and ZSM-11 catalysts. Under liquid phase conditions more similar to those used in the commercial process, ZSM-5 was found to have superior selectivity for MTBE over the broad range of methanol/isobutene ratios investigated as compared to Amberlyst 15. This study by Chu and Kohl is an example of low temperature application of zeolite catalysts. The authors concluded that zeolites ZSM-5 and ZSM- 11 offered a number of distinct advantages over Amberlyst 15 catalyst which are:

(i) high thermal stability,

(ii) no acid effluent,

(iii) high selectivity to MTBE,

(iv) lower sensitivity to methanol/isobutene ratio,

(V) excellent selectivity even at ratios approaching unity,.

(vi) high MTBE output despite unfavorable thermodynamic equilibrium and

(vii) ease of regeneration of the catalyst.

Harandi and Owen [199] disclosed the use of zeolite β as an etherification catalyst in a two-stage process. The first stage involves the isomerization of an olefin-containing feedstock over a silicotitanate catalyst. In the second stage, ether formation occurs by the reaction of methanol and iso-olefins over the zeolite β. This is of interest, since the original study of Chu and Kuhl [29] indicates that the large pore zeolite β is not particularly selective for this reaction.

Knifton [200] described a patented method in which tertiary butyl alcohol is reacted with methanol. The catalysts used were Y-zeolites, super acid alumina, Ni-zeolites, silicates and aluminas. The operating conditions range from 20 to 250 ° C temperature, atmospheric to 1000 psig pressure and molar ratio of 0.1 to 10 moles of methanol per mole of tertiary butyl alcohol. The results indicated that up to 38 weight percent MTBE was obtained in the reaction.

Pien and Hatcher [201] evaluated the catalytic activity of HZSM-5 zeolite for the preparation of MTBE in a fixed bed micro reactor at temperatures ranging from 70 to 115 °C and pressures from 20 to 40 bar. Isobutene conversion ranged from 10 to 89 percent and was completely selective to the formation of MTBE. Dimerization was hindered by the unique pore system of the zeolite. Reaction temperature and the isobutene to catalyst ratios were the significant process variables. Pressure had no significant effect on conversion of the reactants. At 75 °C, Amberlyst 15 was approximately 11 times more active than HZSM-5 zeolite. However, at 100 °C, the two catalysts have about the same activity. This illustrates

the instability of resin catalyst at higher temperatures. The selectivity with the zeolite catalyst was also better as compared to resin catalyst. In another study, it has been suggested that the absence of isobutene dimers in the product was not due to the shape selectivity of HZSM-5 catalyst, but perhaps due to the very high coverage of active sites of the zeolite by methanol which prevents two isobutene molecules from reacting together. The experimental data have shown that methanol adsorptivity is about three times that of isobutene. In the presence of excess methanol, the rate of reaction was zero order and first order with respect to methanol and isobutene respectively [202].

A comparative study has been carried [203] out on the use of different acid catalysts viz. Amberlyst 15 resin, ZSM-5, and Y zeolite, and triflic acid (TFA) modified zeolites (H-ZSM-5 and H-Y) for the gas phase synthesis of MTBE. A vertically mounted stainless steel fixed bed reactor was used for the study. The maximum yield of MTBE was obtained at 68 -70° C for Amberlyst and at 85° C for both zeolites . The maximum MTBE yield with the three catalysts has the following sequence: Amberlyst 15 >> H-ZSM-5 > H-Y. This sequence reflects the situation in terms of acid strength of the catalyst. In particular, the Y type zeolite is much less active than the ZSM-5 zeolite because of its weaker acid strength although its acid density is much higher than that of the ZSM-5 zeolite. In the case of ZSM-5, its lower acid density cannot be readjusted by loading triflic acid (TFA) because of the negative influence of the TFA. TFA loaded Y zeolite appears to be more interesting in the sense that it exhibits the same MTBE yield with lower production of

by-products and thermally more stable than the commercial Amberlyst 15 resin. Therefore, TFA loaded Y zeolite is an alternative to the conventional catalyst, Amberlyst 15, for MTBE production.

Chang et al. [204] have reported the use of titanium modified silicalites at 70 - 110° C under atmospheric pressure in fixed bed reactor for the vapor phase reaction of methanol with isobutene to form MTBE. Infrared spectroscopy and the acidity measurements of the catalyst indicated that there is isomorphic substitution of Ti^{4+} ion into the zeolite lattice sites. The results of reaction studies were compared with HZSM-5 catalyst and it was found that titanium silicalite has higher selectivity for MTBE. Catalyst deactivation or coke formation was not observed in this reaction. The results also indicates that the acid sites responsible for MTBE formation were mainly of weak to medium acid strength. The strength of the acid sites and the adsorption strength of titanium silicalite were found weaker than those of HZSM-5 catalyst.

Nikolopoulos and coworkers [205] have carried out gas phase synthesis of MTBE over acid catalysts using a small fixed bed reactor. In this study, six acid catalysts were tested and compared for their acidic properties, activity and MTBE selectivity. Four of the catalysts were HY zeolites having different acidic properties namely Y62, Y82, S(LZ12)8 and LZ210-12 and the other two were silica-alumina catalyst and Amberlyst 15 resin. The catalytic study shows that the zeolites were superior to resin in terms of acidity and MTBE selectivity. It was found that very strong acidity of the resin favors many secondary reactions

leading to by-product formation. The results of this study suggest that the acid strength has major influence on the catalytic behavior of zeolites for MTBE synthesis. The kinetic data indicate that increased acid strength is favorable for MTBE formation. However, high acid strength also facilitates deactivation of the catalyst. Low acid density tends to reduce overall MTBE formation. Consequently, there seems to be an optimum set of values for acid strength and acid density. At high temperature, thermodynamic limitation dominate the reaction whereas kinetics results for this reaction depends on acid strength. Among the catalysts tested, zeolite LZ210-12 appears to possess the best acidic characteristics for MTBE synthesis.

Kogelbauer et al. [206] investigated the influence of the acid strength of a zeolite upon MTBE synthesis. The other parameters such as crystalline structure, Si/Al ratio, number of acid sites, and charge of balancing cations, were kept constant. A series of HY zeolites that were partially cation-exchanged (cation: Li^+, Na^+, Rb^+) to the same level was used. All zeolite exhibited similar initial activities for the formation of MTBE at temperatures below 100 °C. Steady state activities, however, were found to be strongly influenced by the different deactivation behavior of the investigated samples. For the partially Rb-exchanged sample, blockage of pores caused an expressed decrease in the rate of reaction during the first 30 min on stream. The presence of excess methanol in the pores was regarded as a possible cause for the similarity of the initial reaction rates.

The impact of acidity on zeolite activity for MTBE formation, away from thermodynamic equilibrium limitations, was studied by Nikolopoulos et al. [207]. The catalysts investigated include a series of dealuminated HY zeolites with different acid properties. In addition, H-ZSM-5, an amorphous silica-alumina, and Amberlyst-15 resin were investigated for comparison. An increase in acidity, of HY zeolites produced by dealumination, significantly enhanced the intrinsic activity for MTBE formation. The increased activity of the dealuminated zeolites seemed to be resulted by the formation of extra-lattice Al. The interaction between extra-lattice Al and the acid sites related to lattice Al was most likely responsible for the enhanced activity of the zeolites. It was concluded that the ratio of extra-lattice to lattice Al could be an important parameter for determining the catalytic behavior of zeolites for this reaction.

CHAPTER 3

EXPERIMENTAL

3.1 Synthesis of High-Silica Zeolites

Synthesis of high-silica zeolite involves a large number of variables, such as Si/Al ratio, pH, temperature, time, etc. It is difficult to investigate the effects of each of them separately on the properties of the final products. Therefore, screening of such variables to select the important ones is very important.

3.1.1 Screening of Variables

Plackett-Burman experimental design [208,209] is one of the fractional factorial design which is based on balanced, incomplete blocks, and can serve the required purpose. The application of this statistical method in the preparation of high-silica zeolite is illustrated in this section. The preparation involves variables at the gel formation and hydrothermal crystallization. These variables are listed in Table 3.1. Two response variables are chosen to evaluate the primary variables involved in the preparation : IR-crystallinity and BET surface area of the zeolites prepared.

Table 3.1 Variables affecting the synthesis of high-silica zeolites.

Parameter	levels	
	low	high
A. Silica/alumina ratio	3500	4500
B. Cation (NaCl (g))	45.00	55.00
C. Anion (NaOH (g))	1.50	3.00
D. pH	10.3	9.7
E. Template(g)	5.00	10.00
F. Order of addition	I	II
G. Dummy	NA	NA
H. Homogenization of gel	Mech.	Ultrasonic
I. Aging (48 hr)	No	Yes
J Heating rate (^{o}C/min.)	1.00	3.00
K. Reactor stirring (rpm)	900	1500
L Temperature maximum(^{o}C)	210	250
M. Cooling	X	Y
N. Dummy	NA	NA
O. Dummy	NA	NA

I= (B+C) + A, II=(A+B) + C, X= Ambient temp., Y= Ice water

A basic Plackett-Burman design for studying up to 15 variables is shown in Table 3.2. In the present work, only 12 variables were evaluated leaving three dummy variables and thus three degrees of freedom. Each variable is tried at two levels, "+" denoting high level and "-" low level. Inspection of Table 2 shows that, during the 16 runs, each variable appears at its high level eight times and its low level eight times. The effect of any variable on the response, represented here by the measure of crystallinity and surface area, is simply the difference between the average value of the response for the eight runs at the high level and the average value of the response for the eight runs at the low level, as shown by the following equation:

$$E_A = \frac{\Sigma R(+)}{8} - \frac{\Sigma R(-)}{8} \qquad (3.1)$$

where E_A = effect of variable A and R = response, that is, crystallinity or surface area.

As for the dummy variables, no changes are made in the actual runs. If there are no interactions between variables and all levels are reproduced perfectly with no error in measuring the response, the effect shown by a dummy variable should be zero. However, in reality, this is usually not so, and its effect can then be assumed to be an estimate of the experimental error. Three such estimates, i.e., three dummy variables, will provide adequate confidence. Stowe and Mayer [209] had shown that the standard error of an effect in the Plackett-Burman analysis is related to the root-mean-square of the dummy effects by the following equation:

$$SE_{eff} = (\Sigma(E_D)^2 / n)^{1/2} \qquad (3.2)$$

where SE_{eff} = standard error of an effect; E_D = effect shown by a dummy variable, and n = number of dummy variables.

The significance of each effect can then be determined by using the familiar *t*-test:

$$t = \text{effect} / SE_{eff} \qquad (3.3)$$

This test evaluates the probability of finding an effect this large purely by chance when, in fact, no effect really exists. The confidence level of being correct in accepting that the effect is caused by changes in levels of that particular variable is then 100 x (1 - probability due to chance).

Table 3.2 Plackett-Burman Experimental Design.

Run No	Variable														
	A	B	C	D	E	F	G	H	I	J	K	L	M	N	O
1	+	+	+	+	-	+	-	+	+	-	-	+	-	-	-
2	+	+	+	-	+	-	+	+	-	-	+	-	-	-	+
3	+	+	-	+	-	+	+	-	-	+	-	-	-	+	+
4	+	-	+	-	+	+	-	-	+	-	-	-	+	+	+
5	-	+	-	+	+	-	-	+	-	-	-	+	+	+	+
6	+	-	+	+	-	-	+	-	-	-	+	+	+	+	-
7	-	+	+	-	-	+	-	-	-	+	+	+	+	-	+
8	+	+	-	-	+	-	-	-	+	+	+	+	-	+	-
9	+	-	-	+	-	-	-	+	+	+	+	-	+	-	+
10	-	-	+	-	-	-	+	+	+	+	-	+	-	+	+
11	-	+	-	-	-	+	+	+	+	-	+	-	+	+	-
12	+	-	-	-	+	+	+	+	-	+	-	+	+	-	-
13	-	-	-	+	+	+	+	-	+	-	+	+	-	-	+
14	-	-	+	+	+	+	-	+	-	+	+	-	-	+	-
15	-	+	+	+	+	-	+	-	+	+	-	-	+	-	-
16	-	-	-	-	-	-	-	-	-	-	-	-	-	-	-

3.1.2 Synthesis Procedure

High-silica zeolite (Si/Al ratios 3500 and 4500) were prepared by temperature programmed hydrothermal rapid crystallization method. The composition of the reacting solutions are given in Table 3.3.

Table 3.3 Composition of reacting solutions.

A		B		C	
$Na_2SiO_3.5H_2O$	100.0g	$Al_2SO_4.16H_2O$	0.0456g (0.0789g)	NaCl	45.00g (55.00g)
Water	100.0g				
		Template	5.00g (10.00g)	NaOH	1.50g (3.00g)
		Water	200.0g	Water	100.0g

Values given in parentheses are for high level of variable.

The reaction mixture was prepared as follows: for solution A, 100.00g of sodium meta silicate (98% Fluka AG) was added to 100.00g of distilled water and the mixture stirred at 60.0 °C until a clear solution resulted. The solution remained clear as it was cooled in air to 25 °C. The weight of the solution was checked and distilled water added to the proper value. In a separate container, solution B was prepared by dissolving 0.0456g of aluminum sulphate (> 98%, Fluka AG) in 200.00g of distilled water and mixed with 10.00g of tetrapropyl ammonium bromide (>98%, Fluka AG) as a templating agent. In a separate container, 55.00g of sodium chloride (>99.5%, Merck) was added to 100.00g of distilled water and the mixture was stirred at room temperature until a clear solution resulted. To this clear solution, 3.00g of sodium hydroxide (99.5%, BDH) was added and stirred until it was dissolved which constitutes solution C.

Three solutions A, B, and C were mixed in two different orders of addition. In the first case (low level), solutions B and C were mixed; then solution A was added dropwise, and in the second case, that is high level, solutions A and B were added dropwise to solution C with

continuous stirring in both the cases. The homogeneous mixture formed was stirred for half an hour to ensure thorough mixing. The pH was adjusted with conc. H_2SO_4 (98%, Fisher) to 9.7 and 10.3 for the low and high levels, respectively. As the pH was decreased (initially >13.5), a white solid gel started appearing. After adjusting the pH, the gel was homogenized either mechanically or using ultrasonic homogenizer (Cole Parmer 4710 series). Depending upon the nature of the experiment the gel was subjected to aging at room temperature for 48 hours. No aging was required for the low level of this variable. For these runs, the homogenized gel was fed to the stainless steel autoclave (1 lit. Parr Inc.) for hydrothermal crystallization. The autoclave was purged with nitrogen for five minutes, then was pressurized to 30.0 psig before the heating was started.

Temperature was increased at a rate of 1.0 °C/min. (low level) or 3.0 °C/min. (high level) up to 160 °C. Then the heating rate was increased to 9.0 °C/min. up to 210 or 250 °C. The stirring of the mixture was done at low level (900 rpm) or high level (1500 rpm) according to the requirement of the respective run. After reaching the maximum temperature, the autoclave was cooled to room temperature, either by leaving it outside the heater or by putting it to the ice water (high level).

The final product was filtered, washed with deionized water to the chloride-free condition. The crystals formed were first dried over night in the air at 80 °C and then under vacuum at 120 °C for 2 hr. This sample, designated by as-synthesized sample was subjected to infrared

spectroscopy. For the BET surface area measurement the as-synthesized sample was calcined in air at 550 °C for 2 hours to remove the template.

3.1.3 Ion Exchange of High-Silica Zeolite

For the acid catalysis, the zeolite should be in the hydrogen form to provide active sites for the reaction. A hydrogen form zeolite can be prepared by exchange with mineral acid or by exchanging with NH_4^+ and decomposing the ammonium ion into NH_3 gas and H^+ ion which maintains the charge balance in the structure. High degree of H^+ exchange with acids often collapses the structure of the zeolite, but high degree of H^+ exchange can be achieved without structural collapse if the NH_4^+ exchange technique is used.

To obtain effective ion exchange and to remove the template the as-synthesized zeolites were calcined at 500 °C for 4 hours in air. The following procedure was adopted for the ion exchange:

A known amount of the calcined zeolite was carefully mixed with de-ionized water to form a slurry which was heated at 80 °C. In a tri-neck round-bottom flask, 15.0 ml of 1.0 M NH_4NO_3 solution was taken for every 1.0g of the zeolite sample. The solution was heated to 80 °C and the slurry of the zeolite was mixed with it by vigorous stirring. The treatment was continued for one hour.

The zeolite was then filtered (Whatman # 4), washed thoroughly with deionized water to remove the excess salt. The zeolite was dried in air at 110 °C for several hours, then in the vacuum oven over night at 110

°C . The dried sample was calcined in air at 400 °C for 4 hours for deammoniation. The Na-content of the ion exchanged zeolite was measured by flame photometer and was found to be less than 1 % of the initial amount.

3.2 Modification of High-Silica Zeolites

Modification of a zeolite encompasses a variety of techniques to further control the acid activity and/or the shape selectivity of a specific zeolite structure. Three major types of modifications were applied to the high-silica zeolites:

(i) preparing zeolites with different Si/Al ratio to achieve varying acidic property;

(ii) structural modification by isomorphous substitution of T atoms (where T = Si or Al) with Fe, Cr and Cu, during the synthesis (crystallization);

(ii) the third type of modification applied was reaction with steam to obtain the desired acidic behavior. This can be considered as a post-synthesis modification.

The procedures for different modifications applied to the high-silica zeolites are described in the following sections.

3.2.1 Modification by Varying Si/Al Ratio

The acidity depends on aluminum content of the framework of the zeolite. Various high-silica zeolites were prepared with different amounts of aluminum in the framework structure.

The procedure for synthesis of high-silica MFI zeolites with Si/Al in the range of 30 to 115 was similar to the one described in the Section 3.1.1. The amount of aluminum sulphate was varied to achieve the required Si/Al ratio. The pH of the gel was adjusted at 10.0.

The molar gel composition of a typical zeolite sample with Si/Al ratio of 30 is given here:

63 Na_2O : Al_2O_3 : 60 SiO_2 : 4.0 TPABr : 3066 H_2O : 60 NaCl : 50 H_2SO_4

The synthesized zeolites were calcined and ion exchanged according to the procedure given in the previous section. The as-synthesized and calcined zeolites were characterized using various analytical techniques which will be described in Section 3.3. The hydrogen form of the catalysts was subjected to catalytic evaluations.

3.2.2 Modification by Metal Incorporation

The procedure for synthesis of metal containing zeolites was similar to the one described in Section 3.1.1. Instead of aluminum sulphate, the nitrates of Iron (III), Copper (II) and Chromium (III) were used. One aluminum free (no other metal added) sample was also prepared for comparative characterization studies.

In all the preparations, Si/M (where M = Fe, Cu and Cr) ratio was maintained such that the resulting zeolites would have Si/M ratio of 100.

The synthesized zeolites were calcined at 500 °C in air for 4 hours to remove the organic template. These metal-containing zeolites were ion exchanged with ammonium nitrate for the replacement of residual sodium ions present in the pores of the zeolites. The ion exchanged zeolites were calcined in air at 400 °C for 4 hours to deammoniate it. Therefore, the final zeolite may be considered as HM-zeolite (hydrogen form of metal containing zeolite).

3.2.3 Modification by Hydrothermal Treatment (Steaming)

The apparatus used for zeolite steaming was designed and fabricated in the laboratory, the shematic of which is shown in Figure 3.1. The reaction vessel was a quartz tube (25 mm i.d. x 75 cm length) with ground glass joints at the ends. A vernier needle valve permitted carrier gas (nitrogen 99.999%) to flow through the tube at the desired rate. A tube furnace (electrical resistance, 800W) heated half of the length of the reaction vessel. The unheated section constituted an air condenser, which served to collect the condensed water vapor. Water was pumped at the required rate by a high pressure metering pump (Aldex AS-30).

In a typical experiment, a 5.00g sample of the zeolite (granules of 0.600-1.18 mm size) was loaded into the center of the quartz tube with small amount of glass wool to support the zeolite. Heating was started

from room temperature to 500 °C at a rate of 10 °C/min, the nitrogen was flowing at a rate of 100 cm^3/min When the temperature reached 500 °C, the flow of nitrogen was decreased to 25 cm^3/min and water pump was started simultaneously. The pump was calibrated to deliver 5.00 g/h of deionized water to the preheater. The temperature of the preheater was set at 250 °C to get a regular supply of the steam. After two hours of steaming treatment, the water pump was stoped and the tube was cooled to room temperature. The nitrogen flow was increased back to 100 cm^3/min.

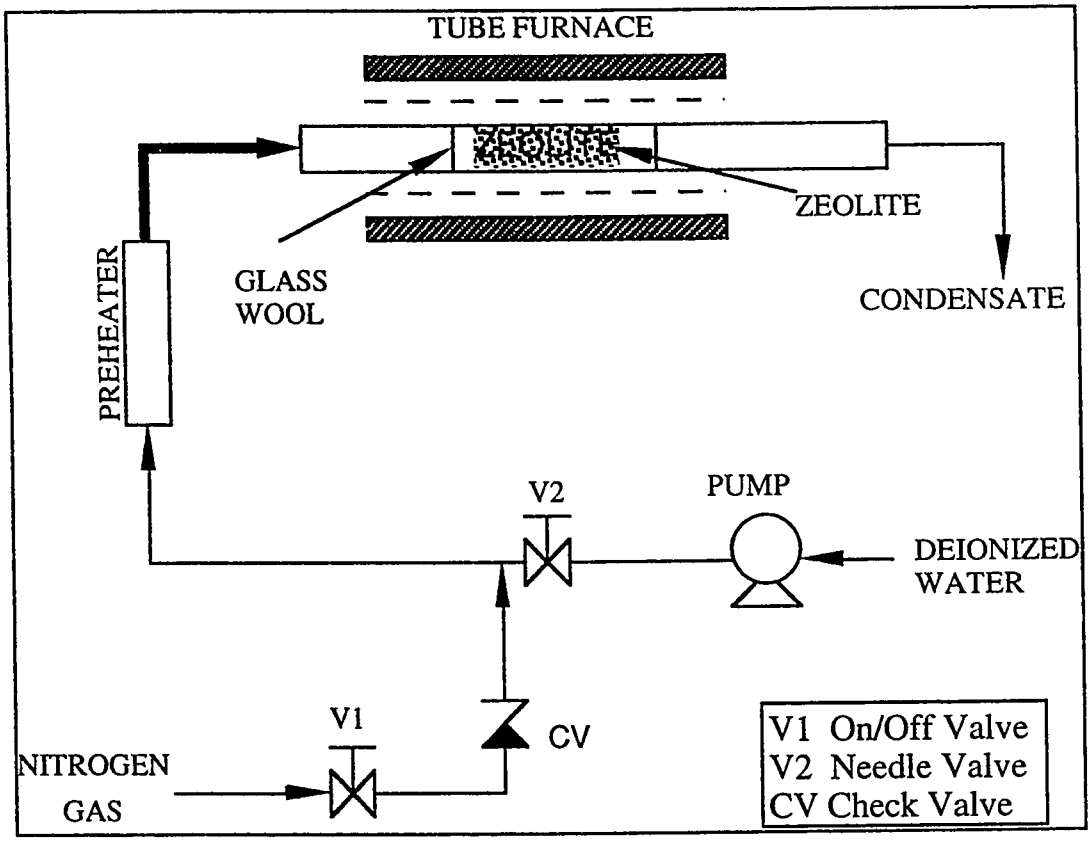

Figure 3.1 Flow diagram for steaming apparatus.

during the cooling stage of the process. The steam treated zeolite was stored ina stopper bottle for characterization and catalytic evaluation for MTBE reaction.

3.3 Characterization of High-Silica Zeolites

After the synthesis and modifications, the zeolites were characterized using the techniques summarized in Table 3.4, and the procedures are described briefly in the following sections.

3.3.1 Elemental Analysis

Elemental analyses were carried out using inductively coupled plasma atomic emission spectroscope (ICP AES) as well as wet analysis methods. The procedures of the analysis are described in this section.

ICP AES

Sample preparation for the analysis of zeolite was done by fusion. A 100 mg sample of dried zeolite was weighed in a 10 ml platinum crucible and mixed with 1.0 gram of lithium metaborate. The crucible was kept in a muffle furnace at 900 °C. When a clear melt was obtained, it was cooled down and the melt was agitated in 4% nitric acid with gentle warming. When completely dissolved it was transferred to a 100 ml volumetric flask and diluted with distilled deionised water to the final volume. This solution was used for the determination of most major and some of the minor elements on ICP.

Table 3.4 Characterization Method and Equipment used.

Characterization Method	Parameter Measured	Equipment Used
Chemical Analysis by ICP-AES; Wet Analysis Metod	Elemental Composition	ARL-3580 (UK); Shimadzu UV-260, (Japan)
BET Method, Nitrogen Adsorption/Desorption	Surface Area	Micromeritics ASAP-2000, (USA)
Centrifugal-sedimentation	Particle Size	Horiba, CAPA-700 (Japan)
XRD	Crystallinity, Cell Parameters	Philips PW/1730 X-Ray Diffractometer (Netherlands)
SEM	Crystal Morphology	JEOL JSM-840, (Japan)
Infrared Spectroscopy (FTIR)	Crystallinity, Acidity (acid type)	Nicolet-5DXB FTIR; Perkin-Elmer-1600-FTIR (USA)
Thermal Analysis (TG, DTA)	Weight Loss, Exothermicity Endothermicity	Simultaneous Thermal Analyzer STA-429, Netzsch, (W. Germany)
TPD of Ammonia	Acidity (acid density)	Chemisorb-2700, Micomeritics Inc. (USA)
ESR Spectroscopy	Transition Metal Siting	Varian E-109.

The instrument used for chemical analysis of the synthesized zeolite samples was the Admiralty Research Laboratory (ARL) atomic emission spectroscope (AES) Model ARL-3580. The equipment uses the Inductively Coupled Plasma (ICP), which is an atomic emission spectroscopic technique where radio-frequency power is coupled to a specially designed quartz torch establishing the plasma in argon. This high temperature plasma source excites the species introduced, and each element emits radiation of a particular wavelength. This emission intensity is measured by a spectrometer that facilitates the elemental determination at the trace level. The ICP model ARL-3580 was equipped with various channels that allow the simultaneous determination of 48 elements.

Wet Analysis

Al, Si, and Na were analyzed using standard procedures [211]. Standard and blanks were run during the analysis for accurate results.

Sample Preparation for Al and Si

Alkaline hydroxide fusion was used for the dissolution of zeolite samples. This fusion decomposes clays, silicates, silicides, and aluminum quite readily. This is also effective for titanium, corundum, bauxite, and phosphates. A sample to NaOH ratio of 1:10 was used in the fusion mixture.

One gram of solid pellets of sodium hydroxide (AR grade) was weighed in a 10 ml platinum crucible. It was melted on the flame until

homogenized. The melt was cooled to room temperature. Then 100 mg of zeolite sample was added to the crucible and it was heated slowly on the flame until the clear fusion melt was obtained. The platinum tipped tong was used to hold the crucible to avoid contamination from the tong material. The melt was transferred to the muffle furnace at 400 °C and kept for 15 minutes to have complete dissolution. The crucible was then cooled to room temperature and transferred into a 100 ml polyethylene beaker. About 70 ml of de-ionized water was added to it and the melt was completely leached in water using a Teflon coated stirring bar and a magnetic stirrer. The solution was quantitatively transferred to a 100 ml plastic volumetric flask and diluted with de-ionized water up to the mark. This solution was used to determine Si and Al. This procedure converts all the silicon into soluble monosilisic acid upon acidification.

Determination of Si

Si was determined by the well known molybdosilisic acid spectrophotometric method. The soluble monosilisic acid reacts with molybdic acid in a medium at pH 1-2 to form a yellow molybdosilisic acid complex $H_4(SiMo_{12}O_{40})$. This yellow color formation obeys Beer's law in the range of 10-100 mg/l silicon and is the basis for the spectrophotometric determination of silicon. A calibration curve was prepared using four standards (10, 20, 30, 40 mg/l Si) and all measurements were made at 400 nm in an one cm path-length cell using Shimadzu Model 260 spectrophotometer.

Determination of Al

Aluminum was determined by complexometric titration. An aliquot from the fused solution was measured by the volumetric pipette and transferred to the beaker. The pH of this solution was adjusted to 3.5 using dilute hydrochloric acid (Supra pure, Merck). A measured amount of excess of standard 0.0100 M EDTA was added to it and the beaker was gently heated to boil for 3-5 minutes. At this temperature, the EDTA complexes all the aluminum quantitatively. The beaker was cooled to room temperature. The excess EDTA was back titrated with standard 0.0100 M zinc solution at pH 5.5. A buffer was added to adjust this pH. Xylenol orange indicator was used to detect the end point. The calculated amount of EDTA solution (total added - excess titrated) used to complex the aluminum was proportional to the aluminum content. A further step of this method is to release the EDTA bound to aluminum by adding sodium fluoride. This released EDTA was then titrated with standard zinc solution. This step was also performed. Since the zeolite samples do not contain other impurities which also complex EDTA, the amount of EDTA bound to Al was similar in both cases.

Sample Preparation for Na

The zeolite samples for sodium analysis were prepared separately. 100 mg of zeolite sample was weighed into a platinum dish. A small amount of de-ionized water was added to it to form a paste. Then 3.00 ml of hydrofluoric acid (Analar, BDH) was added slowly and mixed. The platinum dish was placed on a hot plate at a low heat. Volatile silicon

tetrafluoride SiF_4 was evaporated completely from the platinum dish. It was kept on the hot plate until it was dried. Then 10.0 ml of diluted HCl was added to it to dissolve remaining metals and was heated for 10 minutes. The solution was quantitatively transferred to a 100 ml volumetric plastic flask and diluted with de-ionized water up to the mark.

Determination of Na

Sodium was determined on a flame photometer Model Dr. Lange M7-DC. The detection limit for Na was 0.01 mg/lit in solution with a relative standard error = ±2%. The instrument was calibrated with sodium standard and the blank was subtracted to get accurate results.

Carbon Analysis

The amount of organic template in the as-synthesized zeolite, and the carbon content of the spent catalysts were measured by carbon analyzer. The instrument used was Coulomat-702 from Ströhlein Inst. W.Germany. In this analyzer, a known amount of sample was burnt in oxygen at 1200 °C. The combustion product, carbon dioxide from carbon, was absorbed in 20 % solution of barium perchlorate. The solution was maintained at a certain pH. Due the absorption of carbon dioxide, the pH of the solution decreased. Electrical back-titration was done to bring the solution to its initial pH. The amount of current used in back-titration was evaluated by a precision integrator motor. The amount of current used in back-titration is the basis of material conversion produced electrically. By

the application of Faraday's law, the amount of carbon dioxide absorbed was calculated whcih will be proportional to the amount of carbon dioxide produced. The results of the analysis are discussed in the next chapter.

3.3.2 X-Ray Diffraction

This is obviously the best technique to characterize which type of zeolite is involved in a given sample. Moreover, when isomorphous substitution is carried out, changes in patterns and particularly in unit-cell volume is expected. As already mentioned in previous sections, one of the most important properties of zeolites is their well defined crystalline structure. The various zeolites, being crystalline solids have characteristic X-Ray powder diffraction patterns which are used for their identification and provide an indication of its purity.

The equipment used to measure the crystalline pattern of the synthesized zeolites was a Philips PW-1730 X-Ray diffractometer. For accurate measurements, α-alumina (Ultrex grade) was used as an internal standard (25% by weight).

The operating conditions of XRD analysis were:

Copper K_a radiation from a broad focus tube at 45 kv and 30 mA.

Auto divergence slit, no scatter slit and receiving slit = 0.2 mm.

Scanning speed and interval of data collection was 0.01 degree two theta/sec.

Angle scanned : 4 to 80 degree two theta.

A graphite monochromator was used.

The cell parameters were calculated by using PDP 11 (powder diffraction pattern version 1.1) program of Mario Calligaris [210].

3.3.3 Scanning Electron Microscopy

Scanning Electron Microscopy (SEM) is used to study the crystal morphology and size of the particles. SEM produces clear images of specimens ranging from objects visible to the naked eye to structures as small as several nanometers.

A small amount of the zeolite sample was mounted on a sample holder using double sided scotch tap. The sample was coated with evaporated gold film for 30 sec. The SEM equipment used was JEOL JSM-840. The micrographs were taken for each sample at different magnifications ranging from 1000 to 15000 times or more, in some cases. The microanalyses using energy dispersive spectroscopy (EDS) were also performed. The relative weight percentages of elements were calculated using the standardless semiquantitative analysis program with ZAF correction.

3.3.4 Infrared Spectroscopy

Infrared spectroscopy in the vibrational mode region may also be used to characterize the zeolite type when some absorption bands are

typical. The degree of crystallinity of the as-synthesized high-silica zeolites was measured by FTIR spectroscopy using KBr disc technique.

About 2 mg of the as-synthesized zeolite sample was ground with 200 mg of dry KBr in a small ball-mill apparatus. The pulverized mixture was transfered to a die, 8 mm in diameter, and pressed for few minutes at about 10,000 psi. High-quality, transparent pellets were obtained with this method. The pellets were stored in a dessicator to avoid any surface adsorption by water. The FTIR spectra were recorded by taking 16 scans with a resolution of 2.0 cm^{-1} and a scan range of 400 to 2000 cm^{-1}. The equipments used were Nicolet 5DXB FTIR and Perkin Elmer 1600 Series FTIR.

3.3.5 Thermal Analysis

Catalytic reactions are normally carried out at elevated temperatures. The zeolite over which the reactions take place should maintain thermal stability over the ranges of operating temperatures. Thermal analysis is therefore, done to study the changes in the zeolite properties as it is subjected to a controlled temperature program. The techniques applied are of two types (i) Thermogravimetry (TG) and (ii) Differential Thermal Analysis (DTA). In thermogravimetry, the change in mass of the zeolite sample is measured as a function of temperature. DTA, on the other hand, is a means of determining the amount of heat evolved or absorbed by the material and the temperature at which such changes take place. The temperature difference between the zeolite

sample and a reference material is measured as both the zeolite and the reference material are subjected to a controlled heating program. Among the phenomena that can be identified by these techniques are: melting, dehydration, desorption, solid-state and solid-gas reaction, vaporization, fusion, phase transformation, and crystalline transition.

The instrument used for thermal analysis of the zeolite samples was a Simultaneous Thermal Analyzer (STA-429) manufactured by Netzsch, Germany. The equipment performs both TG and DTA at the same time. In the thermograms, the weight loss, differential temperature and sample temperature are all plotted simultaneously. The catalyst sample to be analyzed (around 100 mg) was placed in one alumina crucible. The same weight of aluminum oxide (Ultrex grade, Baker), which undergoes no thermal change in the temperature range of the experiment, was placed in an identical alumina crucible as a reference sample. Using the sample carrier system, which has two sets of 10 % Pt-Pt/Rh thermocouples, the sample carrier was placed in the middle of the vertical furnace, which was programmed and controlled by the microprocessor temperature controller. The temperature was raised at a uniform rate of 10 °C/min. The analyses were made over a temperature range of 20-1250 °C in a dynamic atmosphere of air flowing at a rate of 100 cm^3/min.

3.3.6 Electron Spin Resonance Spectroscopy (ESR)

ESR spectroscopy is a sensitive tool to check whether or not transition metal cations are incorporated into the zeolite. This is a method

of choice to investigate the coordination chemistry of paramagnetic (systems containing one or more unpaired electron) metal centers. In particular the siting of various cations (Fe^{3+}, Cu^{2+}, Cr^{3+}, Ni^{+} etc.) based on the symmetry of their local environment can be studied.

ESR measurements were performed with a Varian E-109 X-band spectrometer using 100 kHz modulation. The spectrometer is interfaced with an E-935 data acquisition system, which employs the HP-9835B desktop computer for data processing. The spectra, recorded at room temperature for as synthesized and calcined samples, were digitized and stored on cassette tapes. The microwave frequency was measured with a Hewlett-Packard model 5342A digital frequency counter. The magnetic field sweep was calibrated with a Varian E-500-2 self-tracking n.m.r. gaussmeter with an accuracy of ±0.2 mG. Microwave power and field modulation were carefully controlled so that power saturation and line broadening were absent. Measurements were undertaken in X-band at room temperature for both as-synthesized as well as respective calcined samples.

3.3.7 Surface Area Measurement

Catalytic reaction takes place on the surface of the catalyst, and the activity of solid catalysts (which are porous materials) depends on their total surface area. This makes it imperative to know the surface area of a catalyst.

The most common method applied in determining the total surface area of catalyst, is that developed by Brunauer, Emmet, and Teller (called

the BET method). In this technique, the amount of nitrogen adsorbed at equilibrium at its normal boiling point (-195.8°C) is measured over a range of partial pressures below 1 atm. The Langmuir adsorption isotherm is then extended to apply to multilayer adsorption arriving at the following equation:

$$\frac{P}{V(P_o - P)} = \frac{1}{V_m C} + \frac{(C-1)P}{CV_m P_o} \qquad (3.4)$$

where

P = partial pressure (mm)

V = volume of nitrogen adsorbed at pressure P (cm^3 at STP)

V_m = volume of monolayer gas (cm^3 at STP)

P_o = vapor pressure (mm)

C = constant for the particular temperature and gas-solid system

A plot of $P/V(P_o-P)$ versus P/P_o gives a line, which can be extrapolated to $P/P_o = 0$. From the intercept (I) and the slope (S) of the plot, the volume of adsorbed gas corresponding to a monolayer can be obtained using the relation:

$$V_m = \frac{1}{(I+S)} \qquad (3.5)$$

Volume Vm can be readily converted to the number of molecules and hence to the surface area of the solid adsorbent.

All the measurements reported were carried out using fully automatic surface area measuring apparatus Micromeritics ASAP 2000.

The volume of the gas adsorbed was calculated by measuring the pressure variation resulting from the adsorption of a portion of a known volume of nitrogen by the test sample. Results of surface area measurements of the fresh calcined zeolite samples are presented in the next chapter.

3.3.8 Particle Size Distribution Analysis

The average particle size and particle size distribution can affect the properties of catalyst in term of, for example, product distribution of hydrocarbons in methanol conversion reaction. Measurement of the particle sizes of interest in catalysis can be made by sedimentation.

The instrument used for the particle size measurement of the as-synthesized zeolites, was particle size distribution analyzer Model CAPA-700 from Horiba Limited, Japan. The equipment is based on the principle of liquid-phase sedimentation, measurements being made using the optical transmission method. In this method, Stokes' sedimentation equation is combined with the proportional relationship between absorbency and particle concentration.

A particle having diameter (D) and density (ρ) in a solution of density (ρ_o) and viscosity coefficient (η_o) will settle at a constant velocity according to the Stokes' sedimentation law by the effect of gravity. Under normal gravitation, particles settle under the power of 1 G. As smaller particles do not settle rapidly, measurement requires considerable time.

The time required can be greatly reduced by utilizing centrifugal sedimentation (CS). The relationship between the sedimentation time and particle diameter is expressed in Stokes' centrifugal sedimentation equation:

$$D=\left[\frac{18\eta_o \ln(x_2/x_1)}{(\rho-\rho_o)\omega^2(t)t}\right]^{\frac{1}{2}} \qquad (3.6)$$

Where:

D = particle diameter (cm)

η_o = viscosity coefficient of dispersion medium

ρ = density of sample (g/cm^3)

ρ_o = density of dispersion medium(g/cm^3)

t = sedimentation time (sec)

x_1 = distance between center of rotation and sedimentation plane (cm)

x_2 = distance between center of rotation and measuring plane (cm)

$\omega(t)$ = rotation angular velocity (rad/sec).

Samples were prepared by mixing about 50 mg of the zeolite in 10 ml of 0.5% solution of sodium hexametaphosphate, a dispersion medium. The mixture was thoroughly agitated by ultrasonic homogenizer for few minutes. The blank measurement carried out using dispersion medium, before the sample measurement. The results were printed out in the form of distribution table and distribution graph by area basis. The equipment printed out the average particle diameter (median). This indicated the particle diameter for 50 % of the cumulative distribution.

3.3.9 Acidity Measurement by Pyridine Adsorption

Acidity characterization was made by FTIR studies of the pyridine adsorbed on the zeolite samples. The procedure followed for the measurements is as follows:

High-silica zeolites in the hydrogen form (0.5 g) were degassed at 200 °C under high vacuum (10^{-5} mbar) for two hours in a glass tube having a side arm and stopper. After degassing the sample was cooled to 50 °C and the pyridine was introduced through the side arm of the tube under vacuum. The sample was degassed at 200 °C for two hours and cooled to room temperature.

About 15 mg of the pyridine adsorbed zeolite sample was ground with 300 mg of dry KBr in a small ball-mill apparatus. The pulverized mixture was transferred to a die, 8 mm in diameter, and pressed for few minutes at about 10,000 psi. High-quality, transparent pellets were obtained with this method. The pellets were stored in a desiccator to avoid any surface adsorption by water. The FTIR spectra were recorded by taking 16 scans with a resolution of 2.0 cm^{-1} and a scan range of 1350 to 1800 cm^{-1}, on a Perkin-Elmer 1600 Series FTIR spectrophotometer. The blank (without pyridine adsorbed) was subtracted and the integrated absorbence was measured as area under the curve in the absorption mode for the characteristic peaks.

3.3.10 Acidity Measurements by TPD of Ammonia

The acidity measurements were conducted by temperature programmed desorption (TPD) of ammonia. The instrument used was Pulse Chemisorb 2700 by Micromeritics, Inc. USA.

The instrument applied dynamic pulse method for chemisorption. In this technique, an inert gas (helium) was continuously passed over a catalyst and into which small, reproducible volumes of chemisorbate (ammonia) gas were introduced. The injections were done by a built-in calibrated injection loop of a known volume (0.965 cc). The detector was temperature regulated and provided accurate analysis. The output of the detector were plotted using a strip chart recorder.

The procedure used for TPD of ammonia as described by the ASTM method (D 4824-88) for the determination of the distribution of acid sites in a catalyst is given below:

1. The sample (250.0 ±0.1 mg) was degassed at 500 °C under a continuos flow of He. This will ensure complete removal of impurities (such as moistures) present in the solid. The temperature was raised from room temperature up to the final temperature (500 °C) at a rate of 10 °C/min. The sample was kept at 500 °C for one hour.

2. The sample temperature was then reduced to 50 °C. At this temperature, NH_3 was pulsed over the sample till the detector gave a signal indicating a complete saturation of the sample.
3. Temperature was then raised to 175 °C at a ramping rate of 10 °C/min. The sample was kept at 175 °C for one and a half hour so that all physisorbed NH_3 was removed. The base line was re-established for indication of a clean sample just before desorption started.
4. Desorption was then programmed to begin from 175 °C up to the desired (600 °C) temperature. The temperature was increased at a rate of 10 °C/min.
5. All peaks that occurred were recorded at the temperature at which they appeared. The resulting desorption curves were quantified for acid density as volume of ammonia adsorbed per gram of the catalyst.

3.4 Catalytic Evaluation

3.4.1 Experimental Set-Up

The synthesized zeolites were catalytically evaluated using a reaction system design and fabricated in the laboratory. The reaction system was designed in such a way that it can be used for MTBE synthesis and MTO reaction as well. The reaction system, along with the utility cylinders and gas chromatograph is shown in Figure 3.2. The schematic of the

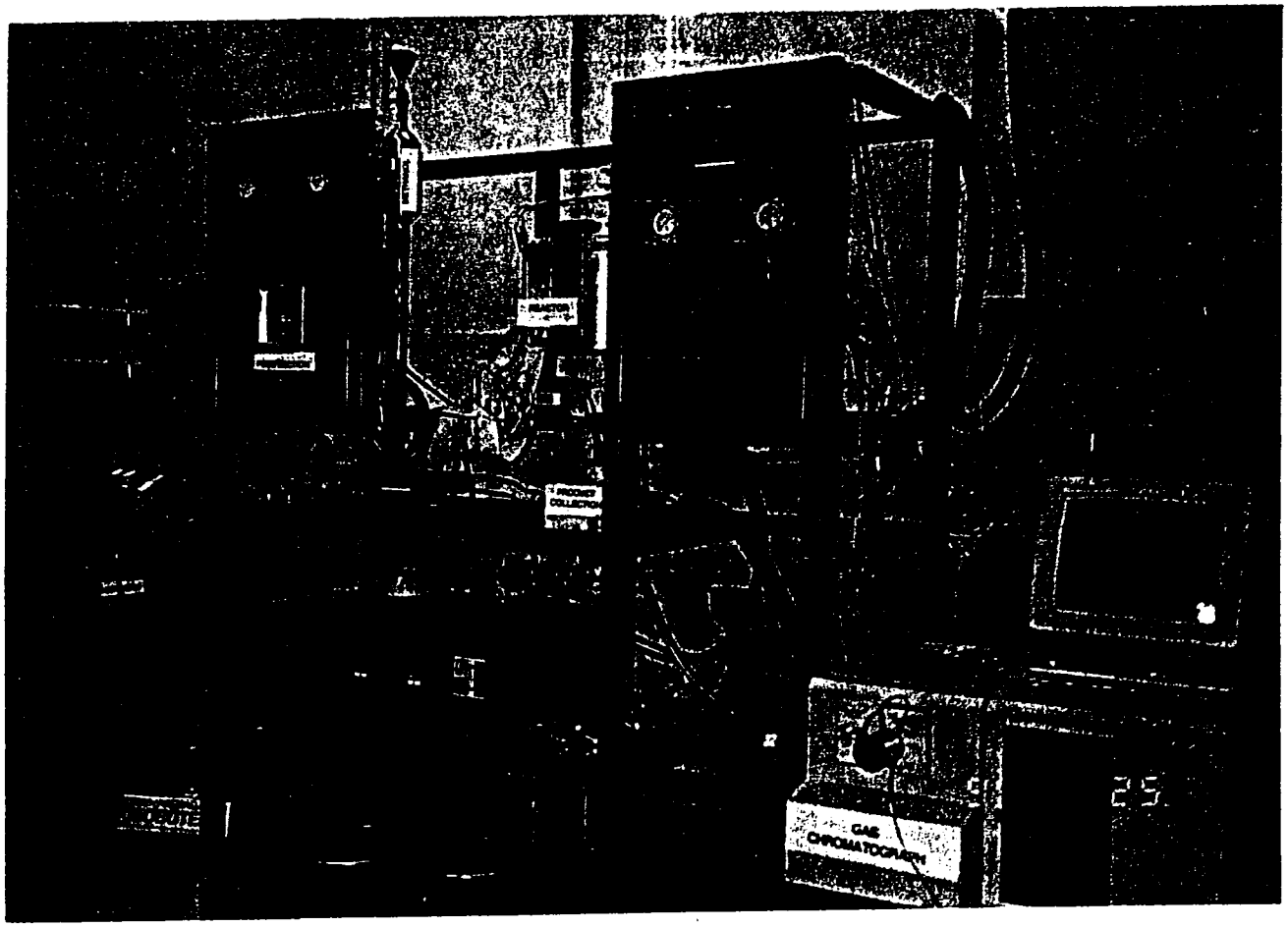

Figure 3.2 Picture of Zeolite Evaluation Reaction System.

experimental set up is shown in Figure 3.3. The set up consisted of four parts: feed section, preheating zone, fixed-bed reactor and product separation section. Experiments were carried out at atmospheric pressure.

Feed Section

The feed section was designed to supply feed to the reactor under controlled pressure and flow rate. It consisted of the following:

i. methanol storage tank;
ii. methanol feed pump;
iii. air, nitrogen and isobutene cylinders;
iv. mass flow controllers for isobutene and air/nitrogen and
v. two single channel mass flow regulators.

The feed tank was equipped with pressure indicator, filling port and a level indicator. Liquid methanol stored in the vessel, was fed to the unit by an Aldex high-pressure metering pump (Model S-60). Isobutene gas from a cylinder, was supplied at a regulated flow rate using Brooks mass flow controller (Model 5896 TR Series) and mixed with the methanol before the preheating zone. Air, also stored in a cylinder, was fed during in situ calcination. The various feeds were delivered to the reaction system through gas lines constructed of 1/4" stainless steel tubing.

Preheating Zone

The methanol and nitrogen (for MTO) was fed to the preheating section in which the methanol was vaporized to provide a homogenous

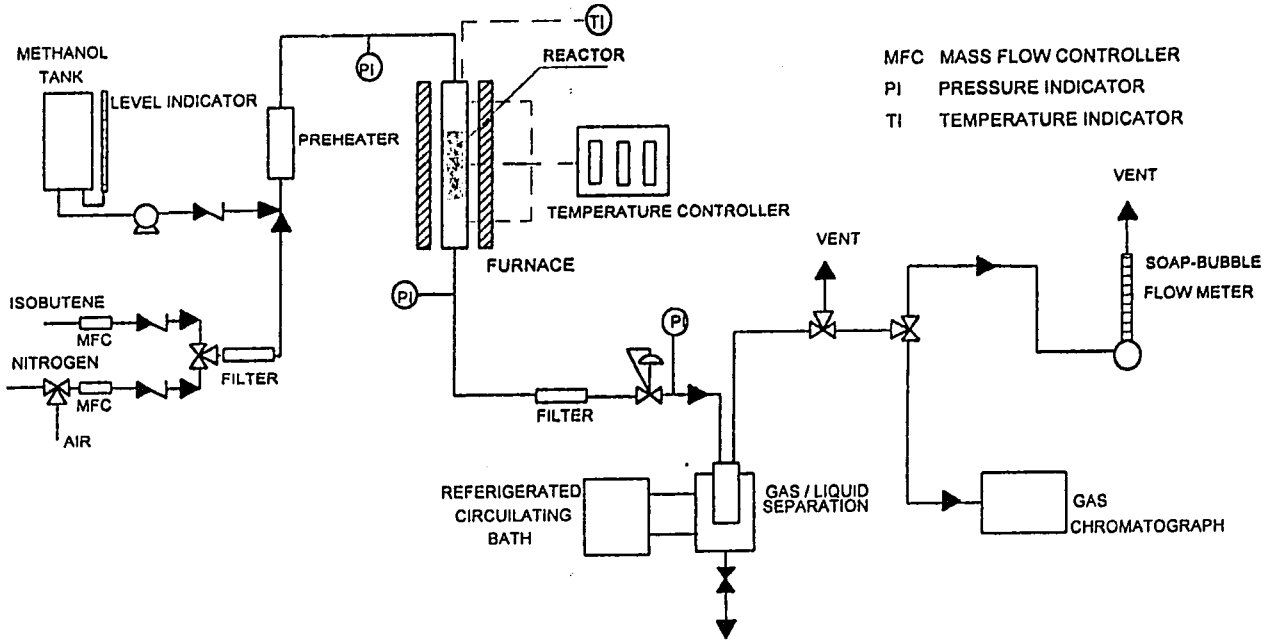

Figure 3.3 Schematic of the Experimental Set-up for Catalytic Evaluation of High-silica Zeollites for MTBE and MTO.

mixture. Similarly, for MTBE synthesis, methanol/isobutene mixture of required molar ratio was vaporized through the preheating zone. The preheator was made of 2.5 m long, coiled 1/4" stainless steel tubing insulated with a heat resistant tape to minimize heat loss and to maintain stable temperature during operation. The temperature was measured using a thermocouple and controlled by a PID controller (Omega, Model D921).

Fixed-bed Reactor

The reactor used was a 35 cm tubular stainless steel 9.5 mm i.d. tube. The schematic of the reactor is shown in Figure 3.4. The catalyst sample was placed in the reactor and held in position using silica wool supports to provide a fixed bed operation. The reactor was heated by a three-zone electric furnace (Thermcarft Inc. USA). Temperature of each zone was controlled by PID controllers. Reactor temperature was monitored by a thermocouple located at the center of the catalyst bed.

Product Separation Section

This section was designed to separate the reaction products into liquid and gaseous fractions. The schematic of the gas-liquid separator is given in Figure 3.5. Reaction products were collected in a gas-liquid separator, which was cooled by circulating ethylene glycol-water mixture using a refrigerating circulator. The circulator was supplied by Brinkmann Instrument Company USA(Model Lauda RK-20). The unit has a capacity of 6 liters and operating range of -15 °C to +120 °C. Condensed

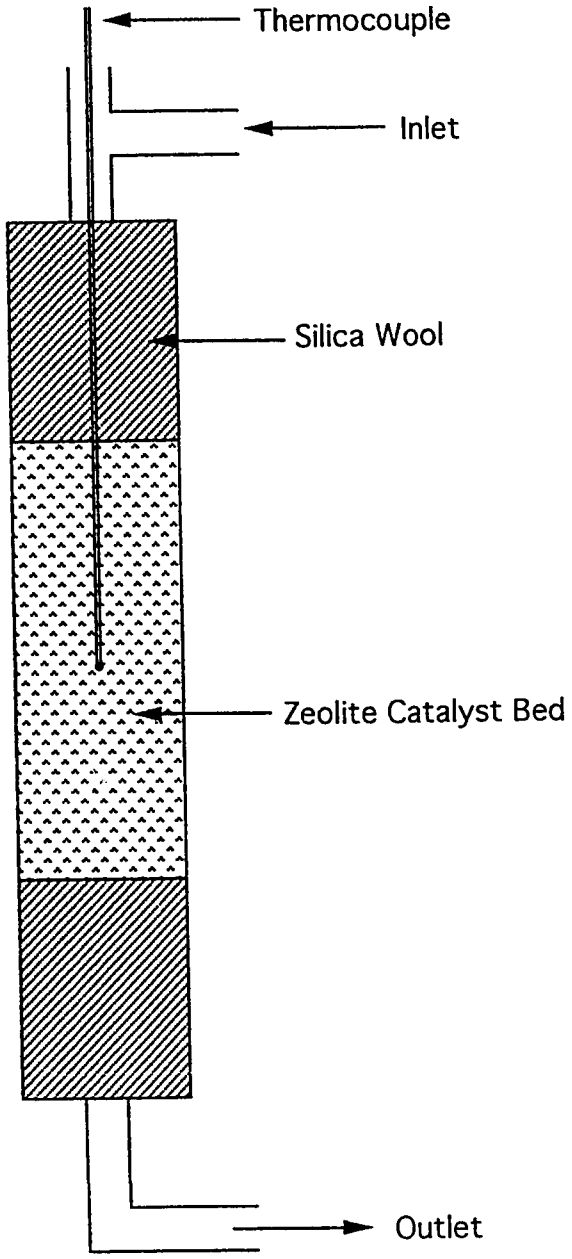

Figure 3.4 Schematic of Fixed Bed Tubular Reactor

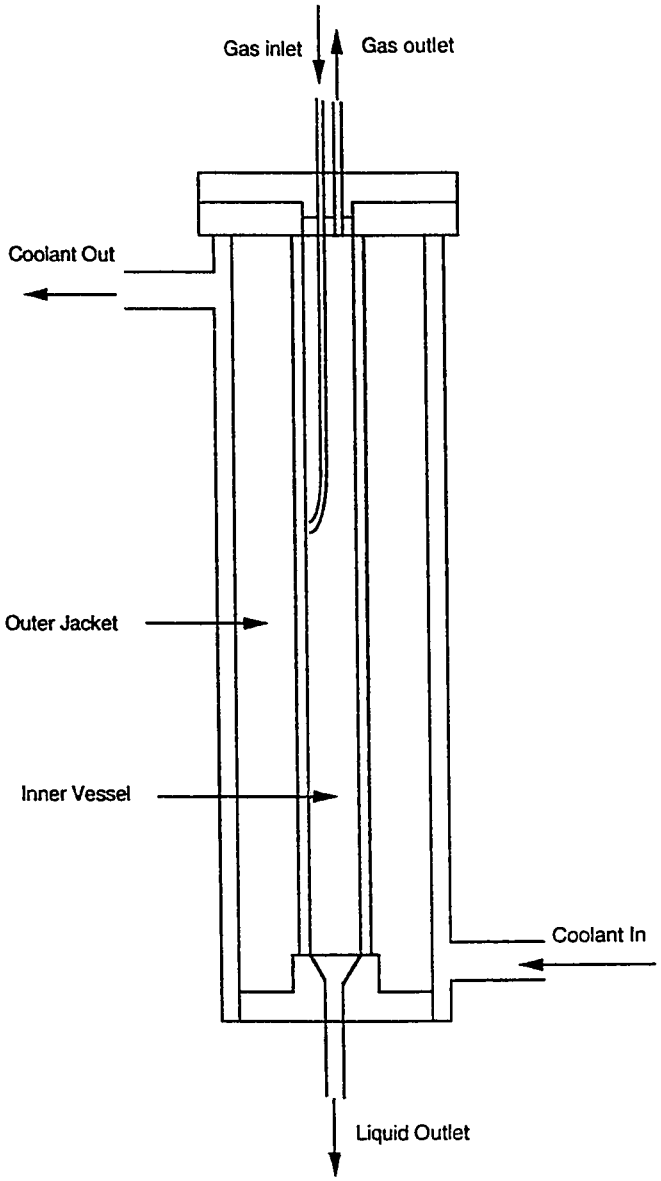

Figure 3.5 Gas Liquid Separator

products were collected through down flow drain valve located at the bottom of the separator. Gaseous products were led through the heat-insulated, 1/4" stainless steel tubing to either the gas chromatograph for the on-line analysis or to the wet test meter for measuring the flow-rate.

3.4.2 Catalytic Evaluation for Methyl tert-Butyl Ether

Materials.

Methanol (B&J HPLC grade), with a minimum purity of 99.9% containing less 0.03% water and isobutene (Fluka AG), with a minimum purity of 99.9% were used with out further purification. Nitrogen with a minimum purity of 99.998% was used to purge the reaction system. Catalyst samples with a particle diameter in the range of 0.600 and 1.18 mm were used. They were obtained by crushing the pellets of synthesized high-silica zeolites in the hydrogen form and sieving them.

Procedure

The reaction of methanol and isobutene for the synthesis MTBE is fairly exothermic. It consists of feeding into the reactor at a given temperature a mixture of methanol and isobutene whose composition corresponds to the required weight hourly space velocity (WHSV) and methanol to isobutene molar ratio. The WHSV was varied either by taking the required amount of catalyst for the fixed amount of the total feed or vice a versa. The experimental procedure consists of the following:

A catalyst bed (3.0-5.5 g of catalyst particles; hight , 7-12 cm) was prepared by placing the catalyst in the middle of the reactor tube. The rest of the tube was filled with glass wool. The reactor was fixed into the three zone heating furnace. The temperature was controlled by three PID controllers, receiving signals from thermocouples located in the middle of each zone of the furnace.

The catalyst was calcined *in situ*, for four hours at 500 °C in air flow of 100 cm^3/min with a heating rate of about 5 °C/min. After the calcination, the reactor was cooled to the desired temperature (75-150 °C) by flowing nitrogen at rate of 100 cm^3/min.

In each run, methanol and isobutene were fed to the reactor through a preheater maintained at 80 °C. The reaction temperature was monitored using a thermocouple located inside the reactor tube at the center of the catalyst bed.

Gas phase reaction, at the range of temperature mentioned above and at atmospheric pressure, was carried out. The reaction was allowed to run till steady state was reached (normally 2-4 hours). Liquid products were collected in a chilled vessel (at -5 °C). Unreacted isobutene was measured and vented to atmosphere.

Analysis

Liquid and gas samples were analyzed by a Perkin Elmer gas chromatograph (Model 8700). A stainless steel column (2 m long; 1/8 in internal diameter) packed with Carbowax 20M 10 % (60/80 mesh) was used with helium (PHGL, He UN 1046) with a minimum purity of

99.998% as carrier gas flowing at a rate of 30 ml-min^{-1}. Column temperature was held at 50 °C for 2 min, increased at a rate of 10 °C/min up to 100 °C, and held for 2 min. For the quantification of the product, internal standard method was used. In this method n-propanol (HPLC grade, Merck), 10 % by weight was added to the liquid product and 0.5 ml of the sample was injected through liquid sampling port of the GC. For the gas phase analysis a heat traced line was attached to the gas sampling port. Therefore, the same gas chromatograph was used on-line, during the run. The material balance was >99.5% for all the experiments.

3.4.3 Catalytic Evaluation for Methanol to Olefins Reaction

Catalytic testing for methanol to olefin (MTO) using some of the synthesized and modified zeolites were carried out by adopting similar procedure as described in the previous section. Methanol was fed to the reactor via a calibrated high pressure piston pump and vaporized in a stream of dry nitrogen to give a controlled feed rate of methanol/N_2. The reaction conditions are summarized in Table 3.5.

Table 3.5 Reaction Parameters for MTO Testing

Catalyst Weight	2.5 g
Methanol Flowrate	10 g/h
Nitrogen Flowrate	100 cc/min
Preheater Temperature	175 °C
Reaction Temperature	375 °C
Reaction Pressure	1 atm
Cooler Temperature	1 °C

The methanol to olefin reaction products consisted of gaseous and liquid phases. The liquid phase usually comprised of two distinct organic and aqueous layers which were separated for analysis.

The gaseous products were analyzed by gas chromatography using Hewlett Packard model HP 5880A Series gas chromatograph. In this GC, three separate columns were used for various components. A 29 ft Bis(-2-methoxy ethyl) Adipate and DC 200 column was utilized to separate C_6,C_5,C_4 and C_3 hydrocarbons. In the second stage, 6 ft Porapak Q column separates C_2 's and CO_2 while a 10 ft Molecular sieve 13X was used at the third stage to separate CO, CH_4, N_2 and O_2. All columns in the 5880A-HP GC were in 1/8 in. OD stainless steel.

The organic layer was separated from the aqueous layer and analyzed by GCMS which gave qualitative analysis of almost all the

hydrocarbons present in the liquid. The aqueous portion of the liquid product, which also contained unreacted methanol, was analyzed using Karlfisher titration (Mettler DL18). This method gave accurate quantitative analysis of water in a mixture. From the results of Karlfisher titration, the amount of unreacted methanol was determined, which was, in turn, used to calculate product yields and conversion.

CHAPTER 4

RESULTS AND DISCUSSION

In this chapter the results of hydrothermal synthesis of high-silica zeolites (HSZ), their modifications and catalytic evaluations for MTBE and methanol to olefins (MTO) reaction will be reported and discussed. Sample description with codes is given in Table 4.1.

4.1 Synthesis of High-Silica Zeolites

Major factors affecting the hydrothermal synthesis of high-silica zeolites were evaluated using the Plackett and Burman experimental design. Here, the IR crystallinity and BET surface area were used as the response variables. The presence of absorption bands at 550 cm^{-1} (band A) and at 450 cm^{-1} (band B) were used as a measure of crystallinity [212]. The IR spectra in the framework absorption region, for some selected samples (a prefix PB is used before the run number), are shown in Figure 4.1. These spectra are typical of silicate materials, with absorption bands at 1200-1150 (sh), 1100-1020 (vs), 800-700 (mw), 650-510 (m), 480-430 cm^{-1} (s). According to the Flanigen-Khatami-Szymanski correlation [213], the absorption near 1100, 700, and 450 cm^{-1} are assigned to internal vibrations of SiO_4, AlO_4 tetrahedra and also present in silica and quartz. The 650-510 cm^{-1} band was empirically assigned to the presence of double-rings of tetrahedra in the framework [213]. The 1200-1150 cm^{-1} band due to an external asymmetrical stretching vibration was observed at

Table 4.1 Description of samples with codes.

Catalyst Code	Description
HSZ-25 HSZ-50 HSZ-75 HSZ-100	High-silica zeolite; the numeric value is indicating the approximate Si/Al ratio
AF-HSZ	Aluminum free high-silica zeolite
Cr-HSZ	Chromium containing HSZ (Si/Cr ratio 100)
Cu-HSZ	Copper containing HSZ (Si/Cu ratio 100)
Fe-HSZ	Iron containing (Si/Fe ratio 100)
PB-1 to 22	Samples of Plackett-Burman experimental design
HSZ-20N	Isothermal synthesis at 160 °C for 4 days; composition similar to that of PB-20

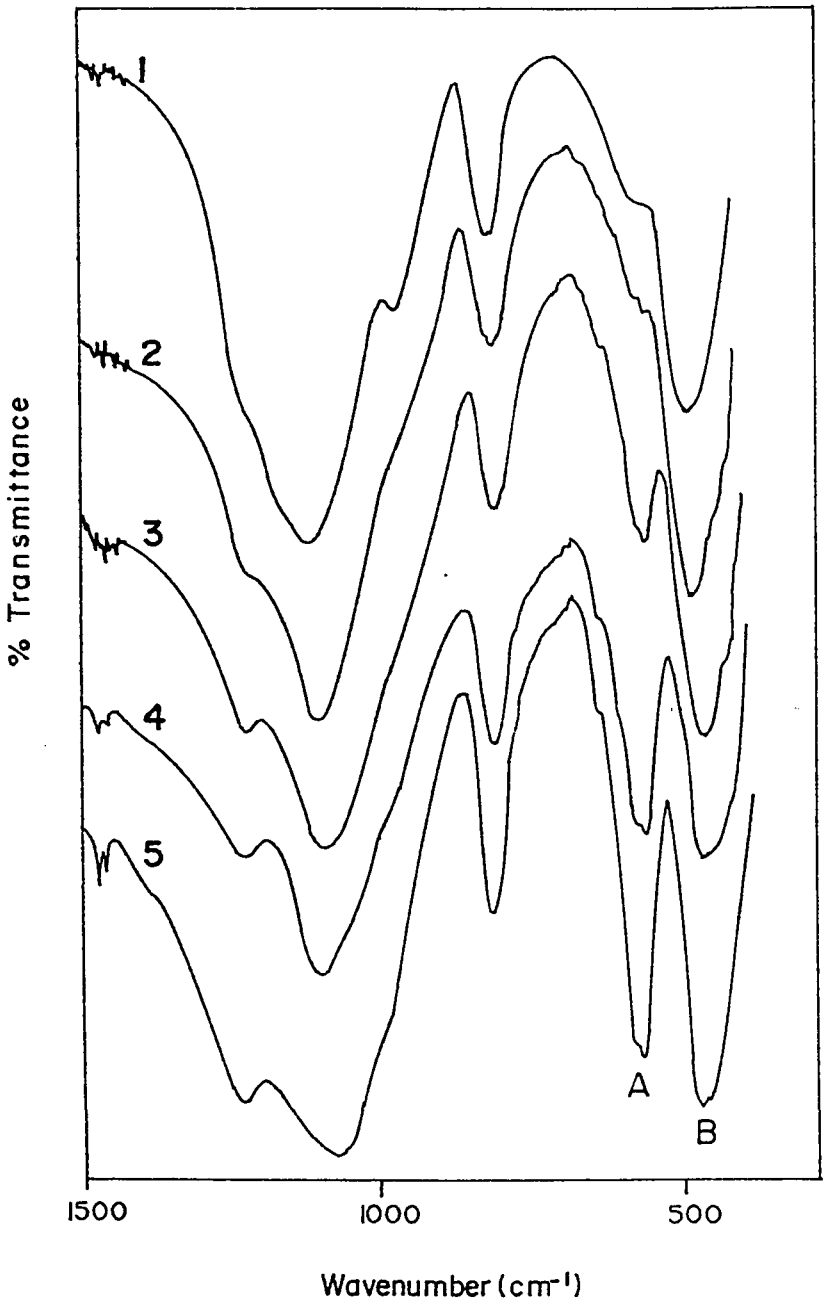

Figure 4.1 FTIR spectra of as-synthesized form of high-silica zeolites: (1) uncrystallized gel; (2) PB-1; (3) PB-5; (4) PB-8 and (5) PB-2 (Absorbance band A is at 550 cm^{-1} and B at 450 cm^{-1}).

a high frequency (1225 cm^{-1}) in our studies. This shift, also found in ZSM-5/11 or mordenite zeolites, could be correlated to a high-silica ratio [214] or to the presence of five-membered rings[215].

As silica does not show any absorption near 550 cm^{-1}, the A:B band ratio may be a good probe to characterize the presence of a zeolite framework. Quantitative IR data are usually unreliable but for a well crystallized sample (specially ZSM-type), the A:B ratio is close to 0.8 [212]. If amorphous silica is present, this ratio will be less than 0.8 in proportion to the amount of disordered silica. The data should also be qualitatively supported by XRD to ensure that no other types of zeolites were present that could contribute to the intensities of these bands.

4.1.1 Experimental Design

Plackett-Burman experimental design (Section 3.1.1) was successful to screen the important variables involved in the synthesis of zeolites. The experimental results of 16 runs are listed in Table 4.2. The IR data show that the A:B (550 cm^{-1}/450 cm^{-1}) band ratios are between 0.0 to 0.834, indicating amorphous to well crystallized (~100%) zeolites, respectively. Similarly the measurements of BET surface area show a broad range, from 0.4 to 333 m^2/g. Based on these results, the Plackett-Burman analysis (shown in Table 4.3) clearly indicates that three variables are significant in the case of IR crystallinity. These variables are: amount of NaCl, the pH and the reactor stirring. However, the results based on the surface area measurements, indicate the heating rate to another important variable in the synthesis of high-silica zeolites in addition to the above

Table 4.2 Results of Plackett-Burman Experimental Design.

Run. No	Absorbance Ratio (A:B)	Surface Area (m^2/g)
1	0.0	25.0
2	0.829	308
3	0.050	17.9
4	0.705	175
5	0.308	70.1
6	0.807	265
7	0.742	167
8	0.831	325
9	0.0	3.35
10	0.629	195
11	0.612	226
12	0.702	244
13	0.809	259
14	0.552	164
15	0.0	0.40
16	0.785	333

Table 4.3 Effects of Variables on Crystallinity and Surface Area.

	Effect on Abs.	Relative significance		Effect on S.A.	Relative significans	
Variable	(-) to (+)	*t*-test	Confidence(%)	(-) to (+)	*t*-test	Confidence(%)
A	-0.064	-1.1		-6.529	-0.191	
B	-0.202	-3.33	97	-62.34	-1.827	89
C	0.0209	0.344		-22.49	-0.659	
D	-0.414	-6.82	99	-146.0	-4.280	97.5
E	0.138	2.29		38.95	1.142	
F	-0.0021	0.035		-27.64	-0.810	
G	0.0643	1.06		31.70	0.929	
H	-0.1371	-2.262		-38.38	-1.125	
I	-0.1486	-2.452		-45.13	-1.323	
J	-0.1686	-2.790		-68.13	1.979	90.5
K	0.2503	4.132	96	82.06	2.406	92.5
L	0.1619	2.672		40.36	1.183	
M	-0.0761	-1.25		-59.33	1.738	
N	0.0783	1.29		12.05	0.353	
O	-0.0271	-0.448		-48.38	-1.418	

Variable: (A), Silica/alumina ratio; (B), NaCl; (C), NaOH; (D), pH; (E), Template; (F), Order of addition; (G), Dummy; (H), Homogenization of gel; (I), Aging; (J), Heating rate; (K), Reactor stirring; (L), Maximum temperature; (M), Cooling; (N) and (M) are Dummy.

three. The similarity between these results was expected because for the well crystallized samples the surface area must also be high.

The samples with very low surface area were found to be amorphous or less crystalline as observed by SEM and XRD. When these samples were calcined, the products turned gray in color. This shows that partially decomposed organic template could not escape from the material because of the unavailability of well-defined pore structure of amorphous particles. The samples remained gray even for prolonged heating at higher temperature. Due to the blockage of the pores, the surface area was found to be very low as compared with the highly crystalline samples. The crystalline zeolite samples remained white after calcination, which showed that the organic template was removed completely. The latter was confirmed by the carbon analysis of the calcined samples.

In Figure 4.2, IR absorbance ratio (A:B) is plotted against the BET surface area. The data were fitted to a third order polynomial having a correlation coefficient of 0.982 which indicates a sound correlation exists between IR absorbance ratio and BET surface area. It is observed that the correlation is not strong around 0.6 IR absorbance ratio. This anomaly can be attributed to the inhomoginiety of the sample which comprised of amorphous and crystalline phase mixture and amorphous could be blocking the pores of the zeolite.

A scanning electron micrograph of a partially crystalline sample (PB-11) having absorbance ratio of 0.612, is shown in Figure 4.3a. The

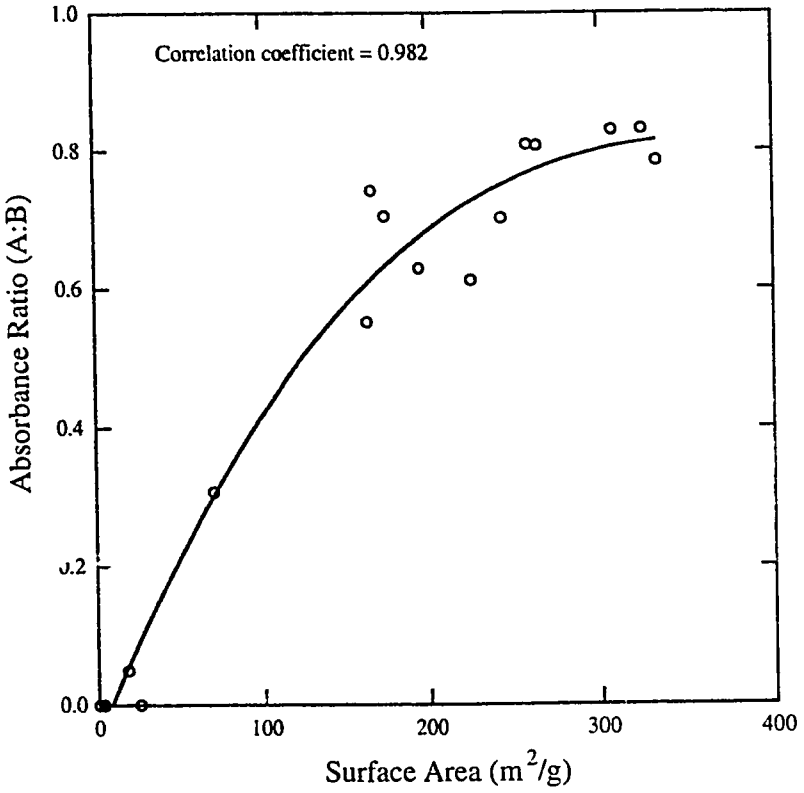

Figure 4.2 Correlation between BET Surface Area and Absorbance Ratio (I.R. Crystallinity) of synthesized High-Silica Zeolites.

a

b

Figure 4.3 SEM of synthesized high-silica zeolite: (a) partially crystalline (PB-11); (b) crystalline (PB-21).

micrograph shows the zeolite crystals are embedded in the bulk, amorphous gel phase. The surface area of such a sample, after calcination is not well correlating with the IR crystallinity which was measured before calcination. Figure 4.3b shows the scanning electron micrograph of a well crystallized (100%) sample (PB-21). The crystals are about 1.5 x 2.1 micro meter in size. The particle size distributions of both the samples are shown in Figure 4.4. The analysis shows that a fairly homogeneous distribution with narrow range of crystal size. In this case, the BET surface area is correlating well with IR absorbance ratio. On the other hand, partially crystalline sample (Figure 4.4a) shows a broad distribution of particle size.

The confidence limit for selecting the variable was 98.5%. The reason for such a high value is that the low and high limits of the variables were quite close between themselves as compared to the reported ranges for such parameters (for example, ZSM-5 could be crystallized with or without template, and SiO_2/Al_2O_3 ratio between 15 to infinity). And also, the experiments with the important variables, other than pH, showed little or no effect on the crystallinity of the zeolite formed. For example, reactor stirring was the second most important variable found in the case of surface area measurements as response variable. The experiments conducted at very low stirring rate or even at unstirred condition gave crystalline zeolite product. Hence, the values below 98.5% confidence level for the variables were rejected and not considered as important within the limits investigated. Therefore, the effect of pH being the most important variable found, on crystallization of high-silica zeolite was

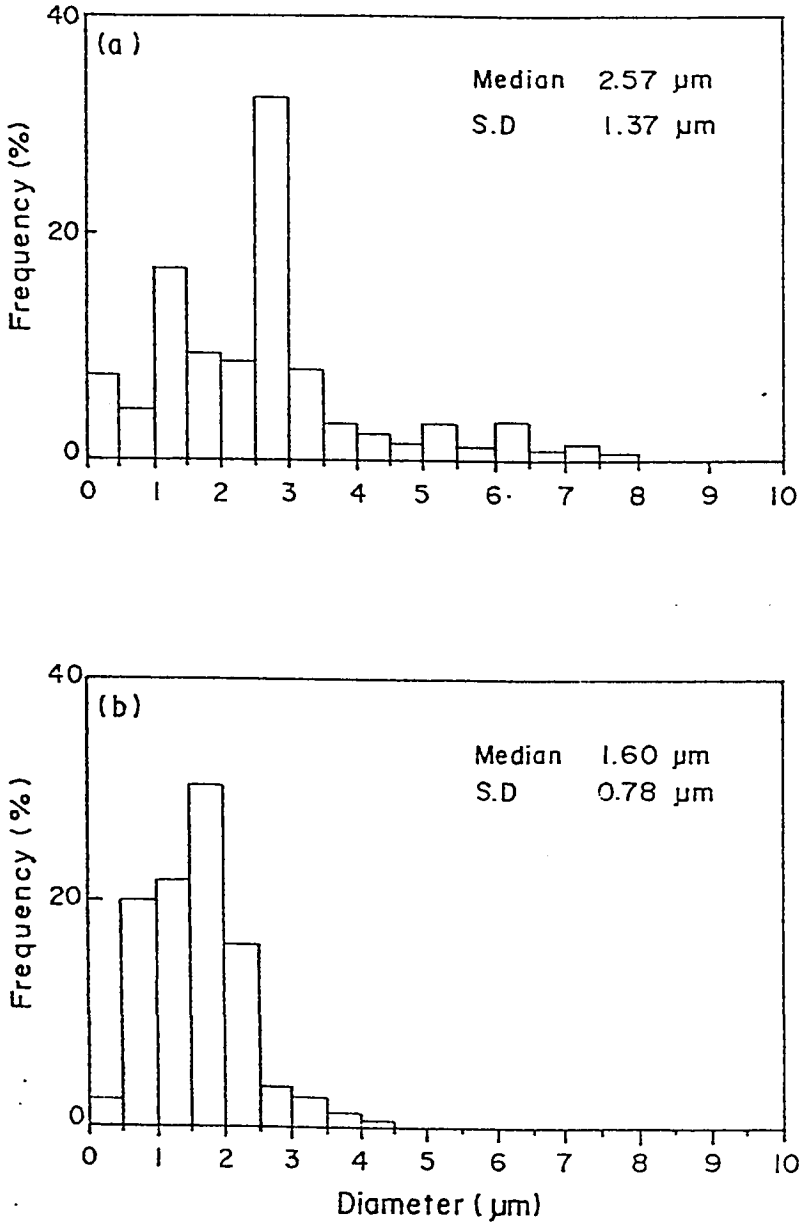

Figure 4.4 Particle size distribution of synthesized high-silica zeolites: (a) partially crystalline, (PB-11) and (b) crystalline, (PB-20).

further studied in detail and the results are discussed in the following section.

4.1.2 Effect of pH on Crystallization

The rate of crystallization is influenced by the alkalinity of the system which was found to be the most important variable in the synthesis of high-silica zeolites. An increasing OH^- ion concentration will generally accelerate crystal growth and shorten induction period before viable nuclei are formed. Table 4.4 shows the effect of pH, at constant level of other variables, on the BET surface area and IR crystallinity. Raising pH of synthesis mixtures using OH^-, mainly influences the crystallization of high-silica zeolite in a positive way within the synthesis field. As depicted in Figure 4.5, increasing the pH shows an increase in the crystallinity and the surface area of the high-silica zeolites synthesized.

The crystallization field was found to be limited by the maximum value of pH 10.3. Above this pH value, hard solid lumps were formed which were dissolved by boiling in concentrated NaOH (50%) for few hours. In some cases, (Si/Al ratio > 4500) even the pH of 10.3 caused the formation of hard lumps. The change in BET surface with an increase in pH suggests that there is a minimum threshold value for pH (around 9.0) above which a sharp increase in the surface area was found and then it reaches a maximum value around pH of 10. This indicates that pH of about 9.0 is needed for the solubility of silica (polymeric forms) to start nucleation process. The change in the slope of curve around pH 10.0

Table 4.4 Effect of pH on IR crystallinity and BET surface area.

Run No.	pH	Absorbance Ratio (A:B)	Surfac Area (m^2/g)
PB-17	8.0	0.05	24.0
PB-18	9.5	0.61	240
PB-19	9.7	0.69	307
PB-20	10.0	0.76	314
PB-21	10.3	0.79	320
PB-22	10.5	*	*
HSZ-20**	10.0	0.81	330

* Hard solid lumps formed.

**Conventional crystallization method.

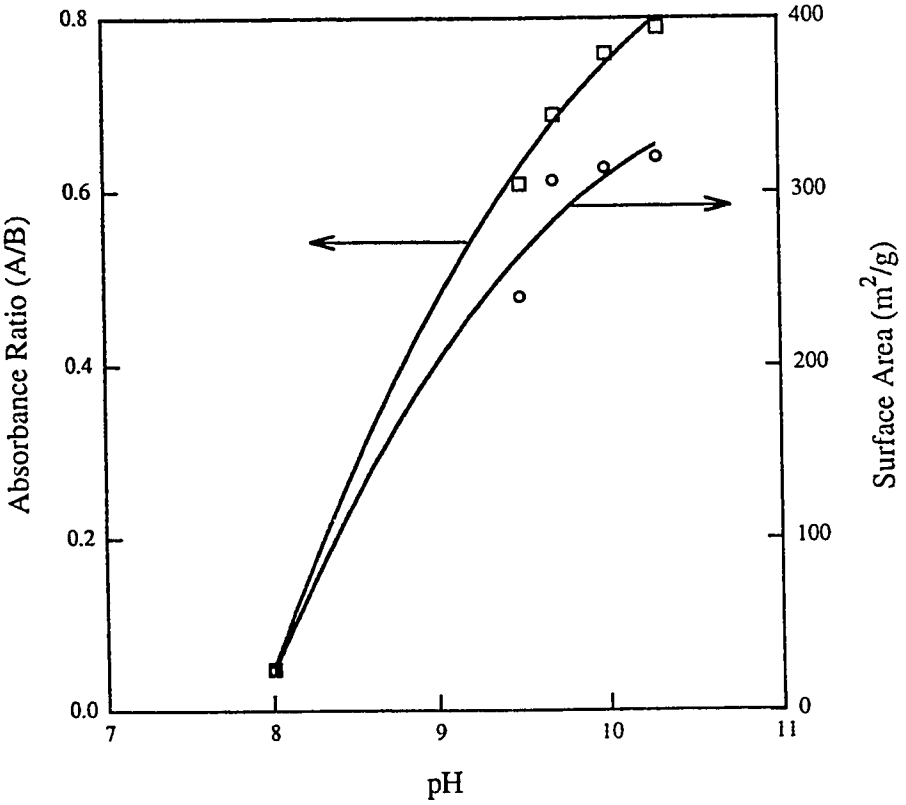

Figure 4.5 The effect of pH on IR crystallinity (Absorbance Ratio) and BET Surface Area.

indicates the growth of crystals is relatively a slower process. The growth of crystals reaches a maximum when the nutrients (mainly SiO_2) are being exhausted. The removal of SiO_2 from the gel mixture, accompanied by the formation of zeolite framework structure, increases the pH of the final mother liquor. This effect will further be discussed in Section 4.3.1.

4.1.3 Comparison of Rapid Crystallization with Conventional Crystallization Method

The narrow crystal size distribution results from short crystallization time (about 2 h) as compared with the conventional synthesis method (for example, for ZSM-5, 20 h-7 days). The crystal size distribution of the sample prepared by conventional synthesis method (HSZ-20N) is given in Figure 4.6b. The synthesis was carried out for 4 days at 160°C with sample mixture composition as used for PB-20. Figure 4.6a shows the particle size distribution of the sample PB-20. The median of the distribution is 1.31μm with a standard deviation (SD) of 0.57μm as compared with fairly large value of SD 1.49μm for the particle size distribution of HSZ-20N. Although, the average particle size in HSZ-20N is smaller than that produced by rapid crystallization method, the distribution is showing a broad range of particle sizes (0.50-7.00 μm). Similar results were obtained by scanning electron microscopy. Figure 4.7 shows the SEM photographs for the samples prepared by rapid crystallization method (4.7a) and by conventional synthesis procedure (4.7b). Crystals of regular size and shape are distinctly visible in Figure

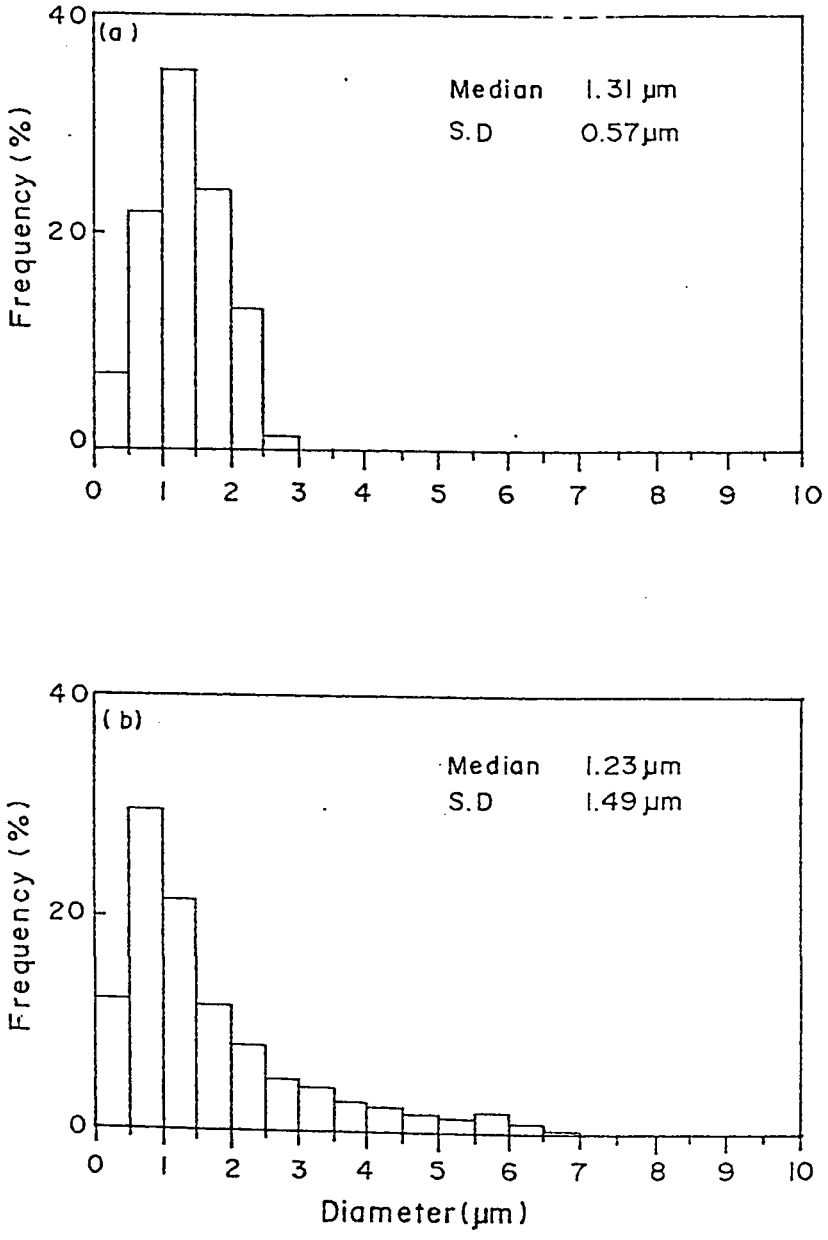

Figure 4.6 Particle size distribution of synthesized high-silica zeolites: (a) Rapid crystallization, time 2 h, (PB-20) and (b) Conventional crystallization, time 4 d, (HSZ-20N).

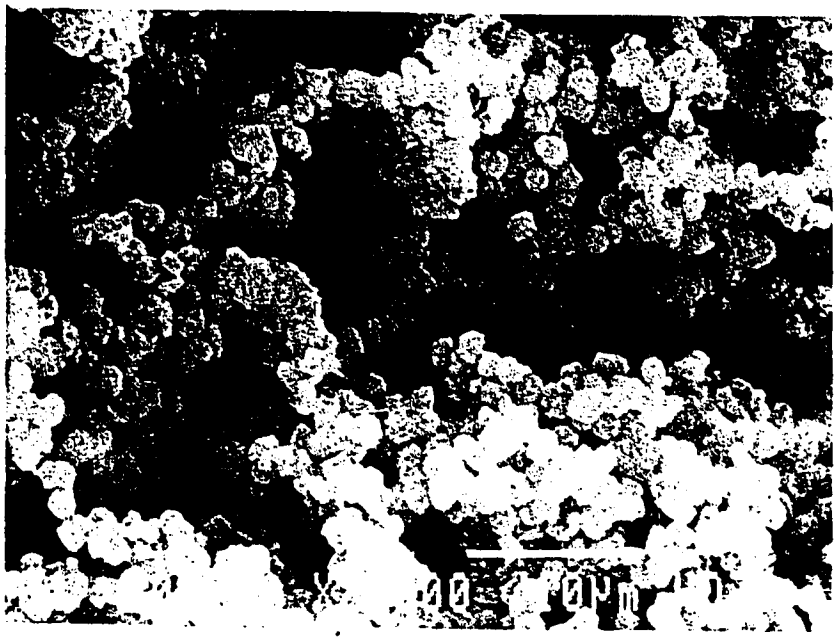

a

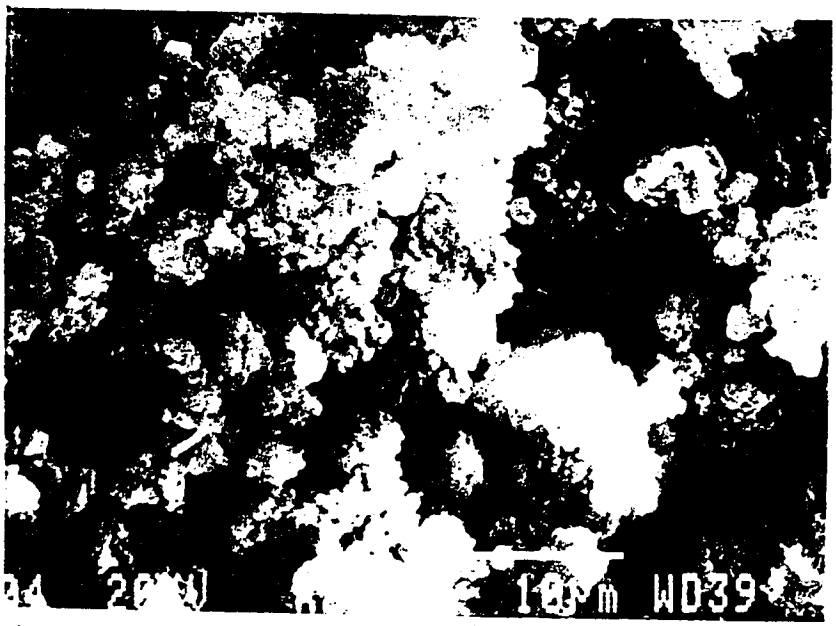

b

Figure 4.7 SEM of synthesized high-silica zeolite: (a) rapid crystallization (PB-20); (b) conventional crystallization method (HSZ-20N).

4.7a, where as crystals of different size and shape are present in the sample prepared by the conventional method.

However, the results of IR crystallinity and BET surface area measurements (given in Table 4.4) were comparable for the samples prepared by rapid crystallization and conventional crystallization methods. This was because the crystallization was almost complete and all of the gel transformed into crystalline material giving high surface area (> 300 m^2 /g).

X-ray diffraction pattern for the synthesized high-silica zeolites, using tetrapropyl ammonium bromide as a template is similar to that of MFI (Mobil-Five) type zeolites. ZSM-5 and silicalite-I are the two well known zeolites commercially produced by Mobil Oil Corporation and Union Carbide, respectively, comprising this class of zeolites. Figure 4.8 shows a typical X-ray diffraction pattern for the as-synthesized high-silica zeolite (HSZ-100) and the simulated XRD pattern taken from the publication of structure commission of the International Zeolite Association [216]. The $\alpha - Al_2O_3$ was used as an internal standard for the accurate measurement of d - spacing. Peaks around two theta 22.5°-25.0° are the characteristic peaks of MFI type structure and their intensities could be used as a measure of crystallinity of the zeolite. Unit cell dimensions were calculated and found to be comparable with the literature values. Other information like phase transition and aluminum content of the framework structure were also obtained from the XRD

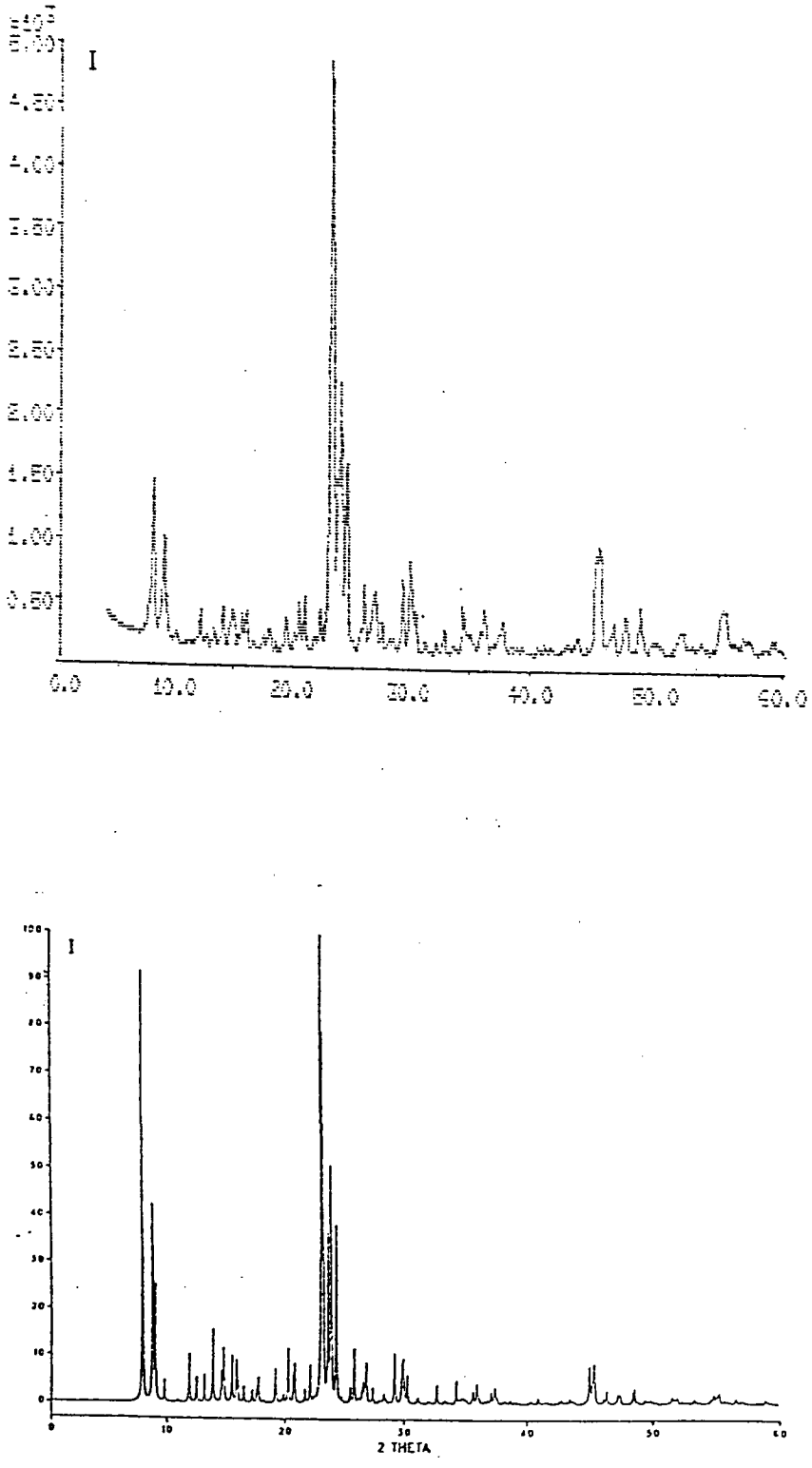

Figure 4.8 XRD pattern of high-silica zeolite: top, as-synthesized HSZ-100; bottom, simulated pattern of MFI zeolite.

pattern of the calcined and H-form of the zeolite samples, respectively. The results will be discussed in the following sections.

4.2 Modification of High-Silica Zeolite

The recent trend in zeolite chemistry is the "tailor made" catalysts produced by adopting different modification procedures. These procedures include modifications at the crystallization stage and post - synthesis modifications. These modifications were applied to further control the acid activity and/or the shape selectivity of a specific zeolite structure.

In our work both types of modifications as mentioned above, were applied. The first one include the synthesis of high-silica zeolites with various Si/Al ratios, to achieve varying acid activity. The second method was incorporation of various metals into the zeolite structure during the synthesis. This could lead to the desired activity and shape selectivity for methanol to olefin (MTO) conversion reaction. The third method used was hydrothermal modification or steaming. The last method may be considered as post synthesis modification procedure.

For each method of modification, a number of characterization techniques have been applied to qualitatively and/or quantitatively identify the resulting changes occured in the zeolite. These techniques include elemental analysis, infrared spectroscopy, BET surface area, X-ray diffraction, scanning electron microscopy, acidity measurements (TPD of

ammonia and FTIR of pyridine adsorption), thermal analysis and electron spin resonance. Of all the techniques utilized, catalytic evaluation remains to be the most powerful tool to discern the effect of the modification methods on the properties of the zeolites. In the following sections results of various methods of modifications will be discussed.

4.2.1 Modification by Varying Si/Al Ratio

High-silica zeolites of various Si/Al ratio were prepared. The lowest Si/Al ratio successfully crystallized was 25. Below this the crystallinity was found to be very low. On the other, hand highly crystalline zeolite samples were prepared with Si/Al ratio as high as 4500 and even without adding aluminum salt into the crystallizing mixture (Al free condition). It was observed that the rate of crystallization is influenced by the Si/Al ratio. The results of IR crystallinity and the amount of template occluded into the zeolite crystals correlate to the Si/Al ratio of the final product. Figure 4.9 shows the correlation of Al content per unit cell and the template (TPA^+) per unit cell of the high-silica zeolite. The curve is a second order fit to the data with correlation coefficient of 0.994. The amount of template incorporated, decrease with increasing aluminum content per unit cell. This indicates that at lower Si/Al ratio the crystallization is slower and the number of TPA cations per unit cell of high-silica zeolite is less than the values reported in the literature (3.3 to 3.8 for MFI zeolite [217].). Whereas, at higher Si/Al ratios (Al content <1/u.c.), time of crystallization being constant (about 2 hours), the amount of template occluded reaches its maximum. The sample

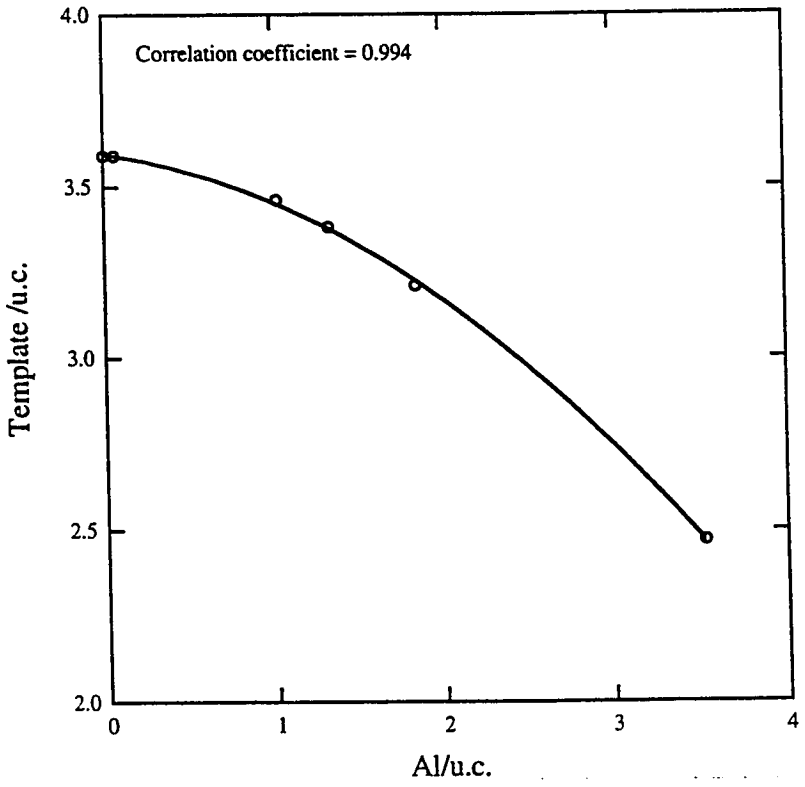

Figure 4.9 Correlation between Al content per unit cell and template content (TPA^+) per unit cell.

with low Si/Al ratio was found comparatively less crystalline as shown in Figure 4.10. Hence the amount of template was relatively lesser than that for the highly crystalline sample. Another interesting correlation was observed between the difference of initial and final pH of the crystallizing mixture and the IR crystallinity of the zeolites formed. Figure 4.10 shows the relation between pH difference (Δ pH) and IR crystallinity. The curve indicates that pH difference increases as the crystallization is completed.

It is mentioned in the literature for high-silica zeolite EU-1 [58], pH increases with the course of crystallization. This rise in pH was attributed to the incorporation of SiO_2 units into the zeolite framework. As the crystals grow, a rise in free OH^-/silica ratio, defined as ([Na_2O] - [Al_2O_3]) /[SiO_2] , results. Similar results were obtained by the examination of SEM photographs and particle size distribution of the high-silica zeolites synthesized with various Si/Al ratios. Large well defined crystals grow when using a synthesis mixture with a lower aluminum content, as shown in Figure 4.11. This has also been observed by Gabelica et al. [218] and Romannikov et al. [65]. The latter authors also suggested an increase in crystallization rate with an increase of Si/Al ratio. Figure 4.11a shows aggregates of tiny crystals which grow to large relatively separate crystals as the aluminum content is decreased or the Si/Al ratio is increased (Figure 4.11c).

The correlation between the Si/Al ratio of the gel and the zeolite product by chemical analysis, is shown in Figure 4.12. The least square fit to the date is given by:

$$(Si/Al)_{zeolite} = 3.53 + 0.777(Si/Al)_{gel}$$

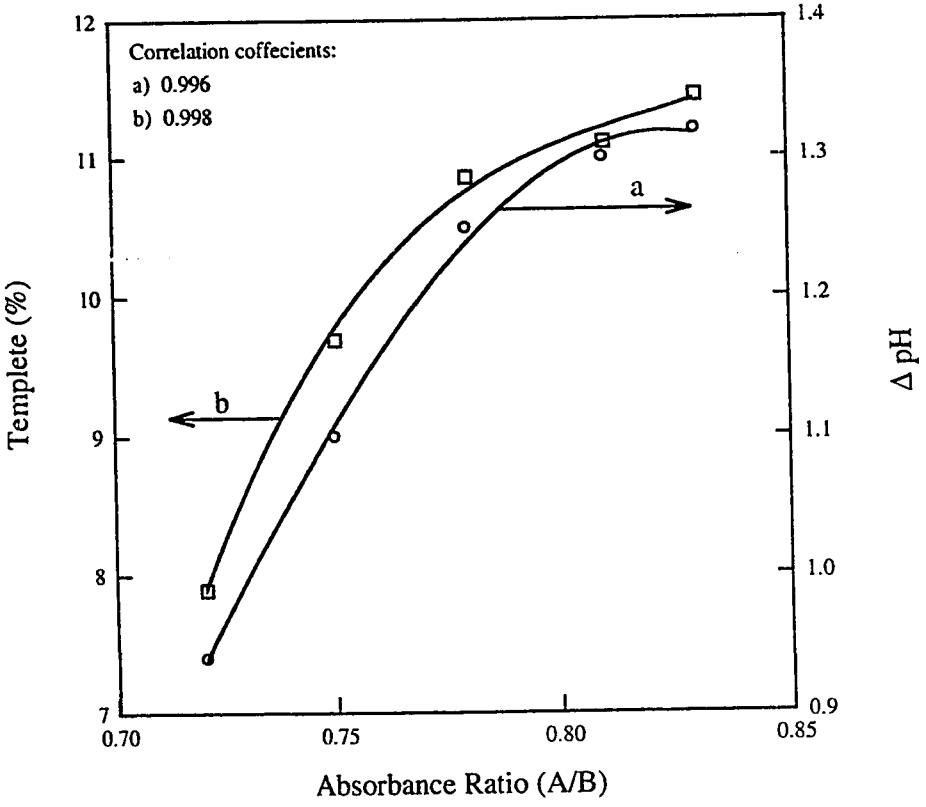

Figure 4.10 Correlation between IR crystallinity (Absorbance Ratio), Template (%) and difference of pH.

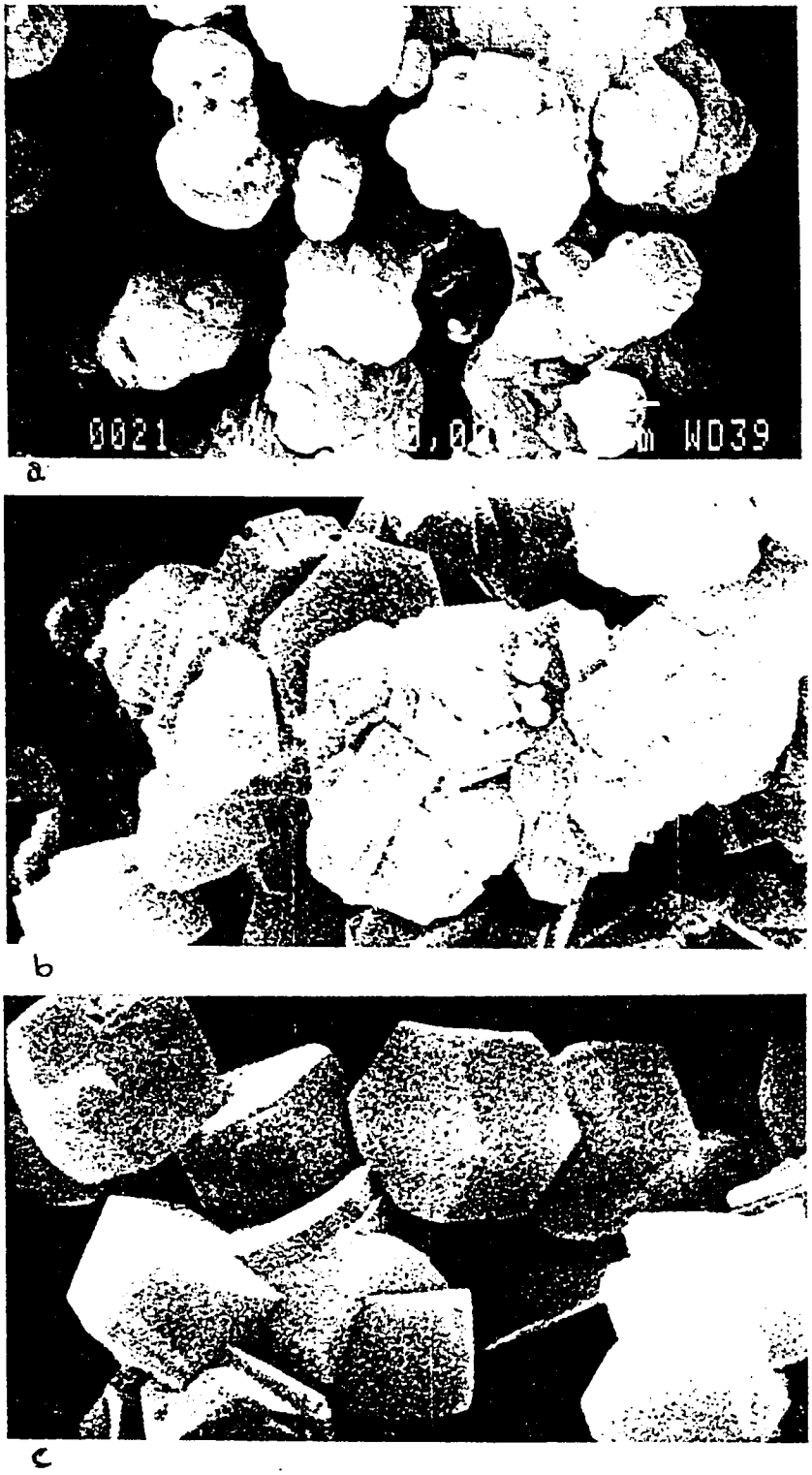

Figure 4.11 SEM of as-synthesized high-silica zeolites: a, HSZ-25; b, HSZ-100; c, AF-HSZ.

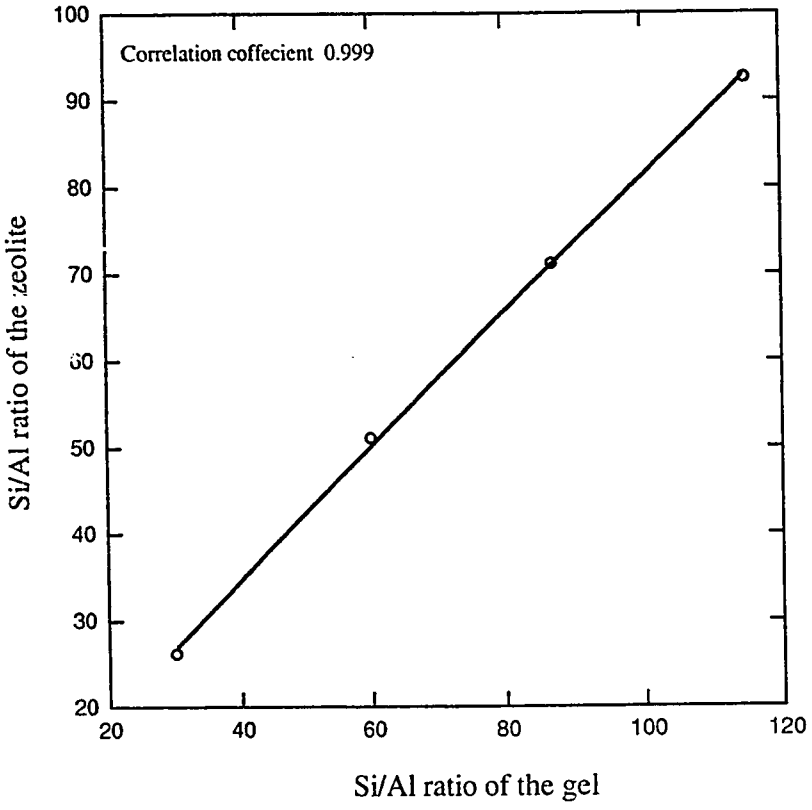

Figure 4.12 Chemical analysis data, plotted as Si/Al ratio of gel vs. Si/Al ratio of zeolite product.

The slope of the curve is less than unity for all compositions. This indicates that Si/Al ratio of the zeolite is always less than Si/Al ratio of the corresponding gel. Thus it can be concluded that aluminum is preferably incorporated in the solid material. This was further confirmed by the chemical analysis of mother liquor, in which aluminum was not detected whereas some of the unreacted silica was remained in the liquid.

A simple correlation was established between the content of zeolite (by chemical analysis) and difference of the two peaks appeared at 2θ 45.0° and 45.5° in the XRD pattern. The XRD patterns were scanned for the H-form of synthesized high-silica zeolites. Figure 4.13 shows the correlation between Al_2O_3 (%) and Δ (°2θ). The least square fit to the data is given by:

$$\% Al_2O_3 = 10.7 - 19.0 \Delta$$

This relation will be used for determining aluminum content of the steam modified samples (Section 4.3.3).

Thermal analysis reveals information concerning the structure and stability of zeolites, which is important for the industrial application of these materials as catalysts and adsorbents. Simultaneous thermal analysis methods (TG-DTA-DTG) gave quantitative information on the dehydration, decomposition of organic template and high - temperature framework stability of the selected synthesized high-silica zeolites.

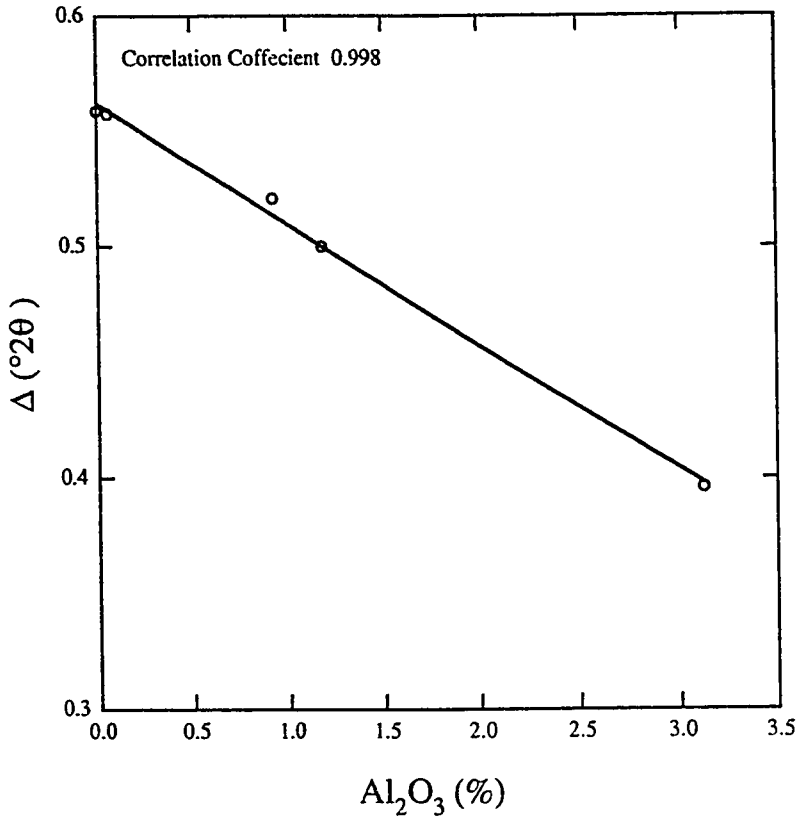

Figure 4.13 Correlation between peak spacing Δ 2 Theta (45.0°-45.5°) and Al_2O_3 (Wt %) of H-form high-silica zeolites.

Figure 4.14 shows a typical combined TG-DTA-DTG thermogram of the synthesized high-silica zeolite (HSZ-100). The DTG curve shows a weak negative peak, for which it was difficult to determine the minimum. This peak is due to the dehydration of mainly physisorbed water in the range of 120-140 °C. A strong negative peak with a relatively sharp minimum at 422 °C was assigned to the removal of organic template incorporated into zeolite structure.

Differential thermal analysis curves for as-synthesized high-silica zeolites of various Si/Al ratios are shown in Figure 4.15. This figure shows an endothermic effect with a minimum at 120-140 °C and a very strong exothermic effect at 350-500 °C, with a shoulder at 438-442 °C and mixima at 470 °C. A sharp exothermic peak appear at higher temperature (>1075 °C).

The endothermic effect at low temperature is related to the removal of water which could be physically adsorbed on the zeolite surface.

The inspection of exothermic peaks on the DTA curves (Figure 4.15) reveals major transitions at 350-500 °C in the as-synthesized form of high-silica zeolites which is accompanied by weight loss, as summarized in Table 4.5. This positive heat effect is related to the oxidative decomposition of organic template stabilized in the zeolite framework structure. Note that pure tetrapropyl ammonium bromide melts with decomposition at 270 °C with a strong endothermic effect. Thus, it can be concluded that TPA cation is probably ionically bonded to the framework aluminum during the hydrothermal crystallization and get stabilized to the extent that it only decomposes at higher temperature. The decomposition

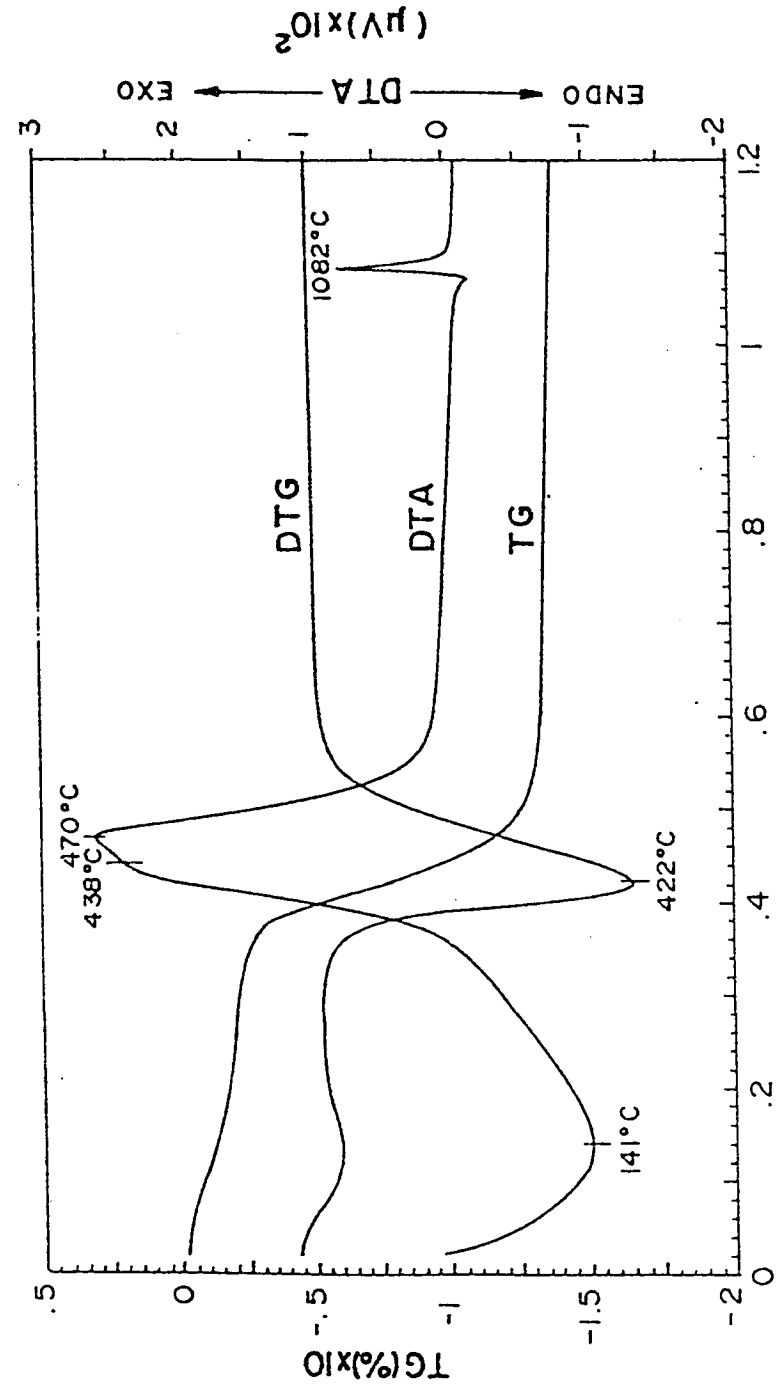

Figure 4.14 TG-DTA-DTG curves of as-synthesized high-silica zeolite HSZ-100.

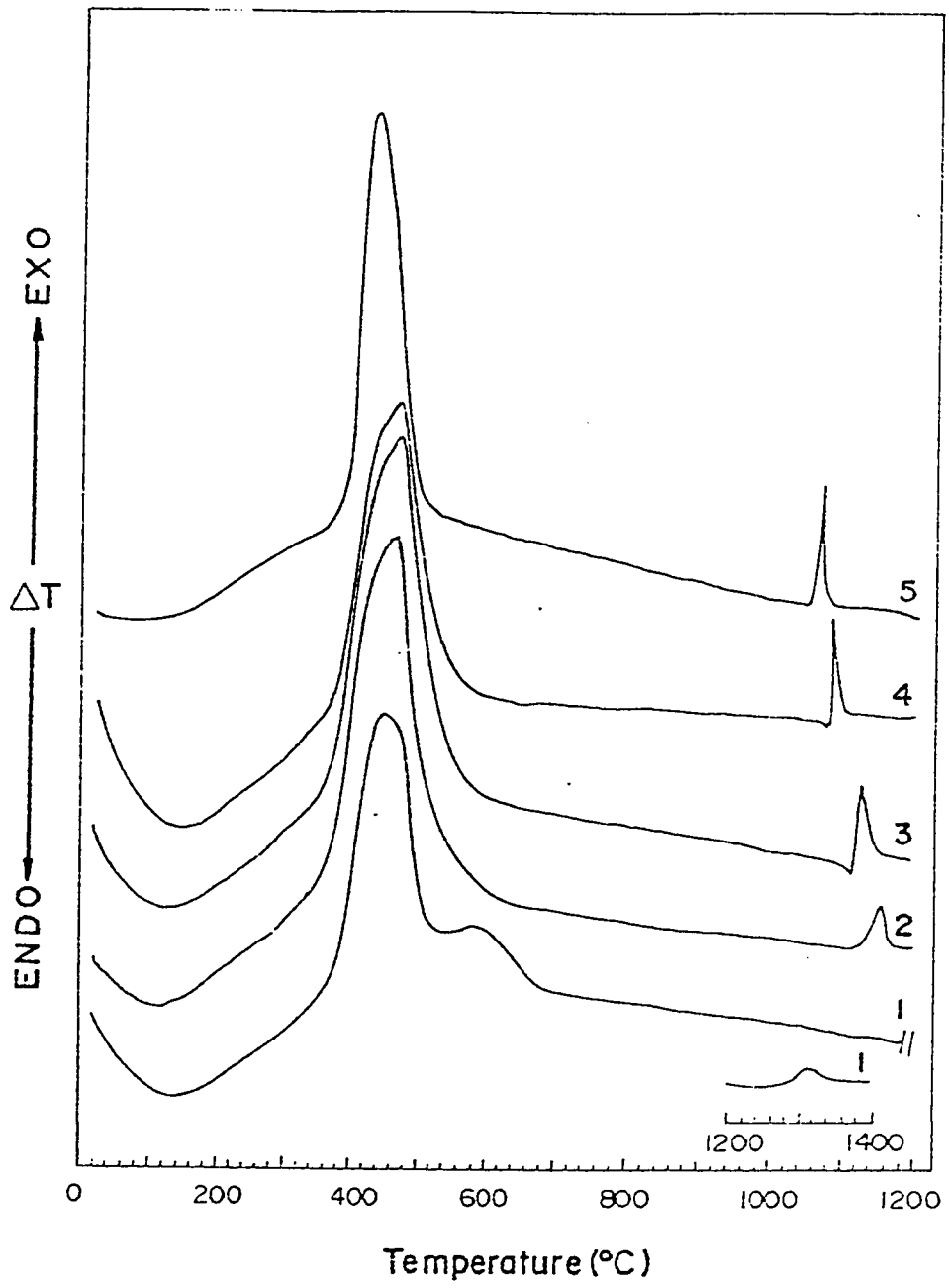

Figure 4.15 DTA curves for as-synthesized forms of high-silica zeolites: (1) HSZ-25, (2) HSZ-50, (3) HSZ-75, (4) HSZ-100 and (5) AF-HSZ.

Table 4.5 Thermogravimetric data for as-synthesized high-silica zeolites

Sample Code	Chemical Analysis		Thermal Analysis			
			H_2O Content		Organic Template	
	Si/Al	Na/Al	Wt. Loss[a] %	Mol./u.c.	Wt. Loss[b] %	Mol./u.c[c].
HSZ-25	26.2	0.75	2.60	8.42	7.90	2.47
HSZ-50	51.1	1.22	3.50	11.24	9.70	3.21
HSZ-75	71.2	1.57	1.96	6.29	10.87	3.38
HSZ-100	92.5	1.96	1.67	5.36	11.12	3.46
PB-2	1565	3.48	1.60	5.12	11.60	3.59
AF-HSZ	∞	0.08[d]	2.00	6.40	11.45	3.59

a Weight loss by TG between 25-225 °C
b Weight loss by TG between 250-630 °C
c Unit cell composition for calcined zeolite, $Na_n\ Al_n\ Si_{96-n}\ O_{192}$, was determined from chemical analysis
d Na wt. % (Na/Al ratio = ∞)

in constrained environment that is, channel intersections could also resist diffusion of product out. A shoulder peak at 442 °C was assigned by Crea et al. [219] to inner-ions neutralizing SiO^- negative charges of defect groups for ZSM-5 zeolite. The higher temperature peak (ca. 470 °C) was attributed to decomposition of TPA in "relaxed" form, although it also neutralizes SiO^- defect groups.

In curve 1 (Figure 4.15, HSZ-25), a relatively broad exothermic effect with a maximum at 595 °C appeared. This peak was accompanied with a weight loss of 2.3 % which is about 30 % of the total weight loss due to the template removal. This peak may be attributed to the TPA cation bound to the structural framework AlO4 tetrahedra. This peak disappears with the increasing Si/Al ratio or with decreasing Al content. Finally, in the aluminum free zeolite sample, a sharp single exothermic effect appeared at 432 °C which may be attributed to the decomposition of TPA bound to defect groups.

The silicalite, aluminum-free analog of ZSM-5, crystals obtained in alkaline conditions contains a large amount SiOR defect sites in their structure, where R = H^+ , alkali cation or TPA^+ [220]. The amount of defect sites can be as large as 32/u.c. in silicalite corresponding to about. 8 missing tetrahedral sites [221]. This means that macrocavities could be formed in these zeolites, where TPA cations are less strongly held than in the zeolitic channels promoting their thermal decomposition.

An exothermic effect at a temperature grater than 1070 °C is assigned to the partial collapse of the framework structure. This was also confirmed by the FTIR spectrum of the zeolite sample heated to that temperature in air. A substantial decrease in the peak intensity at 550 cm^{-1} band was observed which indicates loss of crystallinity due to high temperature heat treatment.

The sharpness of the exothermic peak indicates the crystallinity and homogeneity of the crystal size distribution. As shown in Figure 4.11, zeolite sample with low Si/Al ratio (HSZ-25) has aggregates of small crystals, in this case a relatively broad exothermic effect appear at 1306 °C. Where as, the aluminum free zeolite sample (Si/Al ratio ∞) gave a sharp exothermic effect at 1070 °C.

Increasing aluminum content shifted the high temperature exothermic peak to higher temperature. This behavior is contrary to that reported for high-silica zeolites in which a lower content of aluminum atoms in the lattice exhibits higher thermal stability [222]. A possible explanation is the lower number of defect groups for higher thermal stability of synthesized high-silica zeolites with lower Si/Al ratio. As mentioned earlier, the defect groups increase with increasing Si/Al ratio. This could lower thermal stability of the high-silica zeolites with high Si/Al ratio. The particle size can also affect the relative thermal stability. As the smaller crystals investigated contains probably much less defect than the larger less aggregated, crystals (Figure 4.11). Therefore, high-

silica zeolite with low Si/Al ratio, having less defect groups, are thermally more stable.

Acidity of H-forms of the synthesized high-silica zeolites was measured by temperature programmed desorption (TPD) of ammonia. The results are summarized in Table 4.6. Total acidity, measured as volume of ammonia adsorbed per gram of catalyst, is correlated to Si/Al ratio (aluminum content) of the zeolite catalyst. This was quite expected as the aluminum content of zeolite is responsible for the generation of acid sites. The inspection of TPD curves, shown in Figure 4.16, reveals at least two peaks in the zeolite sample with lowest Si/Al ratio investigated. The temperature of the peak indicates the strength of the acid sites. With increasing Si/Al ratio, the strength of acid sites decreases as marked by the shift of peak temperature toward the lower value. Another effect of Si/Al ratio was the disappearance of two peaks with decreasing aluminum content.

The appearance of two distinct peaks (HSZ-25), one at lower temperature and other at higher temperature, indicates the heterogeneity of Bröensted sites, which may occurred from differences in local composition or the distribution of aluminum atoms in the framework of zeolites. Different types of acidity depend on incipient steaming during calcination. Dealumination to varying extent with various samples could broaden the peaks. Some of the Bröensted sites are also expected to be associated with the Lewis sites.

Table 4.6 Results of temperature programed desorption of ammonia.

Catalyst Code	Total NH_3 Introd. (cc)	Total Area (a.u.)	Peak Area (a.u.)	Peak Temp. (°C)	Total Acidity (cc/g)
HSZ-25	13.51	14.99	4.94	324, 512	17.81
HSZ-50	9.65	10.80	2.88	492	10.29
HSZ-75	6.75	7.84	1.86	442	6.41
HSZ-100	6.75	7.85	1.40	438	4.82
S-350[a]	6.75	8.05	3.10	316, 490	10.40
S-500[b]	7.72	8.90	2.45	409	8.50

a Steam treated HSZ-25 (at 350 °C for 2 h)
b Steam treated HSZ-25 (at 500 °C for 2 h)

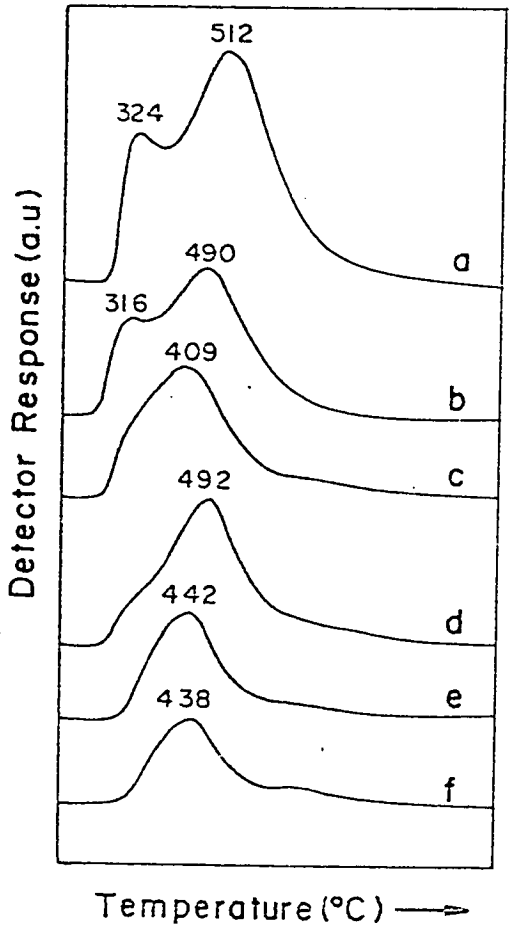

Figure 4.16 Temperature programmed desorption of ammonia for synthesized high-silica zeolites: (a) HSZ-25, (b) S-350, (c) S-500, (d) HSZ-50, (e) HSZ-75, (f) HSZ-100.

The shift in the peak temperature and gradual disappearance of the lower temperature peak suggest that the decrease of Lewis sites with the increasing Si/Al ratio takes place. That could result from lower aluminum content which provide less chances for neighboring aluminum atom in the framework structure of high-silica zeolites.

4.2.2 Modification by Metals Incorporation

High-silica zeolites were modified by incorporation of chromium, copper and iron during hydrothermal synthesis. The metal incorporation was evidenced by utilizing a range of analytical techniques. The results of the characterization methods will be discussed in this section.

The chemical composition of as-synthesized form of metal-containing zeolites and aluminum-free high-silica zeolite is given in Table 4.7. The Si/M ratios, where M = Cr(III), Cu(II), and Fe(III), determined by chemical analyses were close to 100. However, the EDS analyses, which determined the surface composition, showed a close match only for Cr-HSZ. On the other hand, Cu-HSZ and Fe-HSZ gave relatively lower Si/M ratios. This indicates an enrichment of Cu and Fe on the surface of the respective zeolite crystals. While Cr is homogeneously distributed through the crystals. The amount of organic template (TPA^+) incorporated into the zeolite structure is typical for the well crystallized MFI zeolite (3.5 Mol./u.c.).

Table 4.7 Chemical composition of metal-containing synthesized zeolites.

Sample Code	Chemical Analysis		EDS	Thermal Analysis	
	Si/M	Na %	Si/M	H_2O[a] %	Template[b] %
AF-HSZ	∞	0.087	∞	2.00	11.40
Cr-HSZ	98.9	0.968	109	3.20	10.63
Cu-HSZ	103.5	0.595	20.4	2.08	11.14
Fe-HSZ	94.7	0.429	31.4	2.20	11.01

a Weight loss between 25-225°C
b Weight loss between 250-630°C

The scanning electron micrographs shown in Figures 4.17 to 4.19, depict the cubic shaped crystals. The zeolite samples containing Cr and Cu (Fig. 4.17 and 4.18) qualitatively show some amorphous phase along with the well formed crystals. Cu-HSZ showed relatively single crystals whereas, twined crystals are visible in Cr-HSZ sample. The Fe-HSZ (Fig. 4.17) showed agglomerates of small crystals with out any apparently visible amorphous phase. The crystal size and morphology fairly indicated about the incorporation of Fe(III) into the structural (tetrahedral) sites of zeolite framework. The isomorphous substitution of Fe(III), lowered the crystallization rate which prevented the crystals from growing to large single crystals in a given crystallization time. On the other hand, Cr(III) and Cu(II) might not be able to occupy the tetrahedral sites. Hence, relatively large separate crystals grew from the gel matrix containing these elements. In this case, the rate of crystallization was probably comparable to that of Al-free zeolite (AF-HSZ). As the latter also showed single, less twined crystals [Figure 4.11c]. This again indicates slower crystallization with the incorporation of metals (e.g., Al, Fe etc.) in the framework structure of high-silica zeolites.

The ESR spectrum of as-synthesized Cr-HSZ showed a broad nearly isotropic signal at g = 1.983, characteristic of the octahedral symmetry indicating Cr^{3+} ions may be in exchange position (Figure 4.20). Calcination in air oxidized these ions to probably Cr(IV) which is not paramagnetic. The peak almost disappeared after calcination, leaving a very weak signal (< 1%) due to the residual Cr^{3+} ions which could be present inside the pores and channels of zeolite.

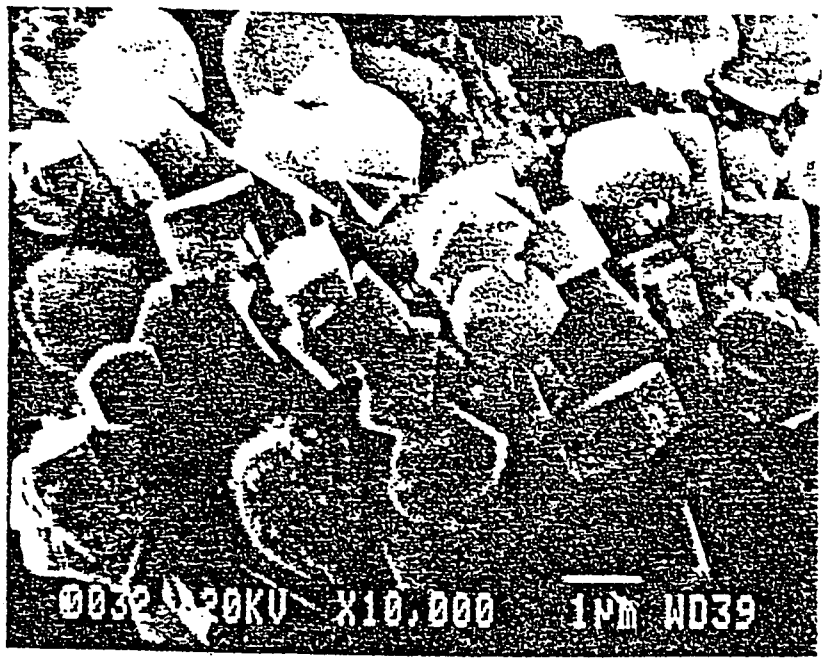

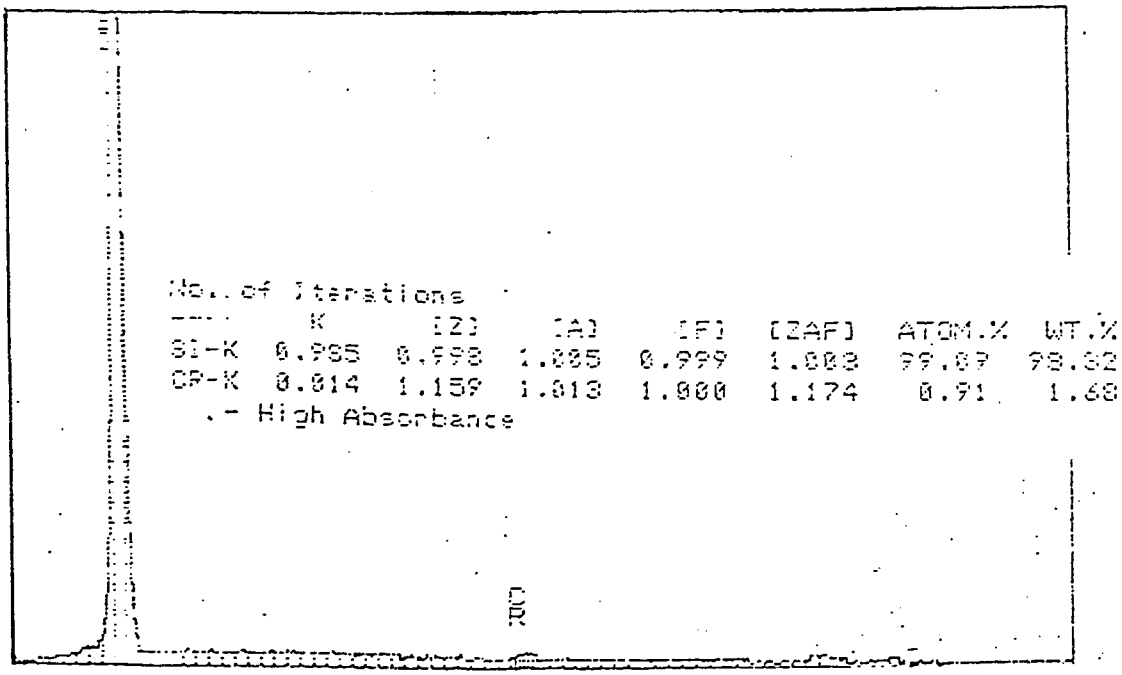

Figure 4.17 Scanning electron micrograph and EDS spectrum of as- synthesized Cr-HSZ.

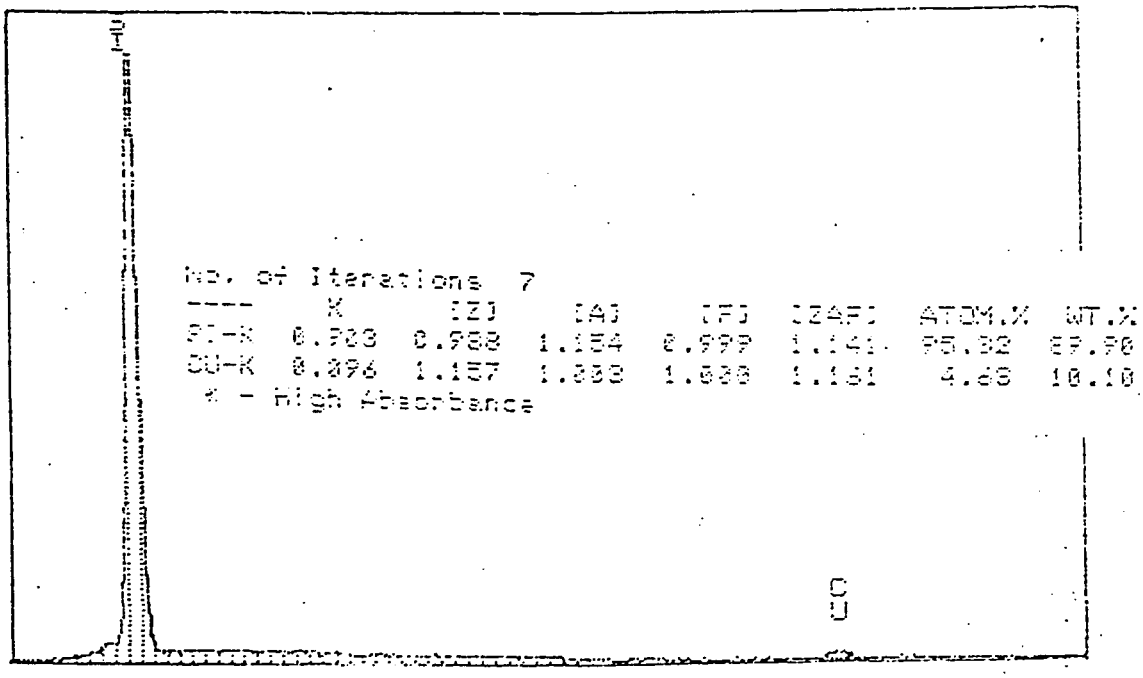

Figure 4.18 Scanning electron micrograph and EDS spectrum of as- synthesized Cu-HSZ.

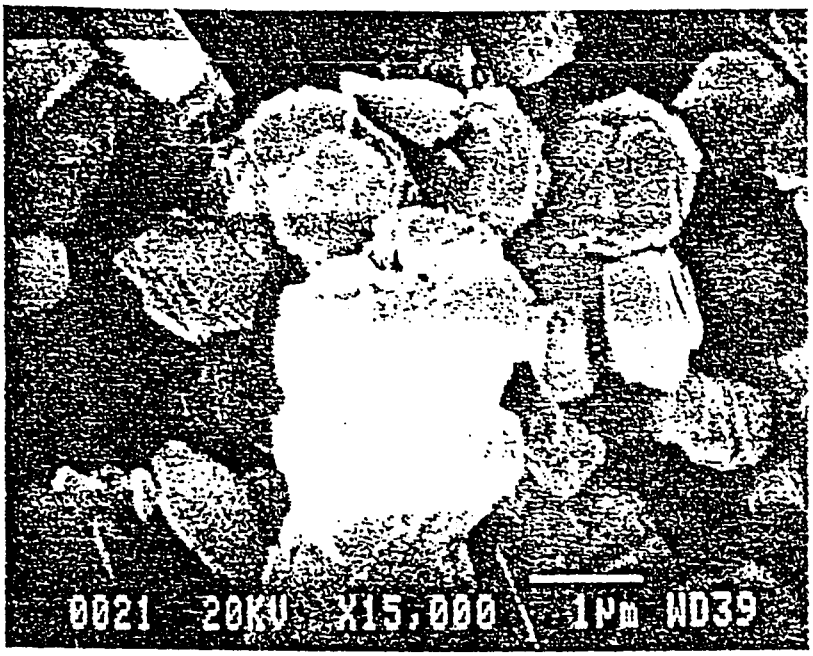

No. of Iterations 3

	K	[Z]	[A]	[F]	[ZAF]	ATOM.%	WT.%
SI-K	0.947	0.993	1.034	0.999	1.017	96.91	94.00
FE-K	0.052	1.167	1.004	1.000	1.172	3.09	6.00

* - High Absorbance

Figure 4.19 Scanning electron micrograph and EDS spectrum of as- synthesized Fe-HSZ.

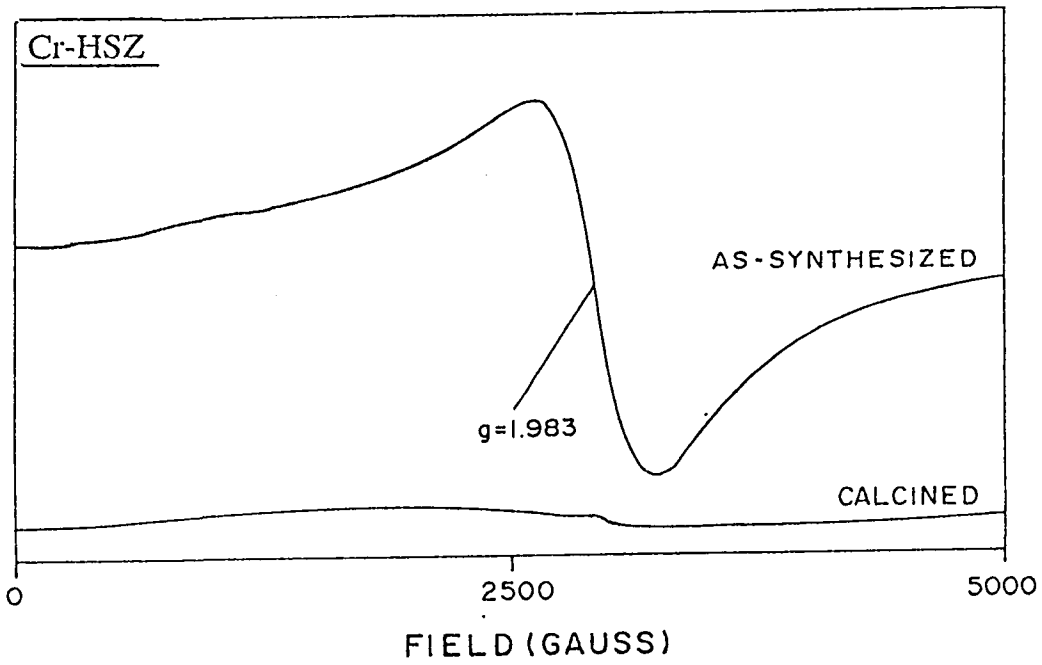

Figure 4.20 ESR spectra of Chromium containg high-silica zeolite, Cr-HSZ: top, as-synthesized, bottom, calcied in air at 550 °C for 1 h.

Copper-containing zeolite (Cu-HSZ) exhibited ESR spectrum typical of powdered sample (Figure 4.21). There is a set of equally spaced four lines assigned as $g_{\parallel} = 2.361$ and another set of four lines with $g_{\perp} = 2.081$. The calcined sample showed a broadening of lines and the signal for $g_{\perp}$ has lost hyperfine splitting pattern. The broadening of the lines could be attributed to the removal water upon calcination. This also indicates the structural changes brought about by the removal of organic template from the zeolite framework. This suggests variability in the framework structure, leading to a distribution of copper (II) ion site symmetries with broadening of the ESR spectral line widths.

Figure 4.22 compares the ESR spectra of as-synthesized and calcined iron - ontaining high-silica zeolite (Fe-HSZ). In the as - synthesized sample, there are three distinct signals at g = 1.996 assigned to hexa coordinated Fe^{3+} aquo/oxy complexes situated at cation sites [223], g = 2.341 (Fe^{3+} ions in oxide/hydroxide phases) and g = 4.369, due to Fe^{3+} in the tetrahedral coordination in the framework. Upon calcination, the intensity of the signal at g = 2.341 decreased and signal at g = 4.4 gained some intensity. This indicates that Fe^{3+} ions in oxide/hydroxide phases might get inserted into the framework at tetrahedral positions. The signal at g = 4.369 in as-synthesized zeolite was shifted upon calcination to g = 4.455 with a broadening of line width. This again, reflects the structural change brought about by the removal of organic template from the zeolite. Similarly, broadening of the signal at g = 2.0 was attributed to the removal of water upon calcination without any appreciable loss of intensity.

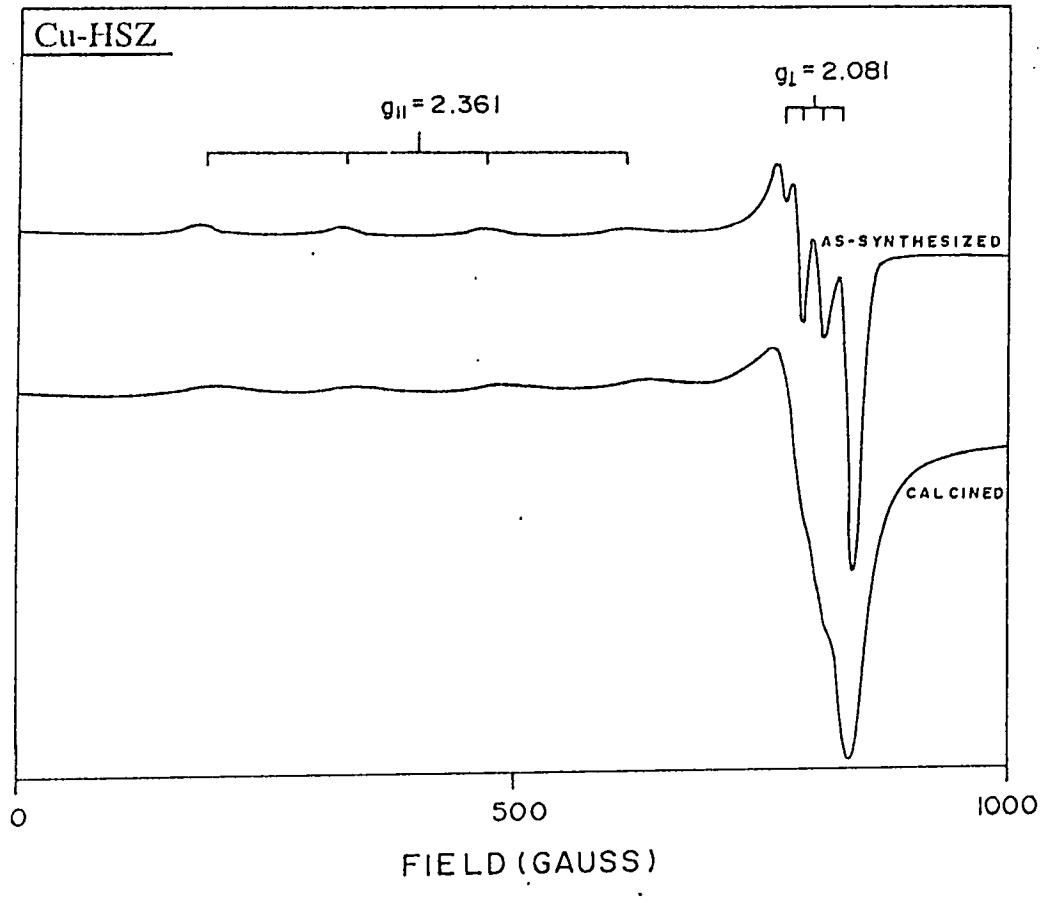

Figure 4.21 ESR spectra of Copper containg high-silica zeolite, Cu-HSZ: top, as-synthesized, bottom, calcied in air at 550 °C for 1 h.

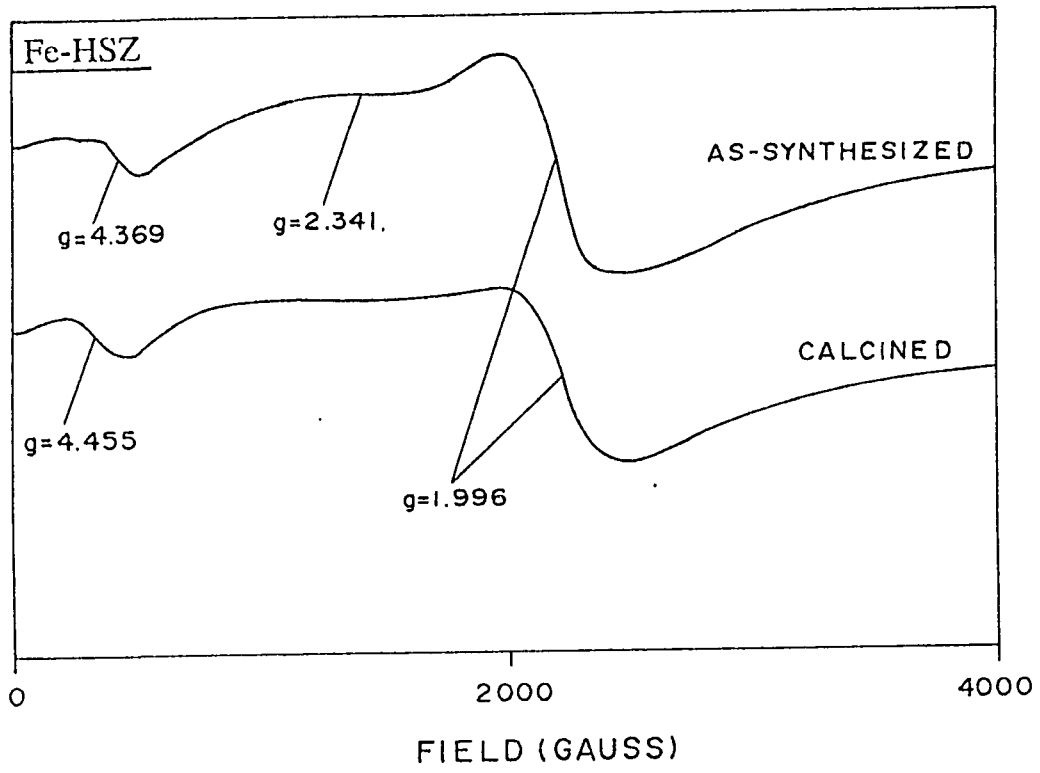

Figure 4.22 ESR spectra of Iron containg high-silica zeolite, Fe-HSZ: top, as-synthesized, bottom, calcied in air at 550 °C for 1 h.

4.2.3 Modification by Hydrothermal Treatment

High-silica zeolite (HSZ-25) modified by hydrothermal treatment or steaming at 350°C and 500°C were characterized by XRD, chemical analysis, thermal analysis and acidity measurements. The results of characterization will be discussed in the following section.

Figure 4.23 shows the XRD pattern of different forms of synthesized HSZ-25. The steam-treated samples did not loose crystallinity significantly. The peak positions are similar to those of the untreated H-form of zeolite (Fig. 4.23b), having no extra peak. This indicates that the framework of zeolite remained unchanged upon the hydrothermal treatment. Only minor differences were observed in the relative peak intensities around $2\theta = 8.2^{\circ}$ and 9.1° for the as-synthesized and other samples. This was attributed to the loss of organic template and water upon calcination which may caused the shrinkage of the unit cell. These results are consistent with reported data for MFI zeolite.

The chemical analysis showed no loss of SiO_2 or Al_2O_3 content of the steamed zeolites in the bulk. However, in the framework, the Al_2O_3 contents determined using the correlation given in Figure 4.13 , were 2.39% and 0.82% for S-350 and S-500, respectively. For the untreated (HSZ-25) sample this value was 3.12%. This indicates that dealumination occurred upon steaming. Dislodged aluminum could provide sites of enhanced activity. This will be further discussed in the following section in connection with the MTBE synthesis.

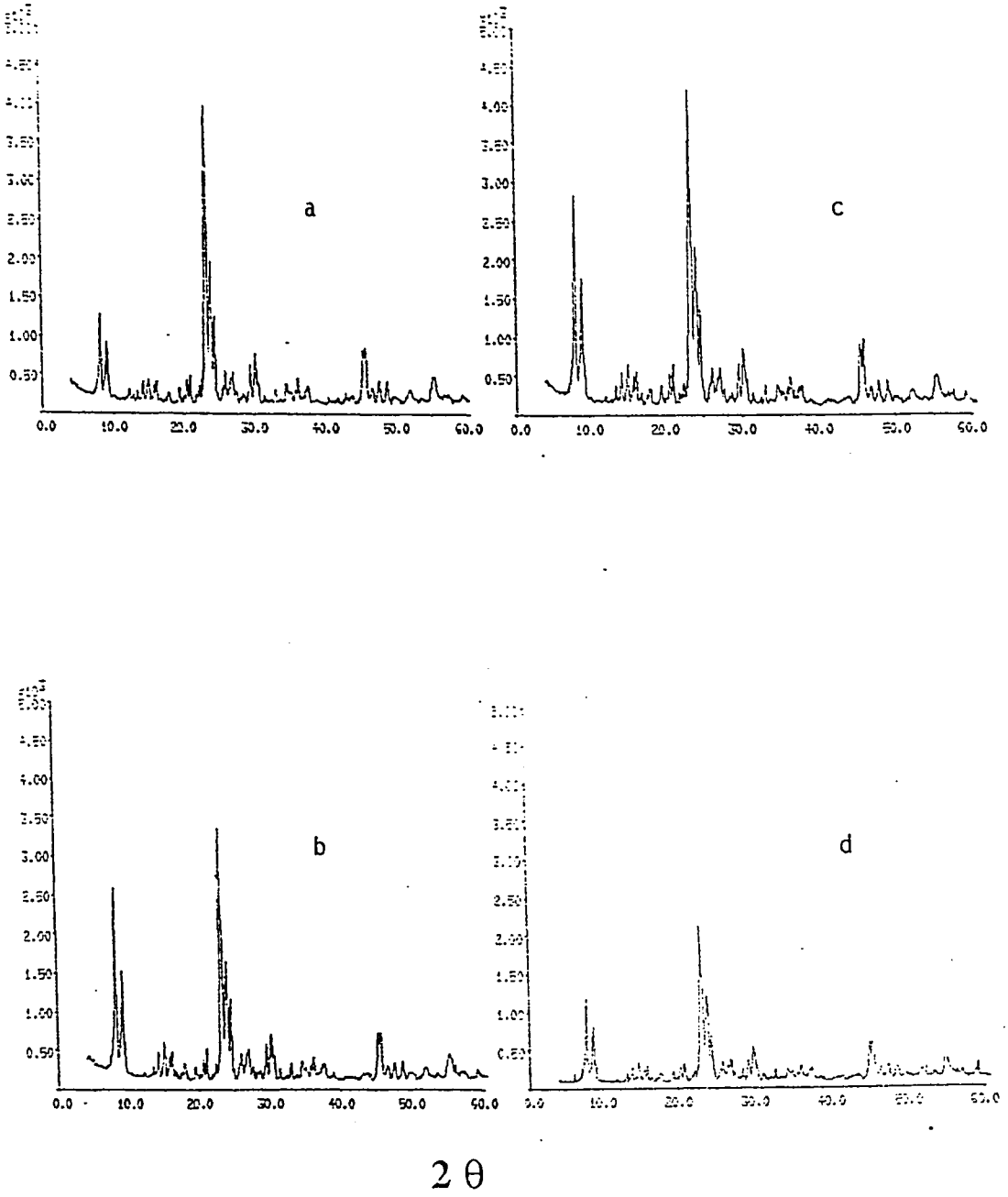

Figure 4.23 X-ray diffraction pattren of synthesized HSZ-25: (a) as-synthesized form, (b) H-form, (c) steam treated for 2 h at 350 °C (d) steam treated for 2 h at 500 °C.

Bröensted and Lewis acid sites can be studied by infrared spectroscopy of pyridine adsorbed on H-form of zeolites. FTIR spectra of pyridine adsorbed on synthesized high-silica zeolites are shown in Figure 4.24. Absorption band at 1545 cm^{-1} is assigned as the pyridinium ion adsorbed on Bröensted acid sites, band at 1455 cm^{-1} is due to the pyridine adsorbed at Lewis acid sites and strong absorption at 1490 cm^{-1} is due to the combined effect of Bröensted and Lewis acid sites.

The inspection of the FTIR spectra revealed that the intensities of all the three peaks mentioned, decreased due to the effect of steaming. The decrease is related to the loss of acid sites and proportional to the extent of the hydrothermal treatment. Similar results were obtained by the TPD of ammonia. Table 4.6 shows quantitative results of the total acidity in terms of volume of ammonia adsorbed per gram of zeolite. About 42% acid density was lost upon mild steaming (at 350°C) which increased to about 52% upon steaming at 500°C. The acid density of the S-350 is comparable to that of HSZ-50 which contains 1.64% Al_2O_3 as compared to 2.39% framework Al_2O_3 of S-350. This indicates that about 30% of framework aluminum of S-350 was probably tricoordinated, providing Lewis acid sites. This semiquantitative analysis is also supported by the FTIR spectra shown in Figure 4.24. The absorption band at 1455 cm^{-1} (Lewis acid sites), in curve 2 has absorbance comparable with that of the untreated zeolite sample (curve 1). However, substantial reduction occurred in the absorption band at 1545 cm^{-1} (Bröensted acid sites).

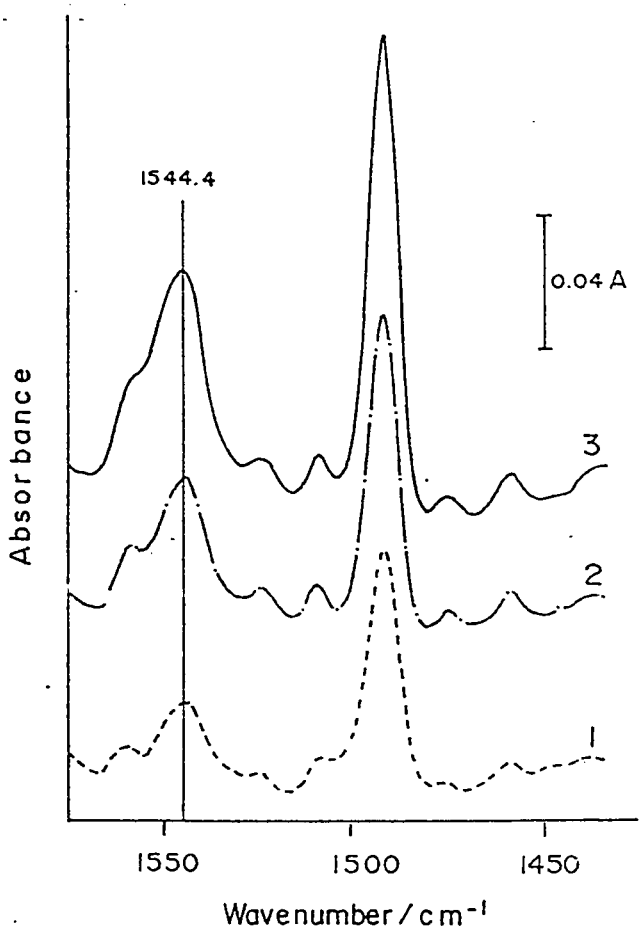

Figure 4.24 FTIR spectra of pyridine adsorbed on high-silica zeolite (H-form, Si/Al ratio 26), Steam treatment for 2 hrs,(1) at 500 °C, (2) at 350 °C, (3) untreated.

The results of differential thermal analysis showed an endothermic effect accompanied by weight lost of about 4.0% with a minima at 140°C. This was attributed to the desorption of water from the steamed samples which were dried in the oven at 110°C over night. There was an exothermic effect at 1300°C due to the partial collapse of structure. This was similar to that for the unsteamed sample. Only a minor shift toward lower temperature was observed in the high temperature exothermic peak. This shift occurred due to the removal of framework aluminum which lowered the thermal stability. But the effect was only minor because the shift was less than 10°C for S-500 as compared to that of the untreated sample. Therefore, it can be concluded that the steaming did not cause severe structure loss except the dealumination of framework aluminum which enhances the acid strength.

4.3 Catalytic Evaluation

Catalytic evaluation is a powerful tool to measure the performance of synthesized zeolite and the effect of its modification . Selected synthesized and modified zeolites were evaluated for their catalytic properties for MTBE synthesis and MTO conversion reaction. The results of the catalytic testing will be presented and discussed in the following sections.

4.3.1 Methyl tert-Butyl Ether Synthesis

Methyl tert-butyl (MTBE) ether was synthesized by the reaction of isobutene and methanol:

$$CH_3OH + (CH_3)_2C{=}CH_2 \rightleftharpoons (CH_3)_3COCH_3$$
$$\Delta_R H^{\circ}_{298} = -37.7 \text{ kJ/mol}$$

The results and experimental condition of the MTBE synthesis reaction are summarized in Table 4.8. The reaction was carried out at atmospheric pressure. Since, the catalyst was in the form of granules (0.6 - 1.2 mm), no back pressure was observed. Major factors which affect the conversion of isobutene are temperature, space velocity, methanol to isobutene molar ratio (m/i) and Si/Al ratio of the catalyst. The effect of these factors was studied for the synthesis of MTBE.

The reactions were conducted between 75-150°C to find the optimum temperature. Figure 4.25 shows the effect of temperature on steady state conversion of isobutene (limiting reactant). It was found that conversion was maximum around 80°C. Reaction being exothermic, the conversion was decreasing with increse in temperature. A decrease in steady state conversion of isobutene below 80°C indicates lower acid activity of zeolite catalysts at lower temperature.

The results concerning acid-catalysed reactions over zeolites can be interpreted in terms of (a) Broensted sites (b) Lewis sites and (c) sites

Table 4.8 Results of catalytic evaluation for MTBE synthesis.

Run No.	Catalyst Code	Temp. (°C)	WHSV (h^{-1})	Molar Ratio (m/i)	Conv. of MeOH %	Conv. of Isobutene %	Product mass distribution		
							MTBE %	MeOH %	Isobutene %
1	HSZ-25	100	4.87	1.70	11.55	19.70	15.68	43.64	40.68
2	HSZ-25	150	4.87	1.70	4.66	7.95	6.33	47.04	46.63
3	HSZ-100	80	4.87	1.70	6.98	11.89	9.47	45.90	44.63
4	HSZ-100	100	4.87	1.70	6.74	11.49	9.15	46.02	44.84
5	HSZ-100	125	4.87	1.70	5.15	8.77	6.98	46.80	46.21
6	HSZ-25	75	4.87	1.70	20.57	35.06	27.91	39.19	32.90
7	HSZ-25	125	4.87	1.70	7.30	12.44	9.90	45.74	44.36
8	HSZ-25	80	4.87	1.70	24.10	41.08	32.70	37.45	29.85
9	HSZ-75	80	4.87	1.70	15.37	26.20	20.86	41.76	37.39
10	HSZ-50	80	4.87	1.70	19.70	33.58	26.73	39.62	33.65
11	HSZ-25	80	3.71	1.61	19.94	31.79	26.14	38.16	35.69
12	HSZ-25	80	3.51	1.58	23.24	36.62	30.28	36.37	33.35
13	HSZ-25	80	3.00	1.20	25.99	32.43	29.75	30.81	39.44
14	HSZ-25	80	3.11	1.89	19.26	36.35	27.48	41.90	30.62
15	HSZ-25	80	2.00	2.00	21.93	43.85	32.16	41.64	26.20
16	Steam-500	80	2.00	2.00	21.20	42.40	31.09	42.03	26.88
17	Steam-350	80	2.00	2.00	23.09	46.18	33.86	41.02	25.12
18	*Amberlist-15	80	2.00	2.00	25.57	50.75	34.32	40.38	22.87
						46.80**			

* Amberlist-15 produced 0.58% TBA and 1.85 % C_8 olefin

** Conversion of isobutene to MTBE (Selectivity for MTBE was 95.2%)

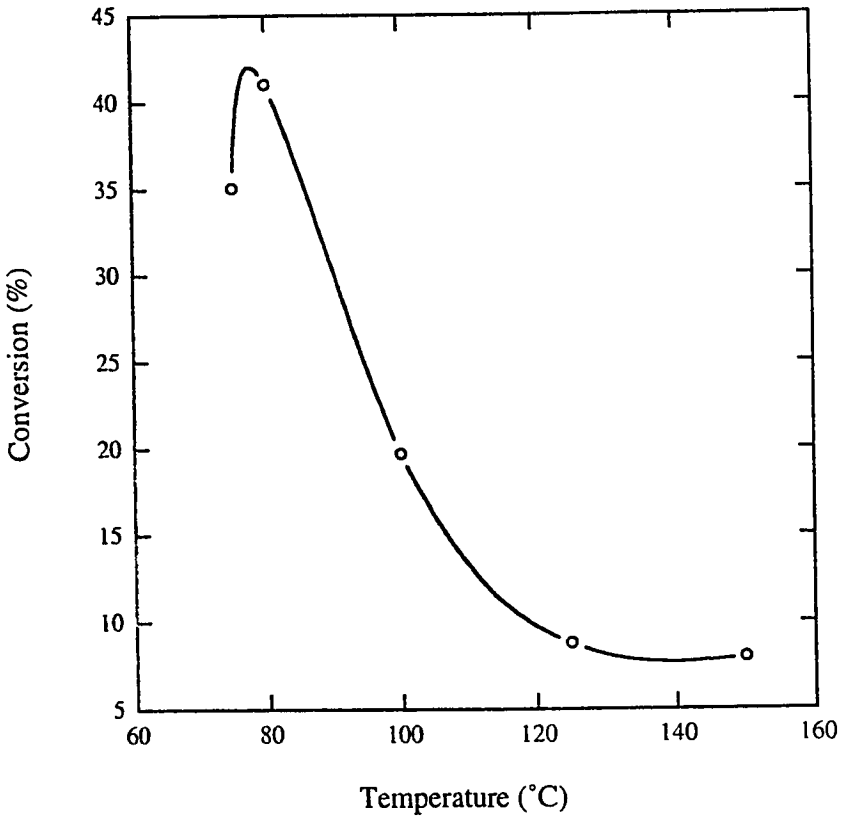

Figure 4.25 The effect of temperature on conversion of isobutene for HSZ-25, WHSV 4.87 h^{-1}, m/i 1.70.

having enhanced activity (supper acids). The different acidity sites are given in Figure 4.26. The reaction, being acid catalyzed, proceeds by the proton transfer from catalyst to isobutene and subsequent attack of methanol to form MTBE. Therefore, Broensted acidity and enhanced acid sites seem to be responsible for the ether formation reaction.

The strength and density of acid sites are function of Si/Al ratio as described in Section 4.3.1. Figure 4.27 shows the effect of Si/Al ratio on the conversion of isobutene at 80°C. It was observed that the conversion of isobutene decreased with increasing Si/Al ratio. This was also correlated to the total acidity of the synthesized zeolites (Figure 4.28). The conversion of isobutene was increasing linearly with acidity between the range of 9 to 18 cm^3/g. Below this range there was a sharp decrease occurred in the conversion of isobutene. This suggested the lower acid activity of the catalyst with increasing Si/Al ratio. From these results it can be concluded that high-silica zeolites with maximum aluminum content or lower Si/Al ratio could be better catalyst for MTBE synthesis.

The effect of space velocity and molar ratio of methanol to isobutene (m/i) on the conversion of isobutene to MTBE is given in Table 4.9. At a constant space velocity, increasing the molar ratio of methanol to isobutene (m/i) has negligible effect on the overall conversion of isobutene. For example, the overall conversion of isobutene was found to be almost same for run number 3 and 4. In these runs, space velocities were comparable, whereas molar ratios were 1.20 and 1.89, respectively. The conversion of isobutene for the former was 0.0405 mol/h and 0.0389

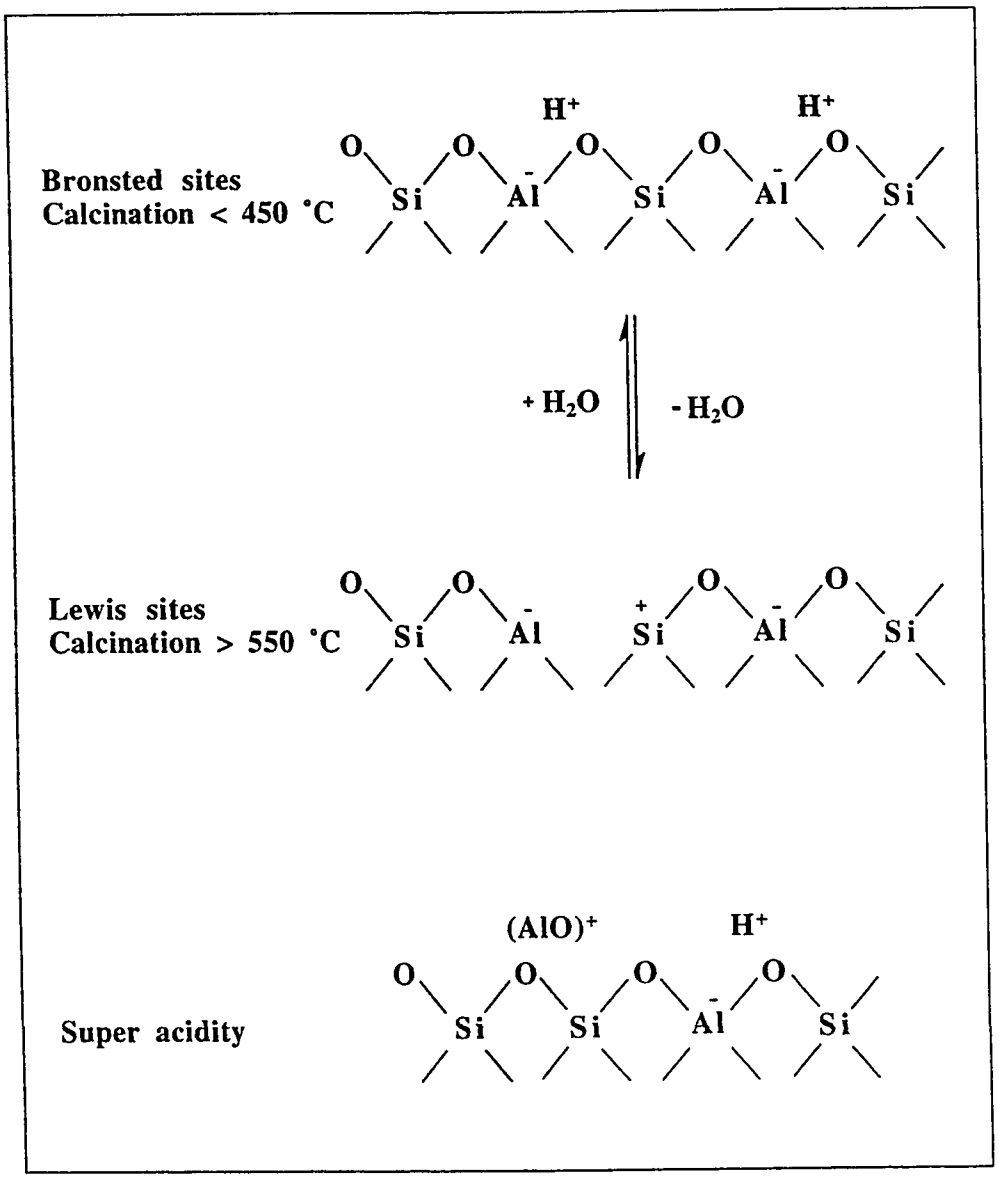

Figure 4.26 Acidity types in zeolite

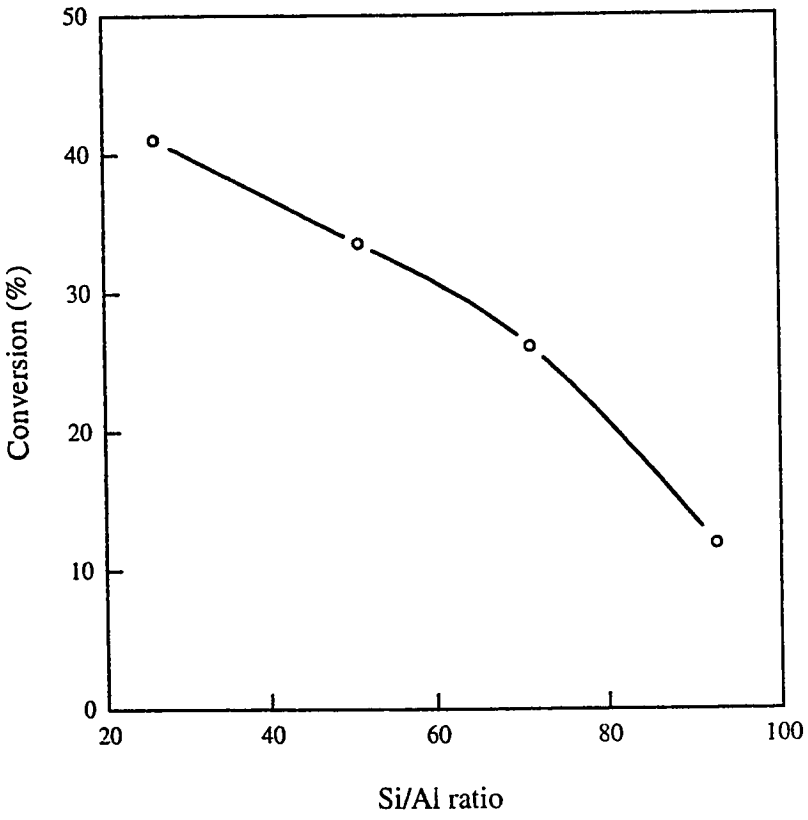

Figure 4.27 The effect of Si/Al ratio on the conversion of isobutene: WHSV 4.87 h-1, m/i 1.70, Temperature 80° C.

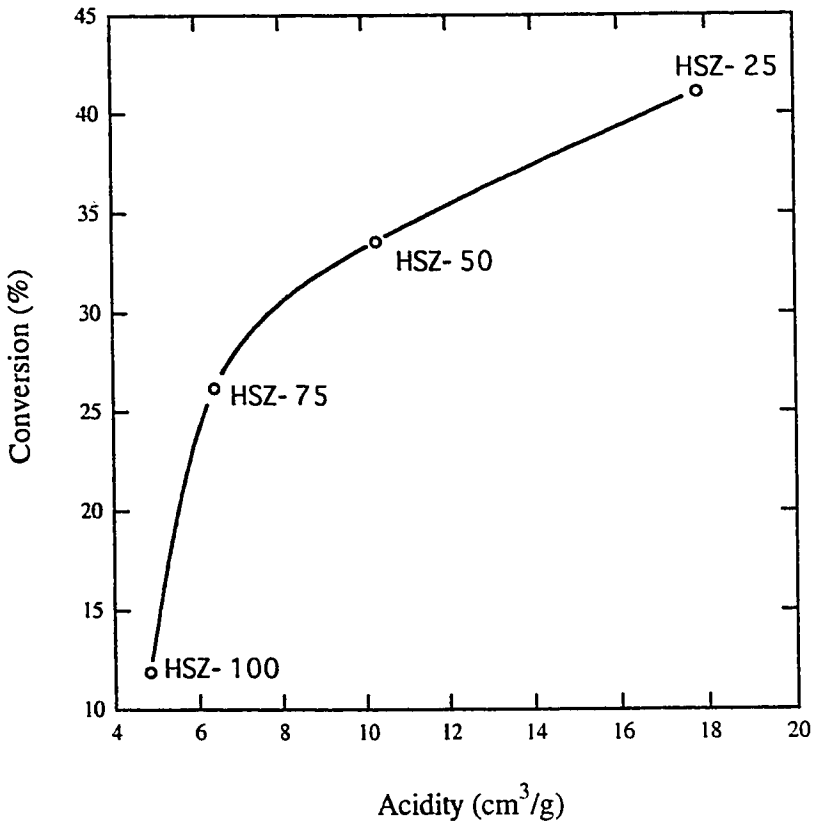

Figure 4.28 Total acidity measured by TPD of ammonia vs. conversion of isobutene (temperature 80° C, WHS 4.87 h^{-1}, m/i 1.70).

Table 4.9 Effect of space velocity and molar ratio on production of MTBE.

S. No	WHSV (h^{-1})	Molar Ratio (m/i)	Productivity (g_{MTBE}-g^{-1}_{Cat}-h^{-1})	Conversion of Isobutene (mol/h)
1	4.87	1.70	1.59	0.0542
2	3.51	1.58	1.06	0.0483
3	3.00	1.20	0.892	0.0405
4	3.11	1.89	0.856	0.0389
5	2.00	2.00	0.643	0.0384

mol/h for the latter run. Similarly, the comparison of run number 4 and 5, in which molar ratios (m/i) were comparable, showed little effect on absolute conversion of isobutene. In run number 4 the conversion was 0.0389 mol/h as compared with 0.0384 mol/h for run-5. Similar results were reported by Pien and Hatcher [201]. The methanol to isobutene ratio in the feed varied from 1.5 to 4.8 with out any significant change in conversion of isobutene. This indicates a zero order rate dependence for methanol as reported by Ancilloti and coworkers [184] in their studies with Amberlyst-15.

Figure 4.29 shows the effect of conversion of isobutene (%) at various space velocities (WHSV h^{-1}) and molar ratios of methanol to isobutene in a three dimensional bar diagram. This figure reveals that at constant space velocity, varying molar ratio (m/i) has less pronounced effect on the conversion of isobutene. However, some variations in conversion were noticed at constant molar ratio. It was observed that carbon content of the spent catalyst was higher for high space velocity runs. Hence for longer catalyst life lower space velocity was found to be appropriate.

The conversion of isobutene to MTBE as a function of time-on-stream for HSZ-25 at 80 °C, m/i 2.00 and space velocity 2.00 h^{-1} is presented in Figure 4.30. After a run of 32 hours no loss in activity was observed. About 1% carbon was determined after 32 hours run time and less than 5% loss in BET surface area was observed. This indicates that the catalyst performed well during the run which was due to the lower space

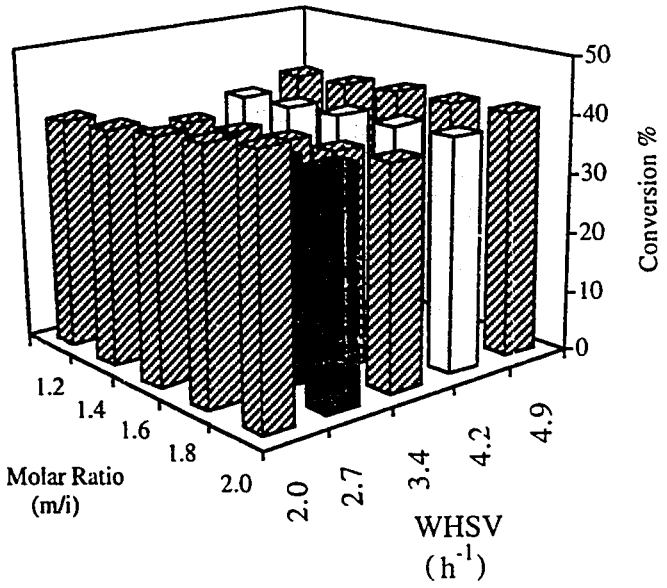

Figure 4.29 Effect of methanol to isobutene molar ratio and space velocity on conversion of isobutene (catalyst, HSZ-25; temp. 80 °C).

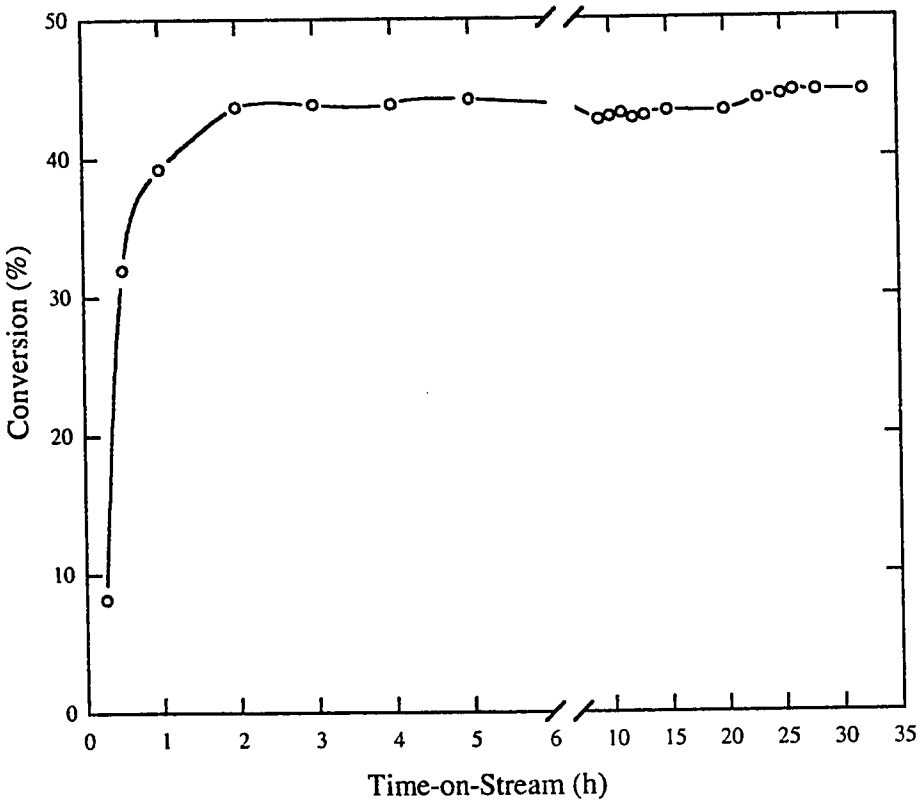

Figure 4.30 Conversion of isobutene vs. Time-on-Stream (catalyst, HSZ-25; temperature, 80 °C; m/i, 2.00; WHSV, 2.00 h^{-1}).

velocity and temperature of the reaction. Due to some experimental limitations it was difficult to achieve space velocity below 2.00 h^{-1}

The steam modified catalysts (S-350 and S-500) were evaluated for MTBE synthesis. Figure 4.31 shows the effect of steaming on conversion of isobutene. Although the effect was not very big, but even then mild steaming (at 350 °C) showed increased conversion as compared to that shown by the unsteamed sample. However, the severity of the treatment (at 500 °C) showed adverse effect on the conversion. This could be the result of loss of acid sites due to excessive dealumination at higher steaming temperature. The steaming affected the induction period (time required to establish the steady state). Steady state was established in relatively shorter time as compared with untreated sample.

The commercially used catalyst, Amberlyst-15 (A-15) was also tested under our experimental conditions. A selectivity of 95.2% for MTBE was achieved even at m/i of 2.00 at 80 °C. The side products included diolefin (dimmer of isobutene, $C_8^=$) and tertiary butyl alcohol (TBA). However, no side product was detected when synthesized high-silica zeolites were used, even at m/i of 1.20. The absence of diolefin in the case of high-silica zeolites demonstrated the shape-selective behavior of medium pore (MFI) zeolite. The TBA was produced due to small amount of water present in the feed when A-15 was used as a catalyst. On the other hand, no alcohol was detected with zeolite catalyzed MTBE synthesis which demonstrated the low affinity of water by the hydrophobic

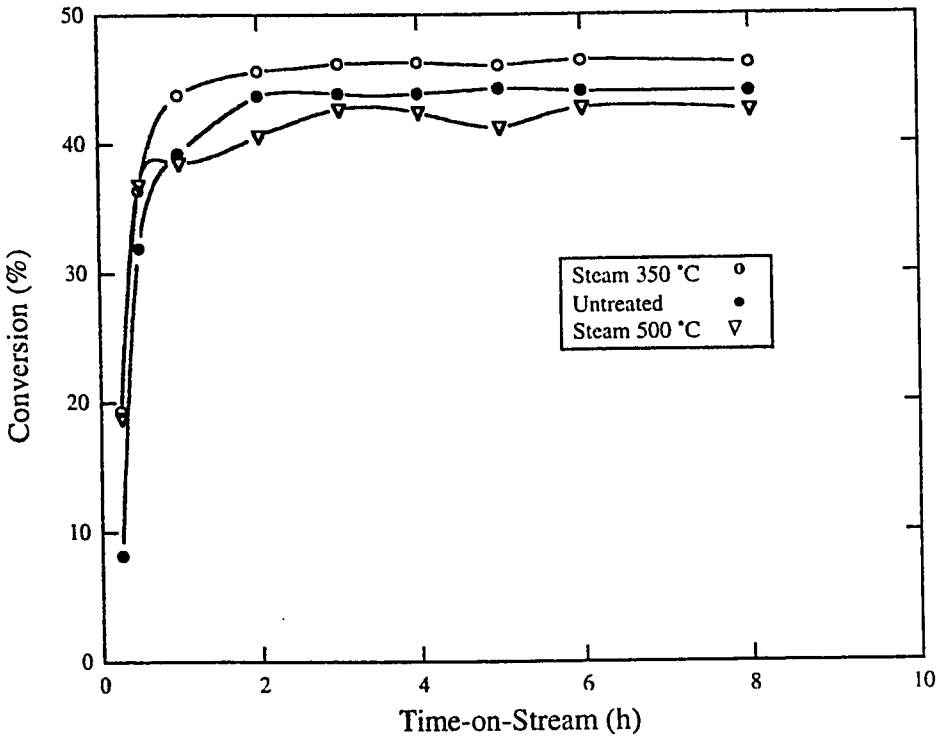

Figure 4.31 Effect of steaming on conversion of isobutene (catalyst HSZ-25, temp. 80 °C, WHSV 2.00 h^{-1} and m/i 2.00).

nature of high-silica zeolite. Hence nearly 100% selectivity for MTBE was achieved with synthesized high-silica zeolites.

4.3.2 Methanol to Olefin Conversion (MTO)

Selected synthesized and modified zeolites were tested for methanol into olefins conversion reaction. The results of catalyst testing for MTO conversion reaction are summarized in Table 4.10. The reaction was carried out at 375 °C and at atmospheric pressure with nitrogen as diluent. The conditions followed were taken from the pervious studies conducted in our laboratory [224].

The results showed that about 85% selectivity (based on gaseous hydrocarbon) for $C_2^=$ - $C_4^=$ olefins was achieved in the case of iron containing synthesized high-silica zeolite (Fe-HSZ). On the other hand, aluminum containing synthesized high-silica zeolite (HSZ-100) gave about 58% selectivity for the target olefins. PB-2, the zeolite with highest Si/Al ratio (~1600) tested, gave a selectivity of only about 24% with a yield of 6.18%.

Inui et al. [225, 143], showed that silicates of Fe, Co, and Pt exhibited the highest selectivity in the formation of light olefins. Since, the incorporation of different metals generates Broensted acid sites with varying strength, the intrinsic activity of metallosilicates also varied. This means that, at constant space time and temperature, more active catalyst

Table 4.10 Results of catalyst testing for Methanol to Olefins conversion.

Catalyst	PB-2 (Si/Al ≈1600)	HSZ-100 (Si/Al ≈100)	Fe-HSZ (Si/Fe ≈100)
Conversion %	100	100	97.5
Product distribution %			
Gaseous HCs	25.99	28.47	25.01
Liquid HCs	13.68	10.91	11.01
Water	54.57	55.01	54.62
$CO_2 + CO$	0.31	0.32	0.87
Coke	3.11	2.79	2.05
Yield[a] %			
Ethene	1.69	2.23	0.91
Propene	1.37	4.82	7.68
Butene	3.12	9.64	12.89
Total $C_2^= - C_4^=$	6.18	16.69	21.47
Methane	0.34	0.40	0.10
Ethane	0.27	0.31	0.18
Propane	4.86	1.95	0.29
Butane	7.28	4.70	0.87
Pentane	7.07	4.42	2.09
Selectivity[b] %			
Ethene	6.47	7.80	3.60
Propene	5.24	16.86	30.35
Butene	11.97	33.73	50.91
Total $C_2^= - C_4^=$	23.68	58.39	84.86
Methane	1.30	1.38	0.39
Ethane	1.02	1.09	0.72
Propane	18.64	6.83	1.15
Butane	27.90	16.46	3.43
Pentane	27.07	15.49	8.24

a Yield = (g product / 100 g of Methanol feed)
b Selectivity = (g product / 100 g of gaseous hydrocarbons)
Reaction Conditions: Temp, 375 °C; WHSV, 4.0; Pressure, 1 atm.

would possibly exhibit a lower selectivity towards light olefins than the less active catalyst. Higher selectivity with Fe-silicate was attributed to the difference in the activity for the disproportionation of olefins to parafins and aromatics. The lower acid strength of Fe-silicate was held responsible for this [143].

The other metal-containing zeolites (Cr-HSZ and Cu-HSZ) were also tested for MTO conversion reaction. But none of the catalyst showed any activity for olefin production. About 5-10 % methanol was converted into dimethyl ether (DME) over these catalysts.

The results of MTO conversion reaction indicates that low and dilute acidity is needed for this reaction. Some of the iron is probably in the framework where as no chromium or copper was incorporated in the framework.

CHAPTER 5

CONCLUSIONS AND RECOMMENDATIONS

5.1 Conclusions

The main conclusions of the study are summarized as follows:

1. Plackett-Burman experimental design was successful to screen the synthesis variables.
2. pH was found to be the most important variable (pH = 10.00 ±0.50).
3. Zeolites prepared by rapid crystallization method showed narrow crystal size distribution as compared to that prepared by conventional zeolite synthesis procedure.
4. The following quantitative relationship was established for the Si/Al ratio of the zeolites produced:

$$(Si/Al)_{zeolite} = 3.53 + 0.777\ (Si/A)_{gel}$$

5. Framework aluminum for the H-form of the synthesized high-silica zeolite was correlated with the peak spacing $\Delta\ 2\theta$ (45.0° - 45.5°) as follows:

$$\%\ Al_2O_3 = 10.7 - 19.0\ \Delta 2\theta$$

6. The effect of temperature, Si/Al ratio, space velocity (WHSV) and molar ratio of methanol to isobutene was investigated for the conversion of isobutene to MTBE. Maximum conversion was achieved at the following conditions:

Temperature	= 80 °C
Si/Al ratio	= 26.2
WHSV	= 2.00 h^{-1}
Molar ratio (m/i)	= 2.00

7. Mild steaming of the synthesized zeolite showed higher conversion of isobutene to MTBE.
8. The synthesized high-silica MFI zeolites performed better than the Amberlyst-15 in terms of selectivity for MTBE.
9. Iron containing synthesized zeolite gave maximum selectivity for C_2-C_4 olefins for methanol to olefins reaction.

5.2 Recommendations for Future Work

The following includes some of the recommendations for future work:

1. Investigation of broader ranges of factors affecting the synthesis of high-silica zeolites.
2. The synthesis of high-silica zeolites at lower temperature may result in different size distribution and morphology. Therefore, rapid

crystallization at maximum temperature, say about 150 °C or below could be investigated.

3. Other organic additives may be used for the synthesis of high-silica zeolites by this method.
4. Some other reactions like n-hexane cracking, alkane aromatization, or *para*-selectivity of xylene isomerization could be investigated using the synthesized high-silica zeolites.
5. Liquid phase synthesis of MTBE using high-silica zeolites prepared in this study, may be investigated because it holds potential for higher conversion of isobutene.
6. Isomorphous substitution of metals, other than the ones investigated in this study, by rapid crystallization should be studied to evaluate selectivity and yield of light olefins.

REFERENCES

1. Weisz, P.B., *Pure Appl. Chem.*, **52,** 2091 (1980).

2. Chen, N.Y. and W.E. Garwood , *Catal. Rev. - Sci. Eng.*, **28,** 185 (1986).

3. Holderich, W.F., *Pure Appl. Chem.*, **58**, 1383 (1986).

4. Bekkum, H.V., and H.W. Kouwenhoven, *Stud. Surf. Sci. Catal.*, **41**, 45 (1988).

5. Jacobs, P.A. J.M. Jacobs and R. Parton, in "*Proc. Int. Symp. on Zeolites as catalysts, sorbates and detergent builders*", Wurburg, FRG 1988, Elsvier, Amsterdam, p163 (1989).

6. Barrer, R.M., *J. Chem. Soc.*, 2158 (1948).

7. Barrer, R.M., ibid, 127 (1948).

8. Barrer, R.M. and Marcilly, C., *J. Chem. Soc.*, A, 2735(1970).

9. Robson, H., *Chemtech*, March 176 (1979).

10. Vaughn, D.E.W., *Chem. Eng. Progress*, **84**, 25 (1988).

11. Barrer, R.M., *Stud. Surfa. Sci. Catal.*, **24,** 1 (1985).

12. Kerr, G.T., *Catal. Rev. Sci. Eng.*, **23**, 281(1981).

13. Barrer, R.M., *Hydrothermal Chemistry of Zeolites*, Academic Press, New York (1982).

14. Meier, W.M. and Olson, D.H., *Atlas of Zeolite Structure Types,* Butterworths, Surrey, (1992).

15. Olson, D.H., *Zeolites*, **14**(5), 389 (1994).

16. Flanigen, E.M., *Adv. Chem. Ser.*, **121,** 119, (1973).

17. Rollmann, L.D. *Adv. Chem. Ser.*, **173**, 387, (1979).

18. Chang, C.D. and A.J. Silvestri, *J. Catal.*, **47**, 249 (1977).

19. Barrer, R.M. *Hydrothermal Chemistry of Zeolites,* Academic Press, London, p. 43 (1982).

20. Lok, B.M., T.R. Cannan and C.A. Messina, *Zeolites,* **3,** 282, (1983).

21. Derouane, E.G., *Appl. Catal.*, **1,** 201, (1981).

22. Boxhoorn,G., *J. Chem. Soc., Chem. Commun.*, 1416 (1983).

23. Groenen, E.J.J., *Zeolites,* **6,** 403, (1986).

24. Milton, R.M., in M.L. Occeli and H.E. Robson (Eds.), *Zeolite Synthesis, ACS , Sympos. Ser.* **389**, ACS, Washington, D.C., pp. 1-10 (1989).

25. Wilson, S.T., B.M. Lock and E.M. Flanigen, *J. Am. Chem. Soc.*, **104**, 1146-47 (1982).

26. Flanigen, E.M., et al., in Y. Murakami and J.W. Ward (Eds.), *New Developments in Zeolite Science and Technology, Pro. 7th Intl. Zeolite Conf.* Tokyo, 1986, Elsevier, Amsterdam, pp. 103-12 (1986).

27. Szostak, R., *Molecular Sieves, Principles of Synthesis and Identification*, Van Norstrand, Reinhold, New York, pp. 205-77 (1989).

28. Berrer, R.M., US Patent, 2,306,610 (1943).

29. Berrer, R.M and White, A.D., *J. Chem. Soc.*, 1561, (1952).

30. Reed, T.B. and Breck, D.W., *J. Am. Chem. Soc.*, **78**, 5972 (1956).

31. Milton, R.M., U.S. Patent, 2,882,244 (1959).

32. Rabo, J.A., Pickert, P.B., Boyle, J.E., U.S. Patent 3,200,082 (1966).

33. Rabo, J.A., Pickert, P.B., Boyle, J.E., U.S. Patent 3,130,007 (1964).

34. Mc Daniel, C.V. and Maher, P.K., in *"Molecular Sieves"* Society of Chemical Industry, London, (1968) p. 186.

35. Argauer, R.J. and Landolt, G.R., U.S. Patent 3,702,866 (1972).

36. Davis, M.E. Saldarriaga,C., Montes, C., Graces, J., and Crowder, C., *Nature* **331**, 6980 (1988).

37. Breck, W.D., *Zeolite Molecular Sieves,* John Wiley & Sons, New York, (1974).

38. Zhdanov, S.P., *Adv. Chem. Ser.*, **101**, 20(1971).

39. Stringham,B., *Econ. Geol.*, **47**, 661(1952).

40. Kulkarni, S.B., et al., *Zeolites,* **2**, 313,(1982).

41. Wilkosz, J., Stobiecka,E. and Dudek,B., *Cryst. Res. Technol.*, **25**(3), 251(1990).

42. Milton, R.M., "*Molecular Sieves", Soc. Cehm. Ind.*, London, (1968) p199.

43. Zhdanov, S.P. and Samulevich, N.N., *Pro. 5th Int. Conf. Zeolites*, (1980) p 75.

44. Quinhua, X., Shulin. B. and Jialu, D., *Scientia Sinica (Ser. B)*, **25**, 39(1982).

45. Chao, K.J., Tasi, T.G., Chen M.S. and Wang, I., *J. Chem. Soc., Faraday I,* **77**, 465(1981).

46. Araya, A. and Lowe, B.M., *J. Chem. Res. (s)* #**912**, (1985).

47. Nastro, A. and Sand. L.B., *Zeolites,* **3**, 57(1983).

48. Barrer, R.M., *Molecular Sieves, Soc. Chem. Ind.*, (1968) p39.

49. Barrer, R.M. and Cole, J.F., *J. Chem. Soc.*, A, 1516(1970).

50. Jacobs, P.T. and Martens, J.A., *Stud. Surf. Sci. Catal.*, **33**, (1987), p64.

51. Suzuki, K., Kiyozumi, Y., Mastsuzaki, K and Shin, S., *Applied Catalysis*, **35**, 401(1987).

52. Suzuki, K., Kiyozumi, Y., Shin, S., Fujisawa, K., Watanabe, H., Satio, K. and Noguchi, K., *Zeolites* , **6**, 290(1986).

53. Hayhurt, D.T. and Sand, L.B., *Molecular Sievs II, ACS Symp. Ser.*, **40**, (1977), p219.

54. Barrer, R.M., *Zeolites*, **1**, 130(1981).

55. Derouane, E.G., Nagy, J.B., Gabelica, Z. and Blom, N., *Zeolites*, **2**, 299(1982).

56. Hogan, P.J., Whittam, T.V., Birtill, J.J. and Stewart,A., *Zeolites*, **4**, 275(1984).

57. Kulkarni, S.J., Hattori, H. and Tanabe, K., *Applied Catalysis*, **49**, 27-44(1989).

58. Casci, J.T. and Lowe, B.M., *Zeolites*, **3**, 186(1983).

59. Casci, J.T., Whittam, T.V. and Lowe, B.M., *Pro. 6th Int. Conf. Zeolites*, (1984) p 894.

60. Flannigen, E.M., Bennett, J.M., Grose, R.W., Cohen, J.P., Patton, R.L., Kirchner, R.M. and Smith, J.V., *Nature*, **271**, 512(1978).

61. Bibby, D.M., Milestone, N.B. and Aldridge, L.P., *Nature*, **280**, 664(1979).

62. Chu, P., U.S. Pat., 3 709 979(1973).

63. Rollmann, L.P., *Zeolite: Science and Technology*, Martinus Nijhoff Publishers, (1984), p109.

64. Lecluze, V. and Sand, L.B., *Rec. Prog. Rep. 5th Int. Conf. Zeolites*, (1980), p 41.

65. Romannikov, V.N., Mastihin, V.M., Hocevar, S. and Drzaj, B., *Zeolites,* **3**, 311(1983).

66. Chao, K.J., Tasi, T.C., Chen, MS. and Wang, I.J., *JCS, Faraday I,* **77**, 547(1981).

67. Dyer, A., *An Introduction to Zeolite Molucular Sieves,* John Wiley & Sons, (1988), p55.

68. Ostwald, W.Z., *Physical Chemistry* **34** 503 (1900).

69. Inuli, T., Ishihara, T. and Takegami, Y., JCS. Chem. Comm., 936 (1981).

70. Inuli, T., Syud. Surf. Sci. & Catal., **44**, 189 (1989).

71. Price, G.D., Pluth, J.J., Smith, J.V., Bennett, J.M. and Patton, R.L., *J. Am. Chem. Soc.*, **104**, 5971(1982).

72. Boxhoorn, et al., *JCS, Chem Comm.,* 264(1984).

73. Bennett, J.M., Cohen, J.P., Flanigen, E. M., Pluth, J.J. and Smith, J.V., *ACS Symp. Series.*, **218**, 109(1983).

74. Scholle, K.F.M.G.T., Veeman, W.S., Frenken, P. and Van Der Velden, G.P.M., *Applied Catalysis,* **17**, 233(1985).

75. Hexuan, L., et al., *Chem. J. Chinese Univ.*, **2**, 517(1981).

76. Grose, R.W., and Flanigen, E.M., U.S. Pat., 4 257 886 (1981).

77. Nastro, A., Aiello, R. and Colella, C., *Stud. Surf. Sci. Catal.*, **24**, 39(1985).

78. Dia, F.Y., Suzuki, M., Takahashi, H. and Saito, Y., *ACS Symp. Series,* **398**, 244(1989).

79. Schwieger, w., Bergk, K.H., Freude, D., Hunger, M. and Pfeier, H., *ACS Symp. Series,* **398**, 274(1989).

80. Freund, E.F., *J. Cryst. Growth,* **34**, 11(1976).

81. Glasser, L.S.D., Lachowski, E.E., *J. Chem Soc. Dalton,* 399(1980).

82. Mostowicz, R., Sand, L.B., *Zeolites,* **2**, 143(1982).

83. Kuhl, G.H., *Molecular Sieve Zeolites-I, Adv. Chem. Series,* **101**, 63 (1971).

84. Culfas, A., and Sand, L.B., *Molecular Sieves, Adv. Chem. Ser.*, **121**, 140(1973).

85. Barrer, R.M., Baynham, J.W., Bultitude, F.W. and Meier, W.M., *J. Chem Soc.*, 195(1959).

86. Kerr, G.T., *J. Phys. Chem.*, **70**, 1047(1966).

87. Kerr, G.T., *J. Phys. Chem.*, **72**, 1385(1968).

88. Cournoyer, R.A., Karnick, W.L., and Sand. L.B., *J. Phys. Chem.*, **79**, 1578(1975).

89. Kacirek, H., and Lechert, H.,*J. Phys. Chem.*, **79**, 1589(1975).

90. Angell, C.L., and Flank, W.H., *Molecular Sieve II, ACS Symp. Ser.*, **40**, 194(1977).

91. Hwakins, D.B., *Clay and Clay Minerarls*, **29**, 331(1981).

92. McNicol, B.D., Pott, G.T., and Loos, K.R., *J. Phys. Chem.*, **76**, 3388(1972).

93. McNicol, B.D., Pott, G.T., Loos, K.R., and Mulder, N., *Molecular Sieves, Adv. Chem. Ser.*, **121**, 152(1973).

94. Polak, F., and Cichocki, A., *Molecular Sieves, Adv. Chem. Ser.*, **121**, 209(1973).

95. Breck, D.W., and Flanigen, E.M., *Molecular Sieves,* Soc. Chem. Ind., London , (1968), p47.

96. Flanigen, E.M., and Breck. D.W., *ACS 137th meeting,* Cleueland Ohio, (1960).

97. Flanigen, E.M., *Zeolite Chemistry and Catalysis,* Rabo, J.A., ed., ACS Monograph, **171**, 80(1976).

98. Kyu-Heon Yi and Son-Ki Ihm, *Microporous Materials*, **1**, 115 (1993).

99. Roozeboom, F., Robson, H.E. and Chen, S.S., *Zeolite: Science and Technology,* Martinus Nijhoff Publishers, (1984), p127.

100. Bodart, P., Nagy, J.B., Gabelica, Z., and Derouane, E.G., *J. de Chimie Physique,* **83**(11-12), 777 (1986).

101. Thompson, R.W., and Dyer, A., *Zeolites,* **5**, 302 (1985).

102. Ciric, J, *J. Colloid Interface Sci.*, **28**, 315 (1968).

103. Mirskii, Y.V., and Pirozhkov, V.V., *Russ. J. Phys. Chem.*, **44**, 1508 (1970).

104. Freund, E.F., *J. Cryst. Growth,* **34**, 11(1976).

105. Kacirek, M., and Lechert, H., *J. Phys. Chem.*, **80**, 1291 (1976).

106. Domine, D., and Quobex, J., *Molecular Sieves, Soc. Chem. Ind.*, London (1968), p78.

107. Meise, W., and Schwochow, F.E., *Molecular Sieves, Adv. Chem. Ser.*, **121**, 169 (1973).

108. Turnbull, D., Solid State Physics, **3**, Academic Press, New York (1956) p252.

109. Culfaz, A., Gunduz, U., and Orbey, H., *Cryst. Res. Technol.*, **28**, 29-38 (1993).

110. Budd, P.M., Myatt, G.T., Price, C., and Carr, S.W., *Zeolites*, **14**, 198-202 (1994).157.

111. Breck, W.D., "*Zeolite Molecular Sieves*", J. Wiley, New York, (1974), p.320.

112. Tielen, M., Geelen, M., and Jacobs, P.A., *Acta Phys. Chem.*, **31**, 1-18 (1958).

113. Koltz, M.R., US Patent, 4 269 813 (1981).

114. Hoelderich, W., Mross, W.D., and Schwarzman, M., G. Offenl. 3,143,045 (1983).

115. Baltes, H., Leupold, E.I., Litterer, H., and Wunder, F., G. Offenl. 3,134,316 (1983).

116. Perego, G., Fattore, V., and Taramasso, M., G. Offenl. 3,316,488 (1983).

117. Barri, S.A.I., and Young, D., EP Appl., 106, 478 (1983).

118. Marosi, L., Stabenow, J., and Schwarzman, M., G. Offenl. 2,831,630 (1980).

119. Taramasso, M., Manara, G., Fattore, V., and Notari, B., U. K. P. Appl., 2,024,790 (1980).

120. Baltes, H., et al., EP Appl., 77, 522 (1982).

121. Baltes, H., et al., G. Offenl. 3, 141, 285 (1983).

122. Koltz, M.R., U.S.P., 4, 405, 502 (1983).

123. McAnnespic, P., Dyer, A., and Mehta, J.B., U.S.P. 4, 329, 328 (1980).

124. Weisser, J., Scharfe, G., Grolig, J. and Waldmann, H., E.P. Appl., 71, 136 (1982).

125. Marosi, L., et al., G. Offnel. 2, 830 (1980).

126. Dwyer, F.G., and Jenkins, E.E., U.S.P. 3, 941, 871 (1976).

127. Boersma, M.A.M., Nanne, J.M., and Post, M.F.M., U.S.P., 4, 337, 176 (1982).

128. Marosi, L., et al., E.P. Appl., 10, 572 (1980).

129. Wilson S.T., et al., "*Interzeolite Chemistry*", The American Chemical Society: Washington, D.C., (1983), p.19-109.

130. Lok, B.M., et al., U.S. Pat. 4 440 871 (1984).

131. Lok, B.M., et al., *J. Am. Chem. Soc.*, **106**, 6092-93 (1984).

132. Wilson, S.T., and Flanigen, E.M., E. P. Appl., 0 132 708 (1985).

133. Wilson, S.T., and Flanigen, E.M., U.S. Pat., 4 544 143 (1985).

134. Ben Taarit, Y., in Zeolite Microporus Solids: Synhthesis, Structure, and Reactivity, Derouane et al., (Eds.), NATO ASI Series 352, Kluwer Academic Publishers, Netherland (1992) p. 291-302.

135. Poncelet, G., Dubrn, M.L., and Lux, T., *Met. Res. Bull.*, **11**, 813 (1976).

136. Lerot, L., Poncelet, D., and Fripiat, J.J., *Met. Res. Bull.*, **9**, 979 (1974).

137. Szostak R., and Thomas, T.L., *J. Catal.*, **100**, 555 (1986).

138. Kotasthane, A.N., Shiralkar, V.P., *Zeolites*, **6**, 253 (1986).

139. Iton, L.E., Beal, R.B., and Hodul, D.T., *J. Hol. Cat.*, **21**, 151 (1983).

140. Dararin, J., Guth, J.L., French Pat., 86/17711 (1986).

141. Inui, T., et al ., Proc. 8th, Int. Congress on Catalysis, Berlin, Verlog Chemie, Vol **III**, (1984) p 569-79.

142. Inui, T., *J. Japan Petrol., Inst.*, **28**, 279-292 (1985).

143. Inui, T., et al., *J. Catal.*, **98**, 491-501 (1986).

144. Taramasso, M., Perego, G., and Notari, B., U.S Pat., 4 410 501.

145. Esposito, A., Neri, C., and Buonono, F., U.S. Pat., 4, 480, 135 (1984).

146. Esposito, A., Neri, C., and Buonono, F., Brit. Pat., 2, 116, 974 (1985).

147. Notari, B., *Stud. Surf. Sci. Catal.*, **37**, 413 (1988).

148. Thangaraj, A., Kumar, A., and Ratnasamy, P., *Appl. Catal.*, **57**, L1 (1990).

149. Notari, B., Presented at the 206th National Meeting of the ACS, Chicago, IL, August 1993; paper PETR 103.

150. Khouw, C.B., and Davis, M.E., *J. Catal.*, **151**, 77-86 (1995).

151. Lok, B.M., Marcus, B.K., Flanigen, E.M., E.P. Appl., 179, 876 (1985).

152. Lok, B.M., et al., E.P. Appl., 181, 884 (1985).

153. Bellussi, G., Giusti, A., Esposito, A., and Buonomo, F., E.P. Appl., 226, 257 (1988).

154. Bellussi, G., et al ., E.P. Appl., 226, 258 (1988).

155. Bellussi, G., et al ., E.P. Appl., 266, 825 (1988).

156. Bellussi, G., et al., *Std. Surf. Sci. Catal.*, **63**, 421-429 (1991).

157. Vedrine, J.C., Auroux, A., Coudurier, G., Engelhard, P., Gallez, J.P., and Szabo, G., *Pro. 6th Int. Conf. on Zeolites*, Olson, Bisio, eds., Butterworth, Guildford, U.K. (1984), 497.

158. Wang, I., Chen, T., Chao, K., and Tasi, T., *J. Catal.*, **60**, 140 (1979).

159. Chu, C.T. and Chang, C.D., *J. Phys. Chem.*, **89**, 1569 (1985).

160. Lunsford, J.H., *J. Phys. Chem.*, **78**, 4163 (1968).

161. Haag, W.O. and Lago, R.M., E.P. 003 444 (1981).

162. Ashton, A,G., Batmanian, S., Clark, D.M., Dwyer, J., Fitch, F.R., Hinchliffe, A. and Machado, F.J., *Stud. Surf. Sci. Catal.*, **20**, (1985), p101.

163. Dwyer, J., *Inovations in Zeolite Materials Science,* P.J Grobet et al. (Eds.), Elsevier (1988) 333.

164. Brunner, E., Ernst, H., Freude, D., Frolich T., Hunger, M., Pfeifer, *J. Catal.*, **127** 34 (1991).

165. Macedo, A., Raatz, F., Boulet, R., Janin, A., and Lavelley, J.C., *Inovations in Zeolite Materials Science*, P.J Grobet et al. eds., Elsevier (1988) 375.

166. Fritz, P.O., and Lunsford, J.H., *J. Catal.*, **118**, 85, (1989).

167. Naccache, C., Chen, F.R., and Coudurier, G., *Zeolites, Facts, Figures, Future*, Jacobs, P.A., and Santen, R.A., (Eds.) Elsevier (1989) 661.

168. Zholobenko, V.I., Kustov, L.M., Kanasky, V.B., Loeffler, E., Lohse, U., and Oehlmann, G., *Zeolites*, **11**, 132 (1991).

169. Luk'Yanov, D.B., *Zeolites*, **11**, 325 (1991).

170. Jarman, R. H., Melchior, M.T., *JCS. Chem. Comm.*, 414 (1984).

171. Piel, W.J., and Thomas, R.X., *Hydrocarbon Processing*, **69**, 68, (1990).

172. Mills, G.A., and Ecklund, E.E., *ChemTech*, **19**, 627 (1989).

173. Ainsworth, S.J., *Chem. Eng. News.* **69**, 13-16 (1991).

174. Suzanne, S., *Chem. Eng.*, **101**(1), 61-63 (1994).

175. Chang, E.J., and Leiby, S,M., *Hydrocarbon Processing*, **71**, 41, (1992).

176. Satterfield, C.N., in "Heterogeneous Catalysis in Industrial Practice" (2nd Ed.), McGraw-Hill, New York, (1990), p.260.

177. Ancilloti, F., Mauri, M.M . and Pescarollo, E., *J. Mol. Catalysis*, **4** (1), 34-37 (1978).

178. Obenaus, F., and Droste, W., Oil Gas J., 77, 76-77 (1979).

179. Texaco, D., German Patent DE 33 22 753 A1 (1985).

180. Erdölchemie, E.C., EP 48 893 A1 (1982).

181. Siger, R.M., *Fuel Refom.*, 46-47, Nov/Dec (1993).

182. Chase, J.D., in "Catalytic Conversion of Synthesis Gas and Alcohols to Chemicals" Herman, R.G., (Ed.), Plenum Press, New York (1984) p. 307.

183. Tjero, J., . Cunill, F., and . Izquierdo, J.F., *Ind. Eng. Chem. Res.*, **28**, 1269 (1989).

184. Ancillotti, F., Mauri, M.M. and Pescarollo, E., *J. Catalysis*, **46**, 49-57 (1977).

185. Voloch, M., Ladisch, M.R., and Tsao, G.T., *React. Polymers*, **4**, 91 (1986).

186. Gicquel, A. and Torck, B., *J. Catalysis*, **83**, 9-18 (1983).

187. Ancillotti, F., Pescqrollo, E., Szatmari, E. and Lazar, L. *Hydrocabon Proc*essing, 63 (1987).

188. U.S. Patent 4 039 590, assigned to Snamprogetti.

189. Refinger, A., and Hoffmann, *Chem. Eng. Sci.*, **45**, 1605 (1990).

190. Tejero, J., Cunill, F., and Izquierdo, J.F., *Ind. Eng. Chem. Res.*, **27**, 338 (1988).

191. Sundmacher, K., and Hoffman, U., *Chem. Eng. Sci.*, **49**, 3077-3089 (1994).

192. Dixon, P.H.O., D'Amico, V.J., Strain, B., Jones, E.M. and Smith, L.A., Paper No. AM89-44. Presented at the National Petroleum Refiners Association Annual Meeting, March 19-21, 1989, San Francisco Hilton, California, USA (1989).

193. Jacobs, R., and Krishna, R., *Ind. Eng. Chem. Res.*, **32**, 1706-1709 (1993).

194. Nijhuis, S.A., Kerkhof, F.P.J.M., and Mak, A.N.S., *Ind. Eng. Chem. Res.*, **32**, 2767-2774 (1993).

195. Norris, J.F., and Rigby, G.W., *J. Am. Chem. Soc.*, **54**, 2088 (1932).

196. Evans, T.W., and Edlund, K.R., *Ind. Eng. Chem.*, **28**, 1186 (1936).

197. Bitar, L.S., Hazbun, E.A., and Piel, W.J., *Hydrocarbon Processing*, 63 (1984).

198. Chu, P., and Kuhl, H., *Ind. Eng. Chem. Res.*, **26**, 365-369 (1987).

199. Harandi, M.N., and Owen, H., U.S. Patent 4, 814, 519 (1989).

200. Knifton, J.F., European Patent EP 333 078 A1, (1989).

201. Pien, S.I., and Hatcher, W.J., *Chem. Eng. Comm.*, **93**, 257-265 (1990).

202. Yavaraski, T., and Hatcher, W.J., Annual Meeting of AIChE, San Francisco, November 8, 1989, Session 51. (1989).

203. Mao, R.L.V., Carli, R., Ahlafi, H., and Ragaini, V., *Catalysis Letters*, **6**, 321-330 (1990).

204. Chang, K.H., Kim, G.T., and Ahn, W.S., *Ind. Eng. Chem. Res.*, **31**, 125-130 (1992).

205. Nikoloupolos, A.A., Oukaci, R., Goodwin Jr. J.G., and Marcelin, G., in '*New Frontiers in Catalysis*' Guczi, L., et al., (Eds.), Proc. 10th Int. Congress on Catalysis, 19-24 July 1992, Budapset, Hungary p 2601-2604.

206. Kogelbauer, A., Ocal, M., Nikoloupolos, A.A., Goodwin Jr. J.G., and Marcelin, G., *J. Catal.*, **148**, 157-163 (1994).

207. Nikoloupolos, A.A., et al., *Appl. Catal.*, **119**, 69-81, (1994).

208. Plackett, R.L., and Burman, J.P., *Biometrica*, **33**, 305-325, (1946).

209. Stowe, R.A and Mayer, R.P., *Industr. and Eng. Chem.*, **58**(2), 36-40 (1966).

210. Mario Calligaris, Third International School and Workshop of Crystallography on XRD and its Applications, January 1990, Cairo Egypt.

211. Furman, N.H., (Ed.), 'Standard Methods of Chemical Analysis', Vol. 1, Krieger Publishers, New York, (1975).

212. Coudurier, G., Naccache, C. and Vedrine, J.C., *J. Chem. Soc., Chem. Commun.*, 1413-15, (1982).

213. Flanigen, E.M., Khatami, H. and Syzmanski, H., *Adv. Chem. Ser.*, **101,** 201 (1971).

214. Pichat, P., Beaumont, R. and Barthomeuf, D., *C.R. Acad. Sci., Ser. C,* Paris, **272**, 261, (1971).

215. Valyon, J., Mihalyfi, J., Beyer, H.K. and Jacobs, P.A., *Proceed. Workshop on Adsorpt.*, Berlin , (1979), p134.

216. Van Ballmoos, R., *Collection of Simulated XRD patterns for Zeolites* Butterworths, (1984).

217. Nagy, B.J, Bordrat, P., Collette, H., *Zeolites*, **3**, 43 (1983).

218. Gabelica, Z., Blous, N. and Derouane, E. G., *Appl. Catal.*, **5**, 227 (1983).

219. Crea, F., Giordano, G., Mostowicz, R., and Nastro, A., *J. Therm. Anal.*, **36**, 2229, (1990).

220. Nagy, J.B., Bordrat, P., Collette, H., *Zeolites,* **8**, 209 (1988).

221. Van Santen, R.A., Keijsper, J., Ooms, G., and Kortbeek, A.G.T.G., *Stud. Sur. Sci. Catal.*, 28 (1986) p.169.

222. Habersberger K., *Thermochim. Acta*, **110**, 337-341 (1987).

223. Wichterlova, B. *Zeolites*, **1**,189 (1981).

224. Abdillahi, M.M., Elnafaty, U.A., and Aljarallah, A.M., *Appl. Catal.*, **91**, 1-12 (1992).

225. Inui, T., et al., in 'New Developments in Zeolite Science and Technology', Murakami, Y., Iijima, A., and Ward, J.W., (Eds.), Elsevier, Tokyo, (1986) p. 859.

226. Adams, J.M., Clement, D.E., and Graham, S.H., *Clays and Clay Minerals*, **30**, 129-134 (1982).